UNIVERSIDADE FEDERAL RURAL DO RIO DE JANEIRO
INSTITUTO DE FLORESTA
CURSO DE PÓS-GRADUAÇÃO EM CIÊNCIAS
AMBIENTAIS E FLORESTAIS

ENTENDENDO OS MECANISMOS DA FLORESTA AMAZÔNICA
PARA MANUTENÇÃO DA SUA PRODUTIVIDADE DIANTE DE
MUDANÇAS ANTRÓPICAS E CLIMÁTICAS

REGIANE SOUZA VILANOVA

Sob a Orientação do Professor
Rafael Coll Delgado

e Co-orientação do Professor
Paulo Eduardo Teodoro

Tese submetida como requisito para obtenção do grau de **Doutora em Ciências,** no Curso de Pós-Graduação em Ciências Ambientais e Florestais, Àrea de Concentração em Conservação da Natureza.

Seropédica, RJ
Agosto de 2021

UNIVERSIDADE FEDERAL RURAL DO RIO DE JANEIRO
INSTITUTO DE FLORESTAS
CURSO DE PÓS-GRADUAÇÃO EM CIÊNCIAS AMBIENTAIS E FLORESTAIS

REGIANE SOUZA VILANOVA

Tese submetida como requisito parcial para a obtenção do grau de **Doutor(a) em Ciências**, no Programa de Pós-Graduação em Ciências Ambientais e Florestais, Área de Concentração em Conservação da Natureza

TESE APROVADA EM 18/08/2021

_____
Rafael Coll Delgado. Dr. UFRRJ
(Orientador)

_____
Carlos Antonio da Silva Junior. Dr. UNEMAT

_____
Marcos Gervasio Pereira. Dr. UFRRJ

_____
Henderson Silva Wanderley. Dr. UFRRJ

_____
Douglas da Silva Lindemann. Dr. UFPEL

MINISTÉRIO DA EDUCAÇÃO
UNIVERSIDADE FEDERAL DO RIO DE JANEIRO
SISTEMA INTEGRADO DE PATRIMÔNIO, ADMINISTRAÇÃO E
CONTRATOS
UFRRJ

FOLHA DE ASSINATURAS

Emitido em 18/08/2021

TERMO Nº 908/2021 - PPGCAF (12.28.01.00.00.00.00.27)

(Nº do Protocolo: NÃO PROTOCOLADO)

(Assinado digitalmente em 20/08/2021 19:05)
HENDERSON SILVA WANDERLEY
PROFESSOR DO MAGISTERIO SUPERIOR
DeptCAmb (12.28.01.00.00.00.00.29)
Matrícula: 2086234

(Assinado digitalmente em 23/08/2021 08:28)
MARCOS GERVASIO PEREIRA
PROFESSOR DO MAGISTERIO SUPERIOR
DeptS (12.28.01.00.00.00.33)
Matrícula: 1060711

(Assinado digitalmente em 20/08/2021 17:51)
RAFAEL COLL DELGADO
PROFESSOR DO MAGISTERIO SUPERIOR
DeptCAmb (12.28.01.00.00.00.00.29)
Matrícula: 1872560

(Assinado digitalmente em 20/08/2021 12:11)
CARLOS ANTONIO DA SILVA JUNIOR
ASSINANTE EXTERNO
CPF: 024.966.381-32

(Assinado digitalmente em 20/08/2021 19:34)
DOUGLAS DA SILVA LINDEMANN
ASSINANTE EXTERNO
CPF: 009.216.190-14

A Deus, pelo cuidado e sustento, à memória de meu pai e a minha família pelo apoio, amor e ajuda em todos estes anos.

Dedico.

AGRADECIMENTOS

Primeiramente a Deus pela dádiva da vida, pelo sustento e por me permitir trilhar esse caminho tão especial e lindo.

À minha família linda que eu tanto amo por ter acreditado e me apoiado durante todos esses anos, em especial, a minha queria mãe Rosilda, por ter sido pai, mãe e amiga, por não ter medido esforços para criar seus 6 filhos e me ensinado valores que me nortearam até aqui.

Ao meu orientador e grande amigo Rafael Delgado, por ter acreditado e me incentivado na carreira acadêmica, ter sido um orientador impecável, com participação efetiva em todos os capítulos desta tese, pela paciência em me ensinar e mostrar como se trabalhar em equipe. Agradeço principalmente por ter ido além, ter me visto como sou, me ouvido, aconselhado e ter tido cuidado e empatia durante todos esses longos 10 anos de amizade.

Agradeço as famílias Pereira, Delgado e Alojamento da Pós-Graduação que me acolheram durante esse período longe de casa. Obrigado por terem me permitido entrar em seus espaços e ocupar um lugarzinho que eu quero sustar para o resto da minha vida. Sou imensamente feliz por ter vocês em minha vida, cada um com suas particularidades e regionalidades que me ajudaram a aliviar os momentos de estresse, me incentivaram, mostram afeto e Amor, me viram chorar, mas também me viram rir e sempre estavam ali, apostos para qualquer necessidade. Não tenho como expressar em palavras o prazer de estar com vocês, cada dia aprendendo e ensinando, moldando e sendo moldada, espero poder ter transmitido o amor que sinto por cada um de vocês em minhas muitas tentativas.

À todas as amizades construídas ao longo dos meus anos, as quais tenho a certeza de que foram escolhidas por Deus, para trilharem esse caminho comigo. Dentre as surpresas que o destino me reservou, está cada um de vocês, agradeço pela paciência, carinho e companheirismo de todos, cada um da sua forma e dentro de suas possibilidades, mas que não permitiram me ver sozinha em nenhum dos meus dias, saibam que tenho imenso amor por vocês. E falando em belas surpresas do destino, agradeço ao meu namorado Gleyton Leonel pelo cuidado, carinho, paciência e amor.

Ao meu coorientador Paulo Teodoro e aos membros da banca pelas contribuições e sugestões neste trabalho tão importante para mim.

À Universidade Federal Rural do Rio de Janeiro (UFRRJ), ao Programa de Pós-graduação em Ciências Ambientais e Florestais (PPGCAF/UFRRJ), pela enorme contribuição em minha formação acadêmica.

Agradeço a todos os meus professores desde os ensinos primários até minha pós-graduação, por terem repassado seus conhecimentos e me formado como acadêmica e cidadã.

Á todos aqueles que de alguma forma contribuíram para realização deste trabalho e que me apoiaram nesta importante etapa da minha vida.

RESUMO GERAL

VILANOVA, Regiane Souza. **Entendendo os mecanismos da floresta amazônica para manutenção da sua produtividade diante de mudanças antrópicas e climáticas.** 2021. 81p. Tese (Doutorado em Ciências Florestais e Ambientais). Instituto de Florestas, Universidade Federal Rural do Rio de Janeiro, Seropédica, RJ, 2021.

As florestas tropicais amazônicas estão entre as áreas mais importantes e de maior biodiversidade da terra. Elas contribuem para as funções do ecossistema, incluindo a regulação do fluxo da água e a manutenção de um dos mais importantes sumidouros de carbono do planeta, e fornecem recursos para atividades econômicas importantes, como madeira e produtos não madeireiros, peixes e outros alimentos. No entanto, o desmatamento tropical-equatorial causado pela expansão das atividades agrícolas e exploração madeireira insustentável tem causado perdas e degradação dessa floresta. A falta de fiscalização e políticas voltadas para a preservação só fortalece esse cenário devastador. Nas últimas décadas, pesquisas têm sido realizadas para quantificar essas perdas e entender melhor os diversos agentes atuantes sobre as florestas Amazônicas. Estudo sobre a evapotranspiração, eventos climáticos extremos, incêndios, carbono e absorção de luz pela planta tem ajudado no entendimento desses fatores, bem como na elaboração de estratégias de mitigação dos impactos. Este estudo investiga os diversos mecanismos utilizados pelas florestas para manter-se em pé e produtiva, diante das intervenções humanas e alterações climáticas severas, combinando, analisando e fazendo projeções futuras de diferentes tipos de agentes atuantes na região Amazônica. A tese foi dividida em três capítulos, onde o primeiro avaliou o estado de saúde da vegetação para o estado do Amazonas, também se verificou correlações positivas e negativas desse índice com outras variáveis como, temperatura do ar, chuvas, umidade do solo, focos de incêndio e temperatura da superfície terrestre. Ainda neste capítulo, foi aplicado o Autoregressive Integrated Moving Average (ARIMA) na série do Vegetation Health Index (VHI) para simulação futura da saúde da vegetação, o que nos permitiu verificar como será o comportamento da floresta no futuro, ano de 2030. No segundo capítulo, foram utilizados dados de sensoriamento remoto, as seis tipologias florestais encontradas para o estado e elementos meteorológicos de quatorze estações meteorológicas convencionais distribuídas em todo o estado do Amazonas, para investigar os processos de degradação da vegetação em ano de eventos do fenômeno El Niño Oscilação-Sul. O terceiro capítulo, foi focado na melhoria dos dados proveniente de torre de fluxo, que são usados para fazer inferências sobre a vegetação. Aplicou-se a metodologia ARIMA no preenchimento das falhas de dados de produtividade primária bruta proveniente de uma torre de fluxo (K34) no estado do amazonas.

Palavras-chave: Modelagem futura, saúde da vegetação, degradação ambiental.

ABSTRACT

VILANOVA, Regiane Souza. **Understanding the mechanisms of the Amazon forest to maintain its productivity in the face of anthropic and climate changes.** 2021. 81p. Thesis (Doctorate in Environmental and Forest Sciences). Instituto de Florestas, Universidade Federal Rural do Rio de Janeiro, Seropédica, RJ, 2021.

Amazon rainforests are among the most important and most biodiverse areas on earth. They contribute to ecosystem functions, including regulating water flow and maintaining one of the planet's most important carbon sinks, and provide resources for important economic activities such as timber and non-timber products, fish and other foods. However, tropical deforestation caused by the expansion of agricultural activities and unsustainable logging has caused losses and degradation of this forest However, tropical-equatorial deforestation caused by the expansion of agricultural activities and unsustainable logging has caused losses and degradation of this forest. The lack of inspection and conservation-oriented policies only strengthens this devastating scenario. A study on evapotranspiration, extreme weather events, fires, carbon, and light absorption by the plant has helped in understanding these factors, as well as in the development of impact mitigation strategies. This study investigates the various mechanisms used by forests to remain standing and productive, in the face of human interventions and severe climate change, combining, analyzing and making future projections of different types of agents operating in the Amazon region. The thesis was divided into three chapters, where the first one assessed the health status of the vegetation for the state of Amazonas, there were also positive and negative correlations of this index with other variables such as air temperature, rainfall, soil moisture, foci of fire and surface temperature. Also in this chapter, the Autoregressive Integrated Moving Average (ARIMA) was applied in the Vegetation Health Index (VHI) series for future simulation of vegetation health, which allowed us to verify how the forest will behave in the future, year 2030 In the second chapter, remote sensing data were used, the six forest typologies found for the state and meteorological elements of fourteen conventional weather stations distributed throughout the state of Amazonas, to investigate the processes of vegetation degradation in the year of events of the El Niño Oscilação-Sul phenomenon. The third chapter was focused on improving the data coming from the flow tower, which are used to make inferences about the vegetation. The ARIMA methodology was applied in filling the failures of raw primary productivity data from a flow tower (K34) in the state of Amazonas.

Keywords: Future modeling, vegetation health, environmental degradation.

SUMÁRIO

INTRODUÇÃO GERAL

A floresta amazônica é o resultado de milhões de anos de evolução com importância ecológica global, e tem sido objeto de diversos estudos ao longo dos últimos anos, na tentativa de entender as respostas das florestas frente as mudanças climáticas, as perturbações humanas, aos regimes de fogo e incertezas políticas. Sabe-se que, além de seu valor estético, as florestas desempenham papel importante na regulação do clima, no avanço medicinal por meio de sua imensa biodiversidade, no orçamento de carbono global, dentre outros.

É notório que existe uma grande preocupação com o futuro dessas florestas, mesmo assim, o desmatamento tem crescido nos últimos anos com a expansão da produção de commodities agrícolas, assim como a ocorrência de incêndios. Combinado a mudanças climáticas globais, o uso da terra, degradação florestal, disponibilidade de água no solo, incêndios e outros distúrbios, vão determinar que tipo de vegetação teremos no futuro.

Vários cenários futuros são projetados para este bioma, que preveem desde o aumento das florestas até uma extinção em grande escala da Amazônia. A grande questão agora é o que fazer a respeito? Combinações de monitoramento ambiental, fiscalização e manutenção de áreas protegidas poderiam trazer um alívio para este último cenário, no entanto, o que vemos são forças políticas e econômicas lutando desesperadamente para se recuperar de uma crise econômica, juntamente com uma grave crise epidemiológica, uma agenda geopolítica pró-desenvolvimentista deixando de lado quaisquer preocupações ambientais.

O risco de transgressão de um ponto de inflexão para a Amazônia, deve ser prioridade no desenvolvimento de pesquisas e políticas de desenvolvimento sustentável, reduzindo sua degradação e perda da biodiversidade. Vale ressaltar ainda que, a degradação ambiental associada a mudanças climáticas, pode gerar um cenário de caos na medida que aumenta a competição por recursos naturais exacerbando as desigualdades sociais e econômicas.

Séries temporais de dados provenientes de satélites e seus sensores, torres micrometeorológicas, índices de vegetação e estações meteorológicas convencionais e automáticas tem ajudado no entendimento e mitigação dos vários fatores que atuam e afetam as florestas tropicais-equatoriais. Porém, os desafios com investimentos nas pesquisas, manutenção de equipamentos, resoluções espaciais e número de estações meteorológicas que apresentam falhas nas séries temporais, ainda são enormes e por vezes dificultam a obtenção de dados para as regiões remotas.

O estado do Amazonas com sua vasta extensão de floresta e território, foi escolhido para ser palco dos estudos realizados nesta tese, o trabalho está dividido em três capítulos. No capítulo I, avaliou-se a saúde da vegetação por meio do índice Vegetation Health Index (VHI), e sua correlação com outras variáveis como, temperatura do ar, chuvas, umidade do solo, focos de calor e temperatura da superfície terrestre. Ainda neste capítulo foi aplicado o Autoregressive Integrated Moving Average (ARIMA) na série do VHI para simulação futura até o ano de 2030 da saúde da vegetação. No capítulo II, foram utilizados dados de sensoriamento remoto, tipologias florestais e elementos meteorológicos de 14 estações meteorológicas convencionais localizadas no estado do Amazonas, para investigar os processos de degradação da vegetação em ano de eventos do fenômeno El Niño Oscilação-Sul. O capítulo III foi focado no preenchimento de falhas de dados obtidos em torres micrometeorológicas. Aplicou-se a metodologia ARIMA no preenchimento das falhas de dados de produtividade primária bruta proveniente de uma torre de fluxo (K34) no estado do amazonas.

CAPÍTULO I

PAST AND FUTURE ASSESSMENT OF VEGETATION ACTIVITY FOR THE STATE OF AMAZONAS-BRAZIL

RESUMO

As atividades de florestas tropicais têm sido sensíveis às mudanças climáticas, tornando o monitoramento dessas florestas cada vez mais necessário. No contexto das mudanças climáticas, a Amazônia Legal é uma região de grande importância global. Neste estudo, foram utilizadas as variáveis temperatura do ar, chuvas, umidade do solo, focos de incêndio, temperatura da superfície terrestre, Normalized Difference Vegetation Index (NDVI) e o Índice de Saúde da vegetação (VHI) de 2001 a 2018 em escala mensal. O Autoregressive Integrated Moving Average (ARIMA) foi aplicado à série VHI e sua capacidade foi analisada na previsão da série temporal observada (2001-2018) e futura (2019-2030). Os resultados mostraram queda nos valores de VHI para o período considerado seco na Amazônia. De cada ano, 2015 registrou a menor média de 30,73%, colocando-a na classe de seca leve. No entanto, em alguns meses, como setembro, outubro e novembro, que apresentaram valores de VHI de 8,42%, 6,08% e 9,47%, respectivamente, indicaram secas extremas. Para a análise de Mann-Kendall, as variáveis umidade do solo e temperatura do ar apresentaram tendência negativa e positiva com valores significativos na maioria dos meses. O cluster baseado na distância euclidiana revelou que as variáveis mais influentes para a região foram VHI e temperatura do ar. A modelagem ARIMA gerada e validada bem simulada VHI, apresentando uma média do coeficiente willmott (d) de 1 para o período de estudo. A projeção futura de 12 anos (2019-2030) de VHI para o estado do Amazonas mostrou que o modelo capaz de representar a sazonalidade da série.

Palavras-chave: Amazônia Legal; florestas tropicais; modelagem de vegetação; vulnerabilidade da vegetação; sensoriamento remoto.

ABSTRACT

Tropical forest activities have been sensitive to climate change, making monitoring of these forests increasingly necessary. In the context of climate change, the Legal Amazon is a region of great global importance. In this study, the variables air temperature, rainfall, soil moisture, fire foci, land surface temperature, Normalized Difference Vegetation Index (NDVI) and the Vegetation Health Index (VHI) from 2001 to 2018 on a monthly scale were used to describe the past condition and future health of vegetation in the state of Amazonas-Brazil. The Autoregressive Integrated Moving Average (ARIMA) model was applied to the VHI series and its capacity was analyzed in the forecast of the observed (2001–2018) and future (2019–2030) time series. The results showed a decrease in VHI values for the period considered dry in the Amazon. Of each year, 2015 registered the lowest average of 30.73%, placing it in the mild drought class. However, in some months, such as September, October and November, which presented VHI values of 8.42%, 6.08% and 9.47% respectively, indicated extreme droughts. For the Mann-Kendall analysis, the variables soil moisture and air temperature showed a negative and positive trend with significant values for most months. The Heatmap clustering based on the Euclidean distance revealed that the most influential variables for the region were VHI and air temperature. The generated and validated ARIMA modeling well simulated VHI, presenting an average of the willmott coefficient (d) of 1 for the study period. The future 12-year projection (2019–2030) of VHI for the state of Amazonas showed that the model able to represent the seasonality of the series.

Keywords: Legal amazon, Tropical forests, Vegetation modeling, Vegetation vulnerability, Remote sensing.

1 INTRODUCTION

In the context of climate change, the Legal Amazon is a region of great global importance. Tree mortality in tropical forests has been increasing significantly and has significant implications for the global and water cycle in these regions, little is known about the factors leading to tree mortality (Aleixo et al., 2019). The Amazon is undergoing profound changes in its landscape through forest degradation, changes in land use and effects of global climate change (Funatsu et al., 2019).

Terrestrial vegetation has determining effects on water and biogeochemical cycles of ecosystems (Piao et al., 2014). Rainforests represent the world's most biodiverse ecosystems, store large amounts of moisture, and provide livelihoods for local populations (Delgado et al., 2018; Kruhlov et al., 2018; Chagas et al., 2019).

Vegetation activities have been sensitive to climate change (Asner and Alencar, 2010), for example, increased temperature and low amount of water in the soil. The intensification of droughts has threatened tropical rainforests, especially younger trees with a smaller root system and those that are concentrated in less humid areas (Giardina et al., 2018).

Higher temperatures caused by El Niño and warmer water in the North Atlantic provides several drought conditions in the region, as rainfall decreases and temperatures rise, resulting in higher fires foci and reduced vegetation activity causing a range of impacts on society (Jiménez-Muñoz, 2016; Stuecker et al., 2017; da Silva Júnior et al., 2019; de Andrade et al., 2019). Therefore, there is a growing need to monitor vegetation activity in the Amazon region.

Various vegetation indices using satellite data are widely used for different types of vegetation studies and monitoring, for example, to monitor vegetation activity and health, in addition to monitoring drought and senescence (Kundu et al., 2016, Bento et al., 2018; Pei et al., 2018). Other indexes are used to examine vegetation activity such as the Vegetation Condition Index (VCI) which is an index derived from the Normalized Difference Vegetation Index (NDVI) that has the ability to distinguish fluctuations due to short term climate change and ecosystem changes. (Kogan, 1990), and the LST-derived Thermal Condition Index (TCI) that was developed by Kogan, (1995) to determine temperature-related vegetation stress and used for the development of the Vegetation Health Index (VHI).

In general, VHI is a time series analysis of the effects of humidity and temperature on plants (Tran et al., 2017), widely applied and effective in assessing vegetation health (Wang et al., 2014; Kundu et al., 2016; Parviz, 2016, Gomes, Bernardo and Alcântara, 2017, Gidey et al., 2018). Some models have been implemented to understand vegetative dynamics and simulate past, present and future distribution patterns (Valipour, 2015; Machekposhti et al., 2017; Rahman, Yunsheng and Sultana, 2017). The Autoregressive Integrated Moving Average (ARIMA) Model allows the use of past data to generate future simulations of environmental processes (Fashae et al., 2019; Lucas et al., 2009) and others.

The increases in deforestation rates in the state of Amazonas causes imbalance in forest ecosystem services, causing major environmental and socioeconomic impacts. Faced with the threat of continuing the trend of increasing deforestation rates across the Amazon, public policies addressing this problem are of paramount importance.

However, many questions still need to be answered, for example: (1) Can ARIMA when applied to the VHI variable be a predictive model in an attempt to detect severe droughts in the Amazon for the future ? and (2) Is the series used satisfactory and shows a positive or negative trend of the biophysical variables studied in the Amazon? In order to answer these questions, this study aims to evaluate the condition of vegetation health in the state of Amazonas through the VHI for the period from 2001 to 2018, and application of the ARIMA model for simulation of the future series for the VHI.

2 MATERIALS AND METHODS

2.1 Study Area

The state of Amazonas is the largest in Brazil in territorial extension, with a surface of 1,559,148,890 km² and a population of 3,938,336 inhabitants (Fig. 1), which corresponds to 18% of the national territory (IBGE, 2017). According to the Koppen-Geiger classification, the predominant climate in the region belongs to group A (tropical), with average temperatures of 24ºC to 26ºC and relative humidity ranging from 76% to 89%, having two well defined seasons, the winter is characterized as the rainy season and summer as the least rainy season (Alvares et al., 2013).

Among the dominant soil classes in the state of Amazonas, Argisols are the most pronounced comprising almost 45% of the entire area of the state. Latosols represent 26% of the area, being predominantly Yellow Latosols, whose occurrence is concentrated near the central region of the state in the terra firme areas (Aquino et al., 2014).

The main forest typologies that occur in the state of Amazonas are the Várzea Forests, Igapó Forest and Terra Firme Forest. In the lower parts closer to the rivers are igapó forests that spend most of the year flooded, unlike the Várzea areas that are subject to flooding more commonly in the rainy season (IBGE, 2012). Dryland Forests are located in the higher parts, where no flooding occurs even temporarily (Lopes et al., 2016).
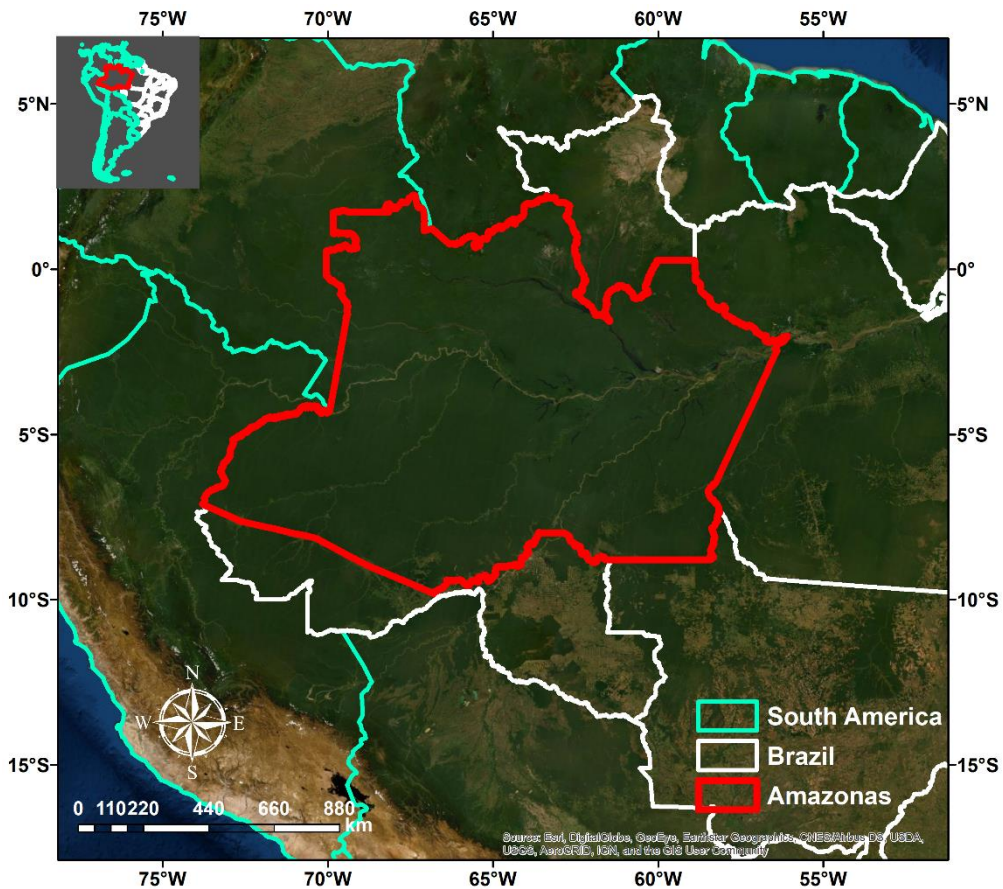

Fig. 1. Geographic localization of the study area.

2.2 Surface Weather Data

Due to the spatial and temporal limitation of automatic and conventional meteorological stations in the northern region and specifically the state of Amazonas, data from Reanalysis 2 in NetCDF format were used (Ruffault et al., 2016; Das et al., 2017).

The rainfall (mm), air temperature (ºC) and soil moisture (mm) in NetCDF format were obtained from NCEP-DOE Reanalysis 2 (https://www.esrl.noaa.gov/psd/data/ gridded / data.ncep.reanalysis2.html) (Kanamitsu et al., 2002). The monthly scale was used for all data and the study period ranged from 2001 to 2018.

2.3 Remote Sensing Products

Data from the fire foci for the same period in question were obtained from the MOD14 collection 6 platforms TERRA and AQUA product (https://earthdata.nasa.gov/firms). Land Surface Temperature (LST) data were used for the state of Amazonas from MOD11B3 V006 (Wan, 2013), derived from the MODIS (Moderate Resolution Imaging Spectroradiometer) sensor aboard the TERRA orbital platform. The MOD11A2 product provides a monthly average day and night terrestrial surface temperature per pixel on a 1200km x 1200km tile and 1km spatial resolution. Monthly Normalized difference vegetation index (NDVI) images were derived directly from MOD13A3 products.

NDVI ranges from -1 to 1 and was proposed by Rouse et al. (1974), where values close to 1 correspond to areas of greater vegetative vigor (Eq. 1).

$$NDVI = \frac{IVP-V}{IVP+V} \tag{1}$$

where IVP is the near-infrared reflectance in the near infrared band and V is the red band reflectance in the visible spectrum.

The MODISsp tool in software R version 3.5.1 was used to download the images from 2001 to 2018 (products MOD11B3, MOD11A2, MOD13A3 V006) for tiles h10v08, h10v09, h11v08, h11v09, h11v10, h12v08 and h12v09 which spatially comprises the state of Amazonas.

2.4 Vegetation Health Index (VHI)

From the LST (MOD11B3) and NDVI (MOD13A3) products we adopted the methodology proposed by Kogan (1997) to estimate the Vegetation Health Index (VHI). VCI and TCI can be estimated using NDVI and LST products (Eq. 2 and 3).

$$VCI = \frac{NDVI-NDVI_{min}}{NDVI_{max}-NDVI_{min}} \times 100 \tag{2}$$

where NDVI is the average value for the year, and NDVI max and NDVI min are the highest and lowest values for the same year for the period 2001–2018, respectively.

Maximum and minimum NDVI values reflect the best and worst conditions for plant growth, respectively. The difference between these two values indicates plant conditions at a given location (Nanzad et al., 2019).

$$TCI = \frac{LST_{max}-LST}{LST_{max}-LST_{min}} \times 100 \tag{3}$$

where LST is the mean value of the year and LSTmax and LSTmin are the highest and lowest values of the same year for the period 2001–2018, respectively.

The Vegetation Health Index (VHI) can be estimated according to (Kogan, 1997; Kogan, 2001; Bento et al., 2018) (Eq. 4). The same constant value of α = 0.5 was adopted. In R environment a grid cell composed for the NDVI and LST values for data extraction was generated, at the end of the process a spreadsheet was generated in .CSV of the monthly values of the VHI for the period from 2001 to 2018, resulting in 216 observations. Lower VHI indicates a high incidence of drought, while a higher value of VHI indicates wet or non-dry conditions (Kogan, 2002).

$$\text{VHI} = \alpha\text{VCI} + (1 - \alpha)\text{TCI} \tag{4}$$

2.5 Statistical Analysis

Through Boxplot statistics, the variables rain, land surface temperature, soil moisture, air temperature, NDVI, fire foci and VHI were characterized.

To better understand the degradation of vegetation throughout the series studied in the State of Amazonas as a function of biophysical attributes, was performed a Heatmap clustering based on the Euclidean distance. All processing was performed in software R version 3.5.1, through libraries (*shiny*, *heatmaply*, *ggplot2*, *plotly*, *plyr* and *shinyHeatmaply*) (R CORE TEAM, 2015).

To detect changes in the time series we use the nonparametric tests of Mann (1945), Kendall (1975) and Pettitt (1979), with a significance level of p = 0.05. The tests were performed using Kendall and TSA packages in software R. The years identified by the Pettitt test that showed significant results for all study variables were then shaved and spatialized in the dry and rainy season for a better analysis of the result. Spatialization of VHI was also performed in climatic months (JFM; AMJ; JAS and OND) for the year with the lowest averages.

2.6 Modeling - ARIMA

The Autoregressive Integrated Moving Average Model (ARIMA) was used to simulate the VHI data series. The ARIMA models have two general forms (p, d and q) and (P, D, Q) m, non-seasonal and seasonal respectively as shown in Eq. 5. The seasonal model I was used in this study where, AR (p) refers to the number of delay observations included in the model, also called the delay order in the regression equation for the Y series. I (d) refers to the number of times gross observations are differentiated, also called degree of differentiation, and MA (q) is the moving average terms, leads to the observation of previous errors.

$$Y_{t=c+\emptyset_1 y_d \ t-1+ \emptyset_p y_d \ t-p \ +\cdots+ \emptyset_1 e_{t-1} + \emptyset_q e_{t-q} + e_t} \tag{5}$$

where y (d) is Y differentiated d times, and c are constants, p is the autoregressive order, d is the differentiation order (1 or 2 typically) and q is the moving average order.

To validate the ARIMA modeling, a 10-year past data series with 120 samples was generated to predict the future. Thus, an estimated monthly series for the years 1991 to 2000 was used to validate the year 2001, for validation of the year 2002, the estimated series from the period 1991 to 2001 was used and validations continued until 2018. All processing was performed in software R version 3.5.1, through libraries (*MASS, tseries, forecast, readxl, raster, rgdal, maptools, RSAGA and ggplot2*) (R CORE TEAM, 2015). All validations were analyzed using the Standard Estimate Error (EPE), coefficient of determination (R^2) and Willmott's

agreement index (d) (Willmott et al., 1985). After the validations, the future simulation of the VHI was generated for the period from 2019 to 2030, totaling 12 years.

3. RESULTS

3.1 Fire Foci

Throughout the period analyzed from 2001 to 2018, the years with the highest occurrence of fire foci were 2005 and 2015 with 24,767 and 21,254, respectively. When analyzing the year 2005, the month of August presented the highest occurrence of fire foci with 9,722, February had the lowest value with only 25 fire foci. For 2015, September was characterized by the highest occurrence with 8,068 fire foci and May with only 13 fire foci represented the lowest value (Fig. 2).

The months from July to October are those with the highest occurrence of fire foci. Among these, the months of August and September have the highest values 86,138 and 83,303 respectively. The months from January to May recorded the lowest occurrences of fire foci. April and May had the lowest values with 468 and 525, respectively (Fig. 2).
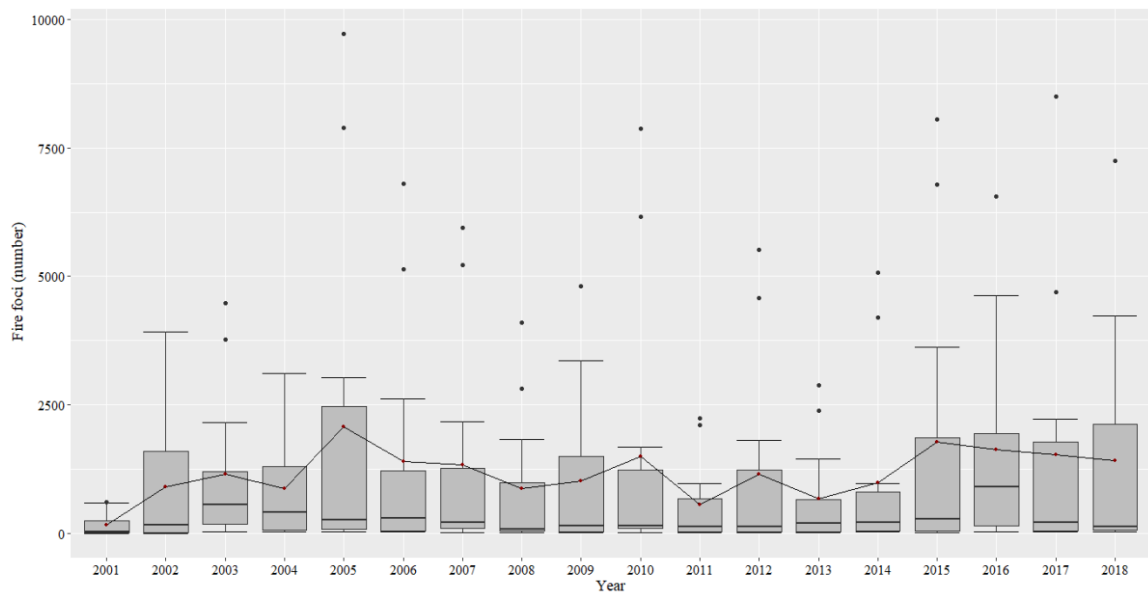
Fig. 2. Fire foci for the state of Amazonas from 2001 to 2018.

3.2 Reanalysis 2 (Surface Weather Data)

In general, the months with the highest amounts of water in the soil corresponded to the wettest months for the state. The month of April presented the highest average value with 589.96 mm of soil water and October the lowest average with 402.16 mm (Fig. 3). The period with the lowest amount of water in the soil from August to November had the highest number of fire foci.

Between December and May, the highest rainfall occurred and from June to November, the lowest. Among the months with the highest rainfall, March was the wettest with an average of 298.14 mm, while the month with the least rainfall for the eighteen years of study was August with an average of 90 mm (Fig. 3). Coincidentally, the months with the lowest rainfall were also those with the highest occurrence of fire foci in the state of Amazonas. The month of

August, for example, which had the lowest rainfall, had the highest occurrences of fire foci (86,138).

For all the years analyzed 2009 presented on average the highest rainfall with 220.07 mm and 2015 corresponded to the lowest average rainfall with 169.18 mm. During the study period, the years 2005, 2010 and 2015 represent three drought events (Fig. 3).

The highest air temperatures in the 18 years of study are distributed from August to November (Fig. 3). Among these, October had the highest temperatures with an average of 27.94ºC. This same period, with the highest temperatures recorded for the state, also presented the highest occurrences of fire foci. The lowest temperatures occurred from May to July, the latter being the month with the mildest temperatures with an average of 26.65ºC (Fig. 3).
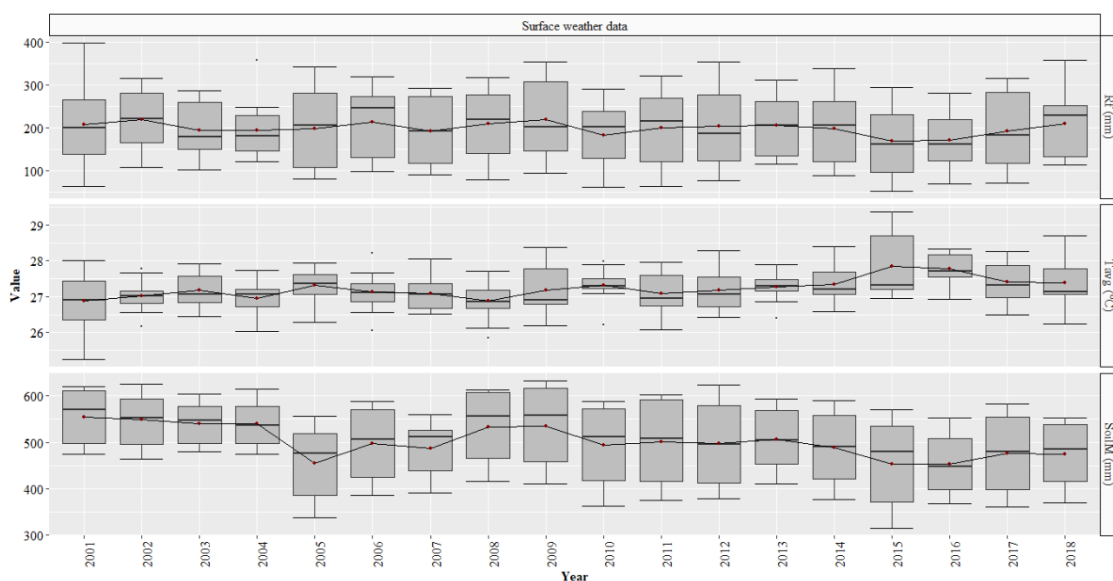
Fig. 3. Rainfall (Rf), average air temperature (Tavg) and soil moisture (SoilM) values for the state of Amazonas.

3.3 Remote Sensing Products

Land Surface Temperature (LST) also has its annual behavior similar to that of rainfall distribution for the state of Amazonas. For all months of the years studied, June recorded the lowest temperatures with an average of 26.72ºC and October the highest with an average of 29.50ºC (Fig. 4), the latter also had the lowest average water value in the soil. The year 2018 had the lowest temperatures, with an average of 27.64ºC (Fig. 4). The highest NDVI values are distributed between June and December, where July obtained the highest average NDVI value 0.83 (Fig. 4). For the lowest values that were recorded between January and May, January had the lowest mean value of NDVI 0.76 (Fig. 5). On average, the year with the highest NDVI was 2016 (0.82), 2001 was the lowest for the index 0.79 (Fig. 4).

The month of January presented the highest values of VHI among all the months analyzed with an average value of 57%, indicating good vegetation health. October, being the month with the lowest VHI values with an average of 21.94%, showed that the vegetation suffered droughts, influencing its condition (Fig. 4).

Overall, we see a drop in VHI values for the period considered dry in the Amazon. The year 2005 presented one of the lowest values of VHI, with an average of 39-70%. Even the average indicating mild drought can be seen that in some months of the year in question, such as October, a value of 21.04% indicating moderate drought was recorded.

In 2010, it also had low VHI values, with an average of 36.91%, indicating mild drought, not compromising the health of the vegetation. In 2014 there is the same scenario with an average VHI of 36.62%, showing the occurrence of a mild drought. But in some months, such as October and November, there was a severe drought, with VHI values of 19.61% and 17.59%, respectively (Fig. 4).
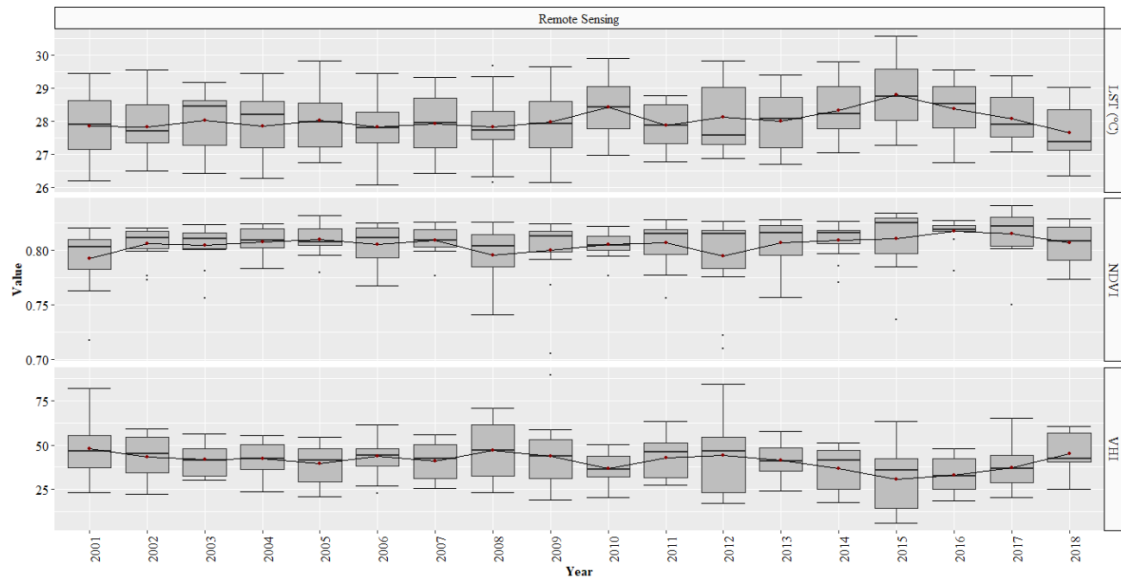
Fig. 4. Land Surface Temperature (LST), NDVI and VHI values for the state of Amazonas.

The months from January to July recorded the best vegetation conditions for the state within the analyzed period because of their higher average VHI values, but spatially analyzing in 2015, the low VHI values were concentrated southwest of the Amazon (Fig. 4 and 5).

The year 2015 recorded the lowest values of VHI for the entire study period, with an average of 30.73%, also placing it in the mild drought class. However, in some months, such as September to November, which presented VHI values of 8.42%, 6.08% and 9.47% respectively, it is possible to see the occurrence of extreme droughts in the southwestern region, mainly in the image and afterwards it spreading throughout the Amazon (Fig. 4 and 5).
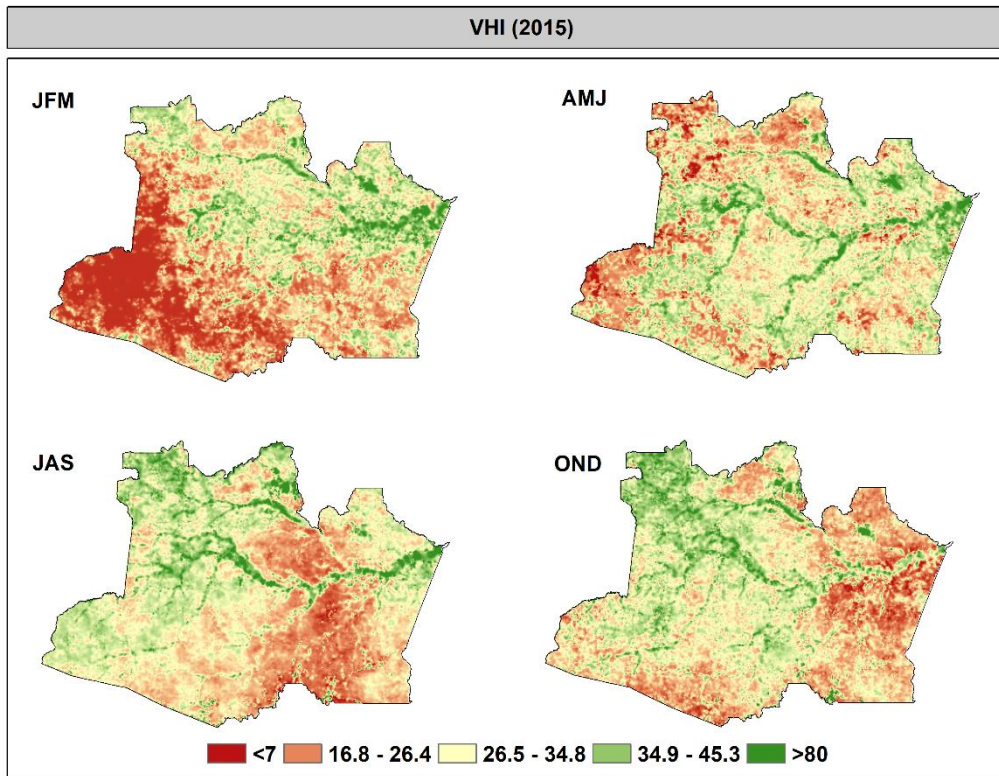
Fig. 5. Spatially VHI values for the quarters of the year 2015 (JFM = January, February and March; AMJ = April, May and June; JAS = July, August and September; OND = October, November and December) in the state of Amazonas.

3.4 Mann-Kendall, Pettitt and Cluster Analysis

Fire foci showed a positive trend in most months with significance, but also showed negative trends for the months from October to January (Table 1). Regarding VHI, every month except January showed a significant negative trend from May to September (Table 1). This result points to a reduction in vegetation health during this period. The LST also showed a positive trend according to the test, with significant values only for the months from May to July, being in those months when the region faces the considered period of drought, resulting in a higher surface temperature (Table 1).

Regarding rain the test showed a negative trend, but only the months of June and October were significant, both months of dry season in the region. A positive trend was shown by the temperature test with significant values for most months (Table 1).

For soil water, the test indicated a negative trend, with significant values for almost every month of the years (Table 1).

Table 1. Mann-Kendall trend analysis of all study variables for the State of Amazonas.

Month	Fire foci Z	Fire foci p-value	VHI Z	VHI p-value	NDVI Z	NDVI p-value	LST Z	LST p-value	Soil moisture Z	Soil moisture p-value	Rainfall Z	Rainfall p-value	Air temperature Z	Air temperature p-value
Jan	-0.04	0.85	0.29	*0.01	-0.16	0.36	0.05	0.82	-0.46	*0.01	0.02	0.94	-0.01	1.00
Feb	0.15	0.40	-0.27	0.13	0.29	*0.01	0.15	0.40	-0.26	0.15	-0.05	0.82	0.14	0.45
Mar	0.38	*0.03	-0.16	0.36	0.32	0.07	0.09	0.65	-0.28	0.11	-0.14	0.45	0.36	*0.04
Apr	-0.01	1.00	-0.09	0.65	0.03	0.88	0.09	0.65	-0.44	*0.01	-0.14	0.45	0.31	0.08

Month	Z	p	Z	p	Z	p	Z	p	Z	p	Z	p	Z	p
May	0.23	0.20	-0.44	*0.01	0.28	0.11	0.36	*0.04	-0.50	*0.00	-0.24	0.17	0.40	*0.02
Jun	0.35	*0.05	-0.43	*0.01	0.33	*0.05	0.41	*0.02	-0.58	*0.00	-0.33	*0.05	0.37	*0.03
Jul	0.16	0.36	-0.50	*0.00	0.48	*0.01	0.53	*0.00	-0.54	*0.00	-0.19	0.29	0.37	*0.03
Aug	0.29	*0.01	-0.29	*0.01	0.41	*0.02	0.27	0.13	-0.44	*0.01	-0.11	0.54	0.26	0.15
Sep	0.22	0.23	-0.29	*0.01	0.50	*0.00	0.22	0.23	-0.39	*0.02	-0.15	0.40	0.50	*0.00
Oct	-0.05	0.82	-0.26	0.15	0.52	*0.00	-0.02	0.94	-0.54	*0.00	-0.33	*0.05	0.27	0.13
Nov	-0.20	0.26	-0.10	0.60	0.16	0.36	0.10	0.60	-0.56	*0.00	0.09	0.65	0.24	0.17
Dec	-0.05	0.82	-0.10	0.60	0.29	*0.01	0.02	0.94	-0.63	*0.00	-0.07	0.70	0.19	0.29

Z = Mann-Kendall test statistical analysis. p-value = *statistically significant trend.

For the variable soil moisture, 2013 showed a significant result for the period considered rainy (Table 2 and Fig. 6). For the dry season 2004 was the year with a p-value below 0.05 (Table 2 and Fig. 6).

Table 2. Pettitt trend analysis of all study variables for the State of Amazonas.

Variable	Rainy		Dry	
	Year	p-value	Ano	p-value
Rainfall	2009	0.39	2009	0.14
Soil moisture	2013	*0.03	2004	*0.05
Fire	2009	0.49	2014	0.15
LST	2012	0.57	2008	0.02
NDVI	2013	0.12	2012	*0.05
Air temperature	2012	0.06	2009	*0.01
VHI	2013	0.26	2009	*0.01

p-value = statistically significant trend*
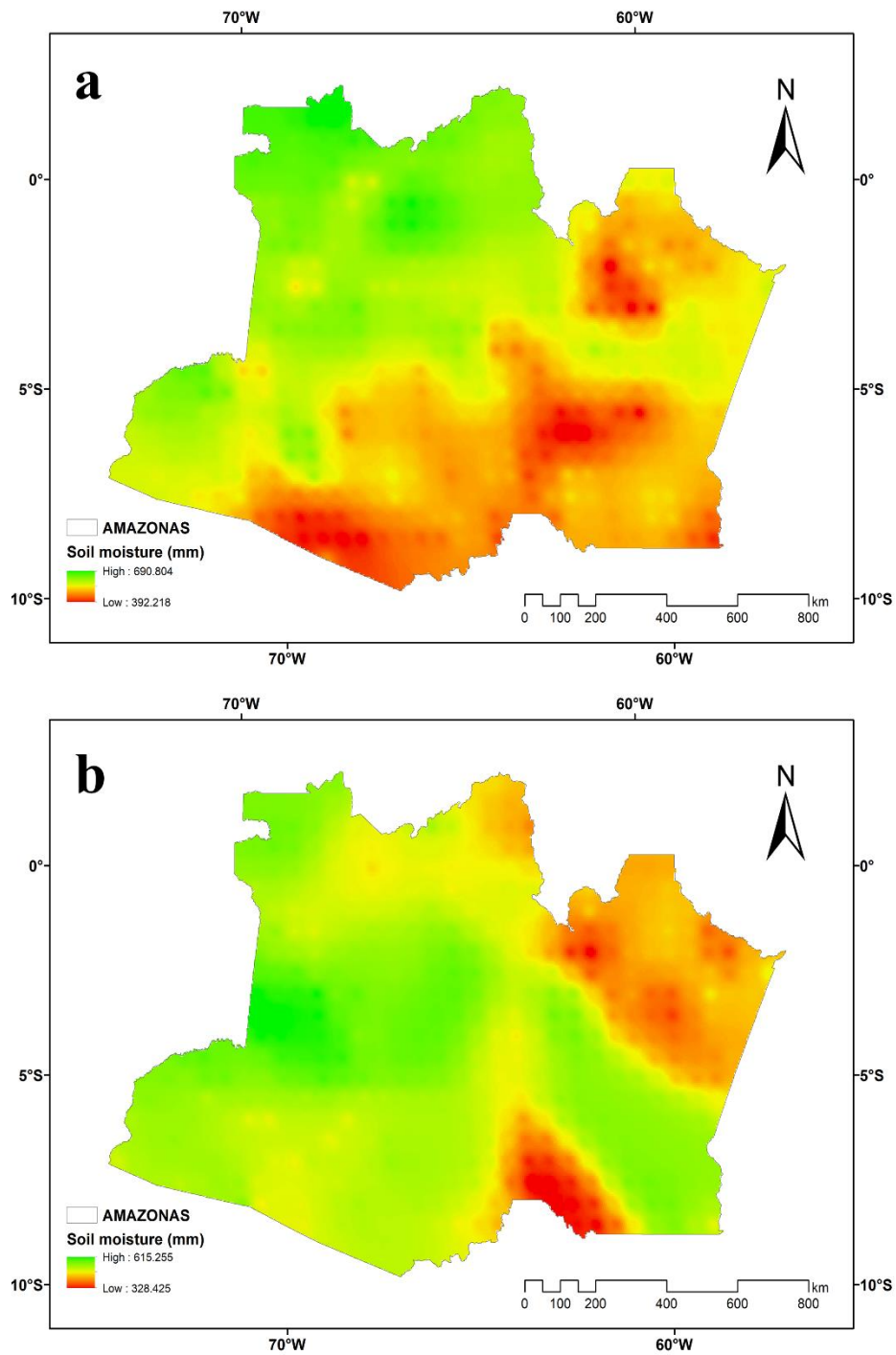
Fig. 6. Soil moisture (mm) values for the dry season in 2004 (a) and rainy season in 2013 (b) in the Amazon.

The drought period of 2009 was also shown by the test as a year where there was a significant change in the temperature of the State of Amazonas (Table 2 and Fig. 7).
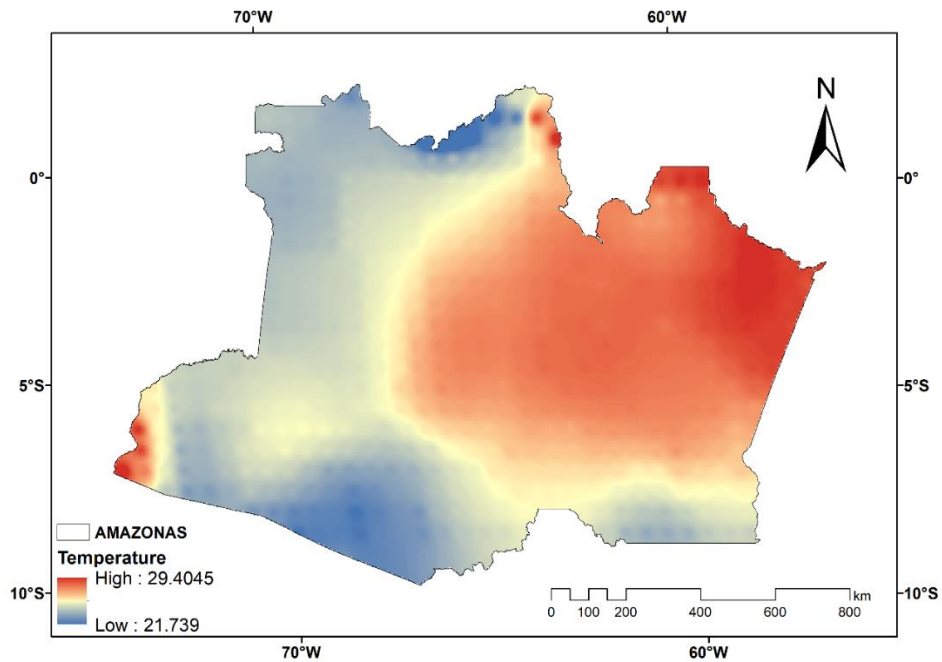
Fig. 7. Average air temperature (℃) values in the year 2009, for the dry season of the region.

The NDVI and VHI variables showed a significant change only for the dry period, for the years 2012 and 2009 respectively (Table 2).

Among all variables analyzed, VHI and air temperature were the most significant for the region within the analyzed period (Fig. 8). It can be noted from the heatmap that rain and VHI correlate positively and both correlate negatively with LST, indicating that the higher the values of VHI and rainfall, the lower the LST values.

It is also seen that fire and temperature correlate negatively with water in the soil, showing that the lower the temperatures and the more water in the soil, the trees tend to be greener and less dry, considerably reducing the combustible material from the fire (Fig. 8).
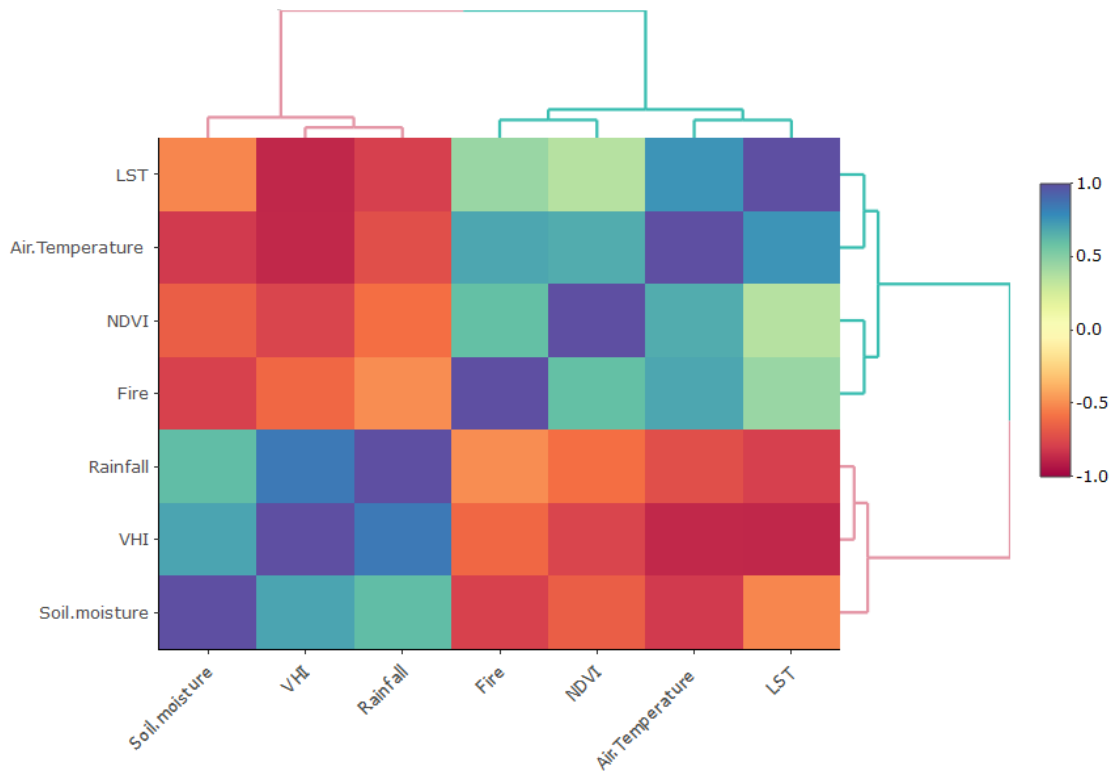
Fig. 8. Heatmap clustering based on the Euclidean distance.

By analyzing the observed data and the prediction (Fig. 9), it can be seen that the model simulated the VHI series well, presenting an average of Willmott's coefficient (d) of approximately 1 for the study period, showing the model's capacity in satisfactorily express the condition of the vegetation.

It is noticeable that for 2010 the data are more grouped and closer to the line; this year presented the highest R^2 (0.90) in the series and a coefficient d = 1. The year 2016 had the worst correlation showing an R^2 of 0.11 and a coefficient d = 1. For the whole series studied (2001 to 2018) the standard error of the estimate (EPE) was considered high with an average value of 7.36%.
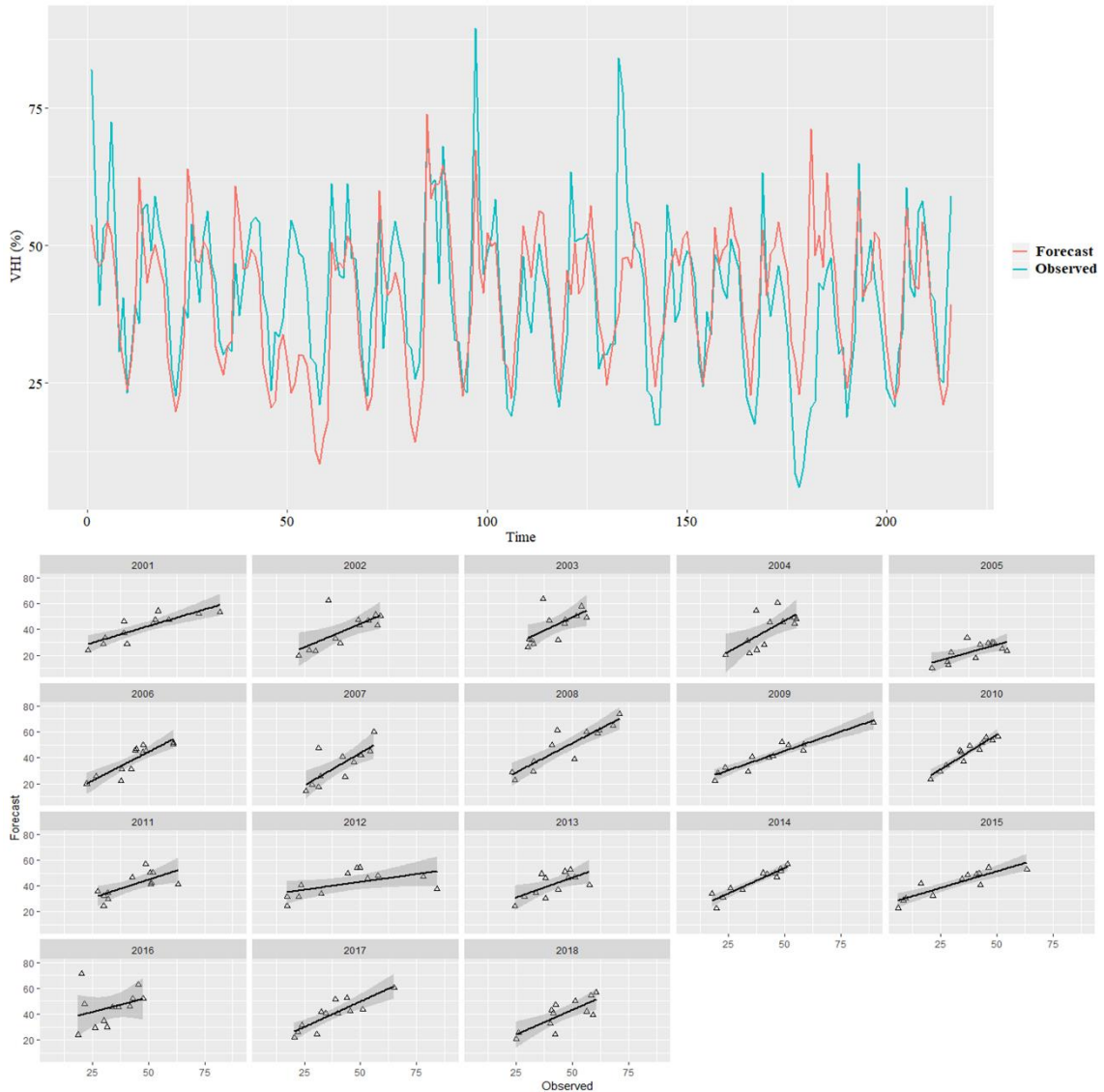
Fig. 9. Observed and predicted VHI temporal behavior (blue and red lines) and below the regression analysis for the study period.

As observed in Fig. 10, the estimated ARIMA model was able to represent the seasonality of the future period. It is remarkable a drop in the value of VHI in the dry period and an increase in the variable in the rainy season of the region.

17
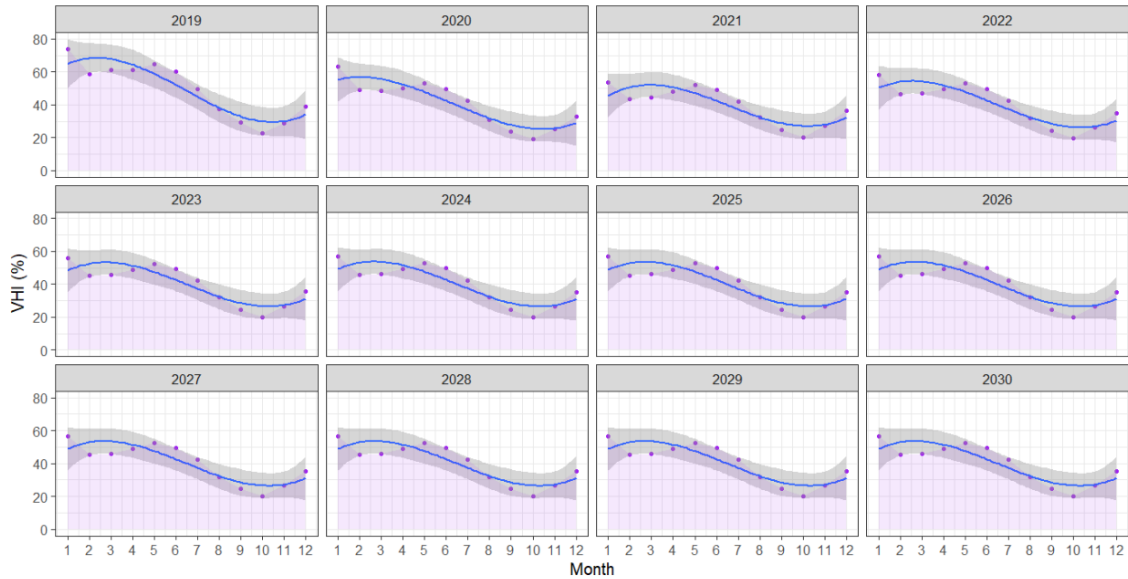
Fig. 10. Future simulation of VHI for the state of Amazonas.

4 DISCUSSION

4.1 Fire Foci and Weather Data

This result can be explained by the fact that in 2005 the Amazon suffered an intense drought caused by warmer water in the North Atlantic and in 2015 was the occurrence of the El Niño phenomenon (Samanta et al., 2010; Jiménez-Muñoz, 2016; Barbosa et al., 2018).

Alencar et al. (2015) in their work for the Amazon, report that in dense forests there is a high susceptibility to fires in years of severe drought caused by El Niño. Asner and Alencar (2010) showed in their Amazon study that the 2005 drought resulted in a 33% increase in fire foci. These studies corroborate the results found in this work, which could be seen, in drought years 2005 and 2015, an aggravating occurrence of fires in tropical forests in the state of Amazonas.

These events, among others occurring in the Amazon, result in severe droughts causing a decrease in rainfall, reduced carbon storage, yield sensitivity of younger trees and plant mortality (Brando et al., 2010; Espinoza et al., 2011; Doughty et al., 2015; Barbosa et al., 2018; Giardina et al., 2018).

4.2 Remote Sensing

The year with the highest temperatures was 2015 recording an average of 28.80ºC, a possible explanation for this is the occurrence of the El Niño phenomenon that occurred this year, which usually causes an increase in temperatures and a reduction in rainfall in the Amazon region (Tedeschi, Grimm, Cavalcanti, 2015; Panisset et al., 2018).

The highest NDVI values were concentrated in the dry season considered for the state of Amazonas. This result may indicate that NDVI in this region is more influenced by solar irradiance than rainfall (Wagner et al., 2017).

Samanta et al. (2010) report in their work that the Amazon rainforest as well as other rainforests record waves of young leaf growth and higher dry season photosynthesis coinciding with the solar irradiance peaks.

18

Parviz (2016) points out that VHI has shown satisfactory results in various parts of the globe when it is used for drought detection, vegetation condition assessment or climate impact assessment. Lee et al. (2013) observed a reduction in productivity of the Amazon ecosystem by 15% during the 2010 dry season drought.

The good health of the vegetation in some years due to the average values of VHI above 40% can be explained by the fact that the Amazonia rainforests have a large extension of the root system, allowing them to capture water in deep areas. Along with this advantage, the closed canopy of the forest and abundant litter makes it difficult for sunlight to enter and allows the soil to keep its moisture longer (Kim et al., 2012).

Bonal et al. (2016) report that when water in the topsoil becomes limited, deep roots can provide water to trees, thereby preventing or delaying the effects of drought on the forest.

Giardina et al. (2018) found that taller, older and denser Amazon forests are more resistant to rainfall variability and maintain their growth during drought due to their deeper rooting.

Guan et al. (2015) state that above an annual rainfall threshold of approximately 2,000 mm yr-1, healthy state is sustained during the dry season in tropical forests worldwide.

4.3 Statistical Analysis and ARIMA Modeling

The NDVI variable showed a positive trend, with significant values mainly in the dry months considered for the region. As previously mentioned in Figure 5, in tropical forests in the dry months there is a record of leaf growth waves and higher photosynthesis, coinciding with solar irradiance peaks (Samanta et al., 2010).

The trends presented by the test when associated with extreme events such as El Nino can reverse forest roles, instead of being sinks they can become carbon sources, for example the mortality of younger, less drought-resistant forests (Giardina et al., 2018). Yang et al. (2018) reports that the Amazonia becomes a net source of carbon in El Nino years.

This result may be associated with the extreme rain event observed in 2009, which softened the region's temperatures (Marengo et al., 2013).

Panisset et al. (2018) reported that increased temperatures may induce increased evapotranspiration in tropical regions, reducing the amount of soil moisture.

Fashae et al. (2019) showed in their study that the ARIMA model modeled with great performance the flow of the Opeki river for the period from 2010 to 2020. Han et al. (2010) demonstrated in their work, through their results, that the ARIMA model can be used for drought prediction.

Machekposhti et al. (2017) in their study for Karkheh River compared the observed and estimated ARIMA series of floods through R^2 and found that the model was suitable for river flood analysis and short-term forecasting of the series in the future.

As the VHI that corresponds to vegetation health is influenced by seasonal climate variables, the generated and validated model can be used to indicate the future condition of vegetation health. Rahman, Yunsheng and Sultana (2017) emphasize the ability of the ARIMA model to detect seasonal changes in time series.

4.4 Importance Of This Study For Future Generations

This study provides practical information for the Brazilian government to adopt future preservation measures for the Brazilian Amazon. Observed data on meteorological variables, fire and VHI present patterns found in recent studies published in the Amazon by other researchers, such as the occurrence of recent extreme drought events in the Amazon (2005, 2010 and 2015). Faced with climate change, extreme drought weather conditions estimated by the VHI condition may represent social, economic and environmental impacts in the state of

Amazonas in the future. Policy and enforcement could play a decisive role in the region's fires, especially in recurring years in El Niño and La Niña, for example.

5 CONCLUSION

The average values of VHI presented mild drought condition for most years, when analyzed the dry period, the index showed severe droughts in the region. The index proved to be a strong tool in detecting vegetation health.

The ARIMA model applied to the VHI series from 2001 to 2018 was able to satisfactorily express the vegetation condition for the period, showing its ability to predict the future of the VHI time series. The Mann-Kendall detailed analysis for VHI shows a negative trend in vegetation health for the Amazonia.

The reduction in vegetation health shown in this paper further emphasizes the concern we should have with our forests and the importance of public policies addressing this problem. Despite significant advances over the past decade with government-implemented projects, there is still a lack of commitment to environmental policies, which is disapproved of by countries that fund preservation projects, and this displaces important financial resources for the preservation of the Amazonia.

7 REFERENCES

Aleixo, I., Norris, D., Hemerik, L., Barbosa, A., Prata, E., Costa, F., Poorter, L., 2019. Amazonian rainforest tree mortality driven by climate and functional traits. Nature Climate Change, 9:384. https://doi.org/10.1038/s41558-019-0458-0.

Alvares, C.A., Stape, J.L., Sentelhas, P.C., Gonçalves, J.L.M., Sparovek, G. 2013. Koppen's climate classification map for Brazil. Meteorologische Zeitschrift, 22:711–728. https:// doi.10.1127/0941-2948/2013/0507.

Aquino, R.E., Campos, M.C.C., Júnior, J.M., Oliveira, I.A., Mantovaneli, B.C., Soares, M.D.R., 2014. Geoestatística na avaliação dos atributos físicos em latossolo sob floresta nativa e pastagem na região de Manicoré, Amazonas. Rev. Bras. Ciênc. Solo, 38:397 – 406. https://doi.org/10.1590/S0100-06832014000200004.

Alencar, A.A., Brando, P.M., Asner, G.P., Putz, F.E. 2015. Landscape fragmentation, severe drought, and the new Amazon forest fire regime. Ecological applications, 25(6):1493-1505. https://doi.org/10.1890/14-1528.1.

Asner, G.P., Alencar, A., 2010. Drought impacts on the Amazon forest: the remote sensing perspective. New Phytologist 187:569–578. https://doi.org/10.1111/j.1469-8137.2010.03310.

Barbosa, M.L.F., Delgado, R.C., Teodoro, P.E., Pereira, M.G., Correia, T.P., de Mendonça, B.A.F., de Ávila Rodrigues, R., 2018. Occurrence of fire foci under diferente land uses in the State of Amazonas during the 2005 drought. Env. Deve. and Sust, 1-14. https://doi.org/10.1007/s1066.

Bento, V.A., Gouveia, C.M., Da Camara, C.C., Trigo, I.F., 2018. A climatological assessment of drought impact on vegetation health index. Agricultural and Forest Meteorology, 259:286-295. https://doi.org/10.1016/j.agrformet.2018.05.014.

Bonal, D., Burban, B., Stahl, C., Wagner, F., Hérault, B., 2016. The response of tropical rainforests to drought—lessons from recent research and future prospects. Ann. For. Sci 73:27–44. https://doi.org/10.1007/s1359.

Box, G.E.P., Jenkins, G.M., 1976. Time Series Analysis: Forecasting and Control. Holden-Day, San Francisco, 525.

Brando. P.M., Goetz, S.J., Baccini, A., Nepstad, D.C., Beck, P.S.A., Christman, M.C., 2010. Seasonal and interannual variability of climate and vegetation indices across the Amazon. Proc. Natl Acad. Sci. EUA, 107:14685–14690. https://doi.org/10.1073/pnas.0908741107.

Chagas, M.C., Delgado, R.C., de Souza, L.P., de Carvalho, D.C., Pereira, M.G., Teodoro, P.E., Junior, C.A.S., 2019. Gross primary productivity in areas of different land cover in the western Brazilian Amazon. Remote Sensing Applications: Society and Environment, 100259. https://doi.org/10.1016/j.rsase.2019.100259.

Das, L., Dutta, M., Mezghani, A., Benestad, R.E., 2017. Use of observed temperature statistics in ranking CMIP5 model performance over the Western Himalayan Region of India. International Journal of Climatology, 38:554–570. https://doi.org/10.1002/joc.5193.

Delgado, R.C., Pereira, M.G., Teodoro, P.E., dos Santos, G.L., de Carvalho, D.C., Magistrali, I.C., Vilanova, R., 2018. Seasonality of gross primary production in the Atlantic Forest of Brazil. Global Ecology and Conservation, 14:1-12. https://doi.org/10.1016/j.gecco.2018.e00392.

da Silva Júnior, L.A.S., Delgado, R.C., Pereira, M.G., Teodoro, P.E., da Silva Junior, C.A., 2019. Fire dynamics in extreme climatic events in western amazon. Environmental Development, https://doi.org/10.1016/j.envdev.2019.06.005.

Doughty, C.E., Metcalfe, D.B., Girardin, C.A., Amézquita, F.F., Cabrera, D.G., Huasco, W.H., Silva-Espejo, J.E., Araujo-Murakami, A., da Costa, M.C., Rocha, W., Feldpausch, T.R., Mendoza, A.L.M., da Costa, A.C.L., Meir, P., Phillips, O.L., Malhi, Y., 2015. Drought impact on forest carbon dynamics and fluxes in Amazonia. Nature, 519:78–82. https://doi.org/10.1038/nature14213.

de Andrade, C.F., Duarte, J.B., Barbosa, M.L.F., de Andrade, M.D., de Oliveira, R.O., Delgado, R.C., Teodoro, P.E., 2019. Fire outbreaks in extreme climate years in the State of Rio de Janeiro, Brazil. Land Degradation & Development, 30(11):1379-1389. https://doi.org/10.1002/ldr.3327.

Espinoza, J.C., Ronchail, J., Guyot, J.L., Junquas, C., Vauchel, P., Lavado, W., Drapeau, G., Pombosa, R., 2011. Climate variability and extreme drought in the upper Solimões River (western Amazon Basin): Understanding the exceptional 2010 drought. Geophys. Res. Lett, 38:1– 6. https://doi.org/10.1029/2011GL047862.

Fashae, A., Olusola, A.O., Ndubuisi, I., Udomboso, C.U., 2019. Comparing ANN and ARIMA model in predicting the dischargeof River Opeki from 2010 to 2020 Olutoyin. River Res. Applic, 35:169–177. https://doi.org/10.1002/rra.3391.

Funatsu, B.M., Dubreuil, V., Racapé, A., Debortoli, N.S., Nasuti, S., Le Tourneau, F.M., 2019. Perceptions of climate and climate change by Amazonian communities. Global Environmental Change, 57:101923. https://doi.org/10.1016/j.gloenvcha.2019.05.007.

Giardina, F., Konings, A.G., Kennedy, D., Alemohammad, S.H., Oliveira, R.S., Uriarte, M., Gentine, P., 2018. Tall Amazonian forests are less sensitive to rainfall variability. Nature Geoscience, 11:405–409. https://doi.org/10.1038/s41561-018-0133-5.

Gidey, E., Dikinya, O., Segosebe, S.R.E., Zenebe, A., 2018. Analysis of the long-term agricultural drought onset, cessation, duration, frequency, severity and spatial extent using Vegetation Health Index (VHI) in Raya and its environs, Northern Ethiopia. Environ. Syst. Res, 7:1-18. https://doi.org/10.1186/s40068-018-0115.

Gomes, A.C.C., Bernardo, N., Alcântara, E., 2017. Accessing the southeastern Brazil 2014 drought severity on the vegetation health by satellite image. Journal of Natural Hazards, 89:1401–1420. https://doi.org/10.1007/s11069-017-3029-6.

Guan, K., Pan, M., Li, H., Wolf, A., Wu, J., Medvigy, D., Caylor, K.K., Sheffield, J., Wood, E.F., Malhi, Y., Liang, M., Kimball, J.S., Saleska, S.R., Berry, J., Joiner, J., Lyapustin, A.I., 2015. Photosynthetic seasonality of global tropical forests constrained by hydroclimate. Nature Geoscience, 8:284–289. https://doi.org/10.1038/ngeo2382.

Han, P., Wang, P.X., Zhang, S.Y., Zhub, H., 2010. Drought forecasting based on the remote sensing data using ARIMA models. Mathe. and Compu. Mode, 51:1398-1403. https://doi.org/10.1016/j.mcm.2009.10.031.

Instituto Brasileiro de Geografia e Estatística - IBGE. 2017. Estados. <http://www.ibge.gov.br/estadosat/perfil.php?sigla=am>. Access in: January 15, 2019.

Instituto Brasileiro de Geografia e Estatística - IBGE. 2012. Manual técnico da vegetação brasileira: sistema fitogeográfico, inventário das formações florestais e campestres, técnicas e manejo de coleções botânicas, procedimentos para mapeamentos. Rio de janeiro: IBGE- Diretoria de Geociências. < https://biblioteca.ibge.gov.br/visualizacao/livros/liv63011.pdf>. Access in: January 15, 2019.

Jiménez-Muñoz, J.C., Mattar, C., Barichivich, J., Santamaría-Artigas, A., Takahashi, K., Malhi, Y., Sobrino, J.A., Schrier, G.V.D., 2016. Record-breaking warming and extreme drought in the Amazon rainforest during the course of El Niño 2015–2016. Scientific Reports, 6:1-7. https://doi.org/10.1038/srep33130.

Kanamitsu, M., Ebisuzaki, W., Woollen, J., Yang, S.K., Hnilo, J.J., Fiorino, M., Potter, G.L., 2002. NCEP–DOE AMIP-II REANALYSIS (R-2). Bulletin of the American Meteorological Society, 83:1631-1644. https://doi.org/10.1175/BAMS-83-11-1631.

Kendall, M.G., 1975. Rank correlation Methods. London: Charles Griffin.

Kim, Y., knox, R.G., Longo, M., Medvigy, D., Hutyrak, L.R., Pyle, E.H., Wofsy, S., Bras, R.L., Moorcroft, P.R., 2012. Seasonal carbon dynamics and water fluxes in an Amazonrainforest. Global Change Biology, 18:1322–1334. https://doi.org/10.1111/j.1365-2486.2011.02629.

Kogan, F.N., 2001. Operational space technology for global vegetation assessment. Bulletin of the American Meteorological Society, 82:1949–1964. https://doi.org/10.1175/1520-0477.

Kogan, F.N., 2002. World droughts in the new millennium from AVHRR-based vegetation health indices. EOS Trans. Am. Geophys. Union, 83:562–563. https://doi.org/10.1029/2002EO000382.

Kogan, F.N., 1990. Remote sensing of weather impacts on vegetation in non-homogeneous areas. Int. J. Remote Sens, 11:1405-1419. https://doi.org/10.1080/01431169008955102.

Kogan, F.N., 1995. Application of vegetation index and brightness temperature for drought detection. Adv. Space Res 15:91-100. https://doi.org/10.1016/0273-1177(95)00079

Kogan, F.N., 1997. Global drought watch from space. Bull. of the Am. Meteorol. Soc 78:621-636. https://doi.org/10.1175/1520-0477.

Kruhlov, I., Thom, D., Chaskovskyy, O., Keeton, W.S., Scheller, R.M., 2018. Future forest landscapes of the Carpathians: vegetation and carbon dynamics under climate change. Regional Environmental Change, 18:1555-1567. https://doi.org/10.1007/s10113-018-1296-8.

Kundu, A., Dwivedi, S., Dutta, D., 2016. Monitoring the vegetation health over India during contrasting monsoon years using satellite remote sensing indices. Arab. J. Geosci, 9:1-15. https://doi.org/10.1007/s12517-015-2185-9.

Lee, J.E., Frankenberg, C., van der Tol, C., Berry, J.A., L, Guanter., Boyce, C.K., Fisher, J.B., Morrow, E., Worden, J.R., Asefi, S., Badgley, G., Saatchi, S., 2013. Forest productivity

and water stress in Amazonia: Observations from GOSAT chlorophyll fluorescence. Proceedings of the Royal Society B, 280:1-9. https://doi.org/10.1098/rspb.2013.0171.

Lopes, M.O., Peralta, D.F., Carmo, D.M.D., Silva, M.R.P.D., 2016. Estudo comparativo de comunidades de briófitas sujeitas a diferentes graus de inundação no município de São Domingos do Capim, PA, Brasil. Hoehnea, 43:159–171. http://dx.doi.org/10.1590/2236-8906-54/2015.

Lucas, E.W.M., Sousa, F.A.S., Silva, F.D.S., Lucio, P.S., 2009. Modelagem hidrológica determinística e estocástica aplicada à região hidrográfica do Xingu – Pará. Revista Brasileira de Meteorologia, 24:308-322. http://dx.doi.org/10.1590/S0102-77862009000300005.

Marengo, J.A., Borma, L.S., Rodriguez, D.A., Pinho, P., Soares, W.R., Alves, L.M., 2013. Recent extremes of drought and flooding in Amazonia: vulnerabilities and human adaptation. American J. of Climate Change, 2:87-96. https://doi.10.4236/ajcc.2013.22009.

Machekposhti, K.H., Sedghi, H., Telvari, A., Babazadeh, H., 2017. Flood Analysis in Karkheh River Basin using Stochastic Model. Civil Engi. J, 3:794-808. https://doi.10.21859/cej-030915.

Mann, H.B., 1945. Non-parametric tests against trend. Econometrica 13:245-259. https://doi.10.2307/1907187.

Nanzad, L., Zhang, J., Tuvdendorj, B., Nabil, M., Zhang, S., Ba, Y., 2019. NDVI anomaly for drought monitoring and its correlation with climate factors over Mongolia from 2000 to 2016. J. of Arid Environments, 164:69-77. https://doi.org/10.1016/j.jaridenv.2019.01.019.

Panisset, J.S., Libonati, R., Gouveia, C.M., Machado-Silva, F., França, D.A., França, J.R., Peres, L.F., 2018. Contrasting patterns of the extreme drought episodes of 2005,2010 and 2015 in the Amazon Basin. International J. of Climatology, 38:1096–1104. https://doi.org/10.1002/joc.5224.

Parviz, L., 2016. Determination of effective indices in the drought monitoring through analysis of satellite images. Agric. Forest, 62:305–324. https://doi.10.17707/AgricultForest.62.1.34.

Patrick, D.K., Edmond, P.P., Jean-Marie, T.M., Louis, E.E., Ngbolua, K., te, N., 2014 Prediction of rainfall using autoregressive integrated moving average model: Case of Kinshasa city (Democratic Republic of the Congo), from the period of 1970 to 2009. Journal of computation in biosciences and engineering, 2:2348 – 7321. https://doi.10.15297/JCLS.V2I1.1.

Pei, F., Wu, C., Liu, X., Li, X., Yang, K., Zhou, Y., Wang, K., Xu, L., Xia, G., 2018 Monitoring the vegetation activity in China using vegetation health indices. Agri. and Forest Meteorology, 248:215–227. https://doi.org/10.1016/j.agrformet.2017.10.001.

Pettitt, A.N.A., 1979. Non-parametric approach to the change-point problem. Applied Statistics 28:126-135. https://www.jstor.org/stable/2346729.

Piao, S., Nan, H., Huntingford, C., Ciais, P., Friedlingstein, P., Sitch, S., Peng, S., Ahlström, A., Canadell, J.G., Cong, N., Levis, S., Levy, P.E., Liu, L., Lomas, M.R., Mao, J., Myneni, R.B., Poulter, B., 2014. Evidence for a weakening relationship between interannual temperature variability and northern vegetation activity. Nature Communications, 5:1-7. https://doi.org/10.1038/ncomms6018.

Rahman, M.A., Yunsheng, L., Sultana, N., 2017. Analysis and prediction of rainfall trends over Bangladesh using Mann–Kendall, Spearman's rho tests and ARIMA model. Meteorol. Atmos. Phys, 129:409–424. https://doi.org/10.1007/s00703-016-0479-4.

Rouse, J.W., Haas, H.R., Schell, J.A., Deering, D.W., 1974. Monitoring vegetation systems in the great plain with ERTS. In: Earth Resources Technology Satellite Symposium. Proceedings. Washington, 1:309-317.

Ruffault, J., Moron, V., Trigo, R.M., Curt, T., 2016. Daily synoptic conditions associated with large fire occurrence in Mediterranean France: evidence for a wind-driven fire regime. Inter. J. of Climatology, 37:524–533. https://doi.org/10.1002/joc.4680.

Samanta, A., Ganguly, S., Hashimoto, H., Devadiga, S., Vermote, E., Knyazikhin, Y., Nemani, R.R., Myneni, R.B., 2010. Amazon forests did not green-up during the 2005 drought. Geophy. research letters, 37:1-5. https://doi:10.1029/2009gl042154.

Stuecker, M.F., Timmermann, A., Jin, F.F., Chikamoto, Y., Zhang, W., Wittenberg, A.T., Widiasih, E., Zhao, S., 2017. Revisiting ENSO/Indian Ocean dipole phase relationships. Geophys. Res. Lett, 44:2481–92. https://doi.org/10.1002/2016GL072308.

Tedeschi, R.G., Grimm, A.M., Cavalcanti, I.F.A., 2015. Influence of Central and East ENSO on extreme events of rainfall in South America during austral spring and summer. Int. J. Climatol, 36:4797– 4814. https://doi.org/10.1002/joc.4106.

Tran, H.T., Campbell, J.B., Tran, T.D., Tran, H.T., 2017. Monitoring drought vulnerability using multispectral indices observed from sequential remote sensing (Case Study: Tuy Phong, Binh Thuan, Vietnam). GIScience & Remote Sensing, 54:167–184. https://doi.10.1080/15481603.2017.1287838.

Valipour, M., 2013. Use of surface water supply index to assess-ing of water resources management in Colorado and Oregon. US. Adv. Agric. Sci. Eng. Res, 3:631–640. https://doi.10.5707/aaser.v3i2.247.

Valipour, M., 2015. Long-term runoff study using SARIMA and ARIMA. modelsin the United States. Meteo. Applications, 22:592–598. https://doi.10.1002/met.1491.

Wagner, F.H., Hérault, B., Rossi, Hilker, V.T., Maeda, E.E., Sanchez, A., Lyapustin, A.I., Galvão, L.S., Wang, Aragão, Y.L.E.O.C., 2017. Climate drivers of the Amazon forest greening. PLoS ONE, 12:1-15. https://doi.org/10.1371/journal.pone.0180932.

Wang, H., Lin, H., Liu, D., 2014. Remotely sensed drought index and its responses to meteorological drought in Southwest China. Remote sensing letters, 5:413–422.

Willmott, C.J., Ckleson, S.G., Davis, R.E., 1985. Statistics for the evaluation and comparison of models. Journal of Geophysical Research, 90:8995-9005. https://doi.org/10.1029/JC090iC05p08995.

Yang, J., Tian, H., Pan, S., Chen, G., Zhang, B., Dangal, S., 2018. Amazon droughts and forest responses: largely reduced forest photosynthesis but slightly increased canopy greenness during the extreme drought of 2015/2016. Glob. Change Biol, 24:1919-1934. https://doi.org/10.1111/gcb.14056.

CAPÍTULO II

VEGETATION DEGRADATION IN ENSO EVENTS: DROUGHT ASSESSMENT, SOIL USE AND VEGETATION EVAPOTRANSPIRATION IN THE WESTERN BRAZILIAN AMAZON

RESUMO

A degradação da floresta Amazônica tem sido palco de estudos nos últimos anos a nível global, na tentativa de identificar elementos e fatores que influenciam neste processo. Assim, este estudo teve como objetivo geral estudar a degradação da vegetação em ano de eventos do fenômeno El Niño Oscilação Sul (ENSO) no estado do Amazonas. Foram utilizados dados de sensoriamento remoto, tipologias florestais e elementos meteorológicos de 14 estações convencionais localizadas do estado do Amazonas. Os dados das estações meteorológicas serviram para estimar a evapotranspiração de referência para 7 métodos empíricos de evapotranspiração. O método padrão FAO-56 foi utilizado como comparativo para os métodos empíricos e o método derivado do sensoriamento remoto. The Standardised Precipitation-Evapotranspiration Index foi utilizado para verificar a intensidade da seca no período observado. Os resultados evidenciam diferenças nas correlações entre os métodos de evapotranspiração utilizados. A maior evapotranspiração foi encontrada na floresta ombrófila aberta. Os focos de calor concentraram-se em áreas de floresta ombrófila densa. O The Standardised Precipitation-Evapotranspiration Index (SPEI) mostrou ser um indice eficiente para caracterização da seca em anos de eventos do El Niño, além de evidenciar a expansão agrícola na região. As maiores tendências dos elementos meteorológicos e do SPEI foram durante o fenômeno El Niño. Uma melhor compreensão dos efeitos do fenômeno ENSO sobre a vegetação poderia evitar a perda de floresta descontrolada. Intervenções de governança, envolvendo atores nacionais e financeiro, bem como populações locais, também tem seu papel nisso.

Palavras-chave: evapotranspiração, Amazônia Legal, mudança climática, clima, índice de seca.

ABSTRACT

In recent years, the degradation of the Amazon forest has been the target of studies at the global level to identify elements and factors influencing this process. Thus, this study had as objective to study the vegetation degradation during the years of El Niño Southern Oscillation (ENSO) phenomenon in the State of Amazonas. We used remote sensing data, forest typologies, and weather elements from 14 conventional stations located in Amazonas. Evapotranspiration images obtained from the MODIS Global Evapotranspiration Project (MOD16A2), and data from fire sources from the Terra and Aqua collection (MOD146) platforms were used. The 6 different forms of forest typologies found in the region were also used, in addition to the climatic elements maximum, minimum temperature, relative humidity, sunshine and wind speed of 14 conventional stations in the state of Amazonas. The weather station data were used to estimate the reference evapotranspiration, using the empirical methods Val-1, Val-2, Val-3, Val-4, Irmak-1, Irmak-2 and Alex. The results show differences in the correlations between the evapotranspiration methods used. The highest evapotranspiration was found in the Open Ombrophilous Forest. Fire foci were concentrated in Dense Ombrophilous Forest areas. The Standardised Precipitation-Evapotranspiration Index (SPEI) showed to be an efficient index to characterize the drought in El Niño events, besides showing the agricultural expansion in the region. The largest trends of the weather elements and the SPEI were during the El Niño phenomenon. A better understanding of the ENSO effects on vegetation could prevent uncontrolled forest loss. Governance interventions involving national and financial actors, as well as local populations, also play a role in this.

Keywords: Evapotranspiration, Legal Amazon, Climate change, Weather, Drought index.

1 INTRODUCTION

Climate variability, as well as changes in the earth's climate, has been an issue of extensive discussion over the last decades around the world due to the various impacts caused on water resources, vegetation, energy generation, and even irreversible damage to society (Marengo; Espinoza, 2016; Sousa; Candido; Andreoli, 2018).

The El Niño Southern Oscillation (ENSO) is a phenomenon characterized by changes in the sea surface temperature (SST) of the Pacific, Equatorial, and Atlantic oceans, with two phases: one warm and another cold. El Niño is characterized by the abnormal warming of the Pacific Ocean waters, while La Niña comprises the abnormal cooling of these waters (Rossi; Soares, 2017; Lu et al., 2018).

Overall, the effects on atmospheric circulation caused by ENSO are quite expressive. Climate responses to ENSO patterns are very complex, where regional differences in the Pacific areas are very notable, varying according to the influence on various atmospheric mechanisms in the region. For this reason, the occurrence of this phenomenon is seen as an agent of climate anomalies (Bonfils et al., 2017; Lu et al., 2018).

In Brazil, there is a significant influence of the ENSO phenomenon on the South, Northeast, and eastern Amazon regions, which has caused anomalies such as decreased rainfall or more abundant rainfall, increased average temperature, and severe droughts (Barbosa et al., 2019).

Variability in rainfall and temperature regimes influences plant growth, thereby altering vegetation conditions on the surface (Barbosa, 2015). For example, Wright and Calderón (2006), when studying a lowland forest in central Panama, observed that trees had higher growth during moderate El Nino events, but when the phenomenon coincided with severe droughts, there was a reduction in tree growth.

Nowadays, it is widely recognized that the climate modulates the behavior of different plant typologies and that the evapotranspiration promoted by them makes their participation in the balance of atmospheric processes and maintenance of temperature expressive (Van Der Werf et al., 2008; Rosemback et al., 2010).

Although several studies have shown the influence of ENSO on single weather variables, there is still a need to investigate relationships between the phenomenon and more complex processes requiring even an interaction between weather and agricultural systems. Among them, evapotranspiration is a crucial component of the water cycle, and its changes are studied for good planning of water resources, irrigation control, among others (Zhang et al., 2015).

Because of the large effect of ENSO on climate variability and hence on the vegetation dynamics and evapotranspiration process, it is necessary to have adequate knowledge of the consequences of ENSO, particularly for the State of Amazonas, which plays an essential role in the thermal and hydric regimes in Brazil.

Although many studies have addressed vegetation degradation due to environmental conditions and climate variability, some questions remain unanswered: i. Which phase of the ENSO event does the degradation of the Amazon occur most? ii. Which conventional weather stations have the highest correlation with the FAO-56 standard? iii. Which vegetation is under the most water stress conditions? iv. Can the SPEI be an index used to monitor vegetation degradation in Amazonas? v. Does demographic expansion and agricultural crops have a positive correlation with increased degradation and fire foci in Amazonas? To answer these

questions, this study investigated the processes of vegetation degradation in years of El Niño Southern Oscillation (ENSO) events in the State of Amazonas.

2. MATERIAL AND METHODS

2.1 Study Area

The State of Amazonas has the largest territorial extension in Brazil, with a surface area of 1,559,148.890 km², which corresponds to 18% of the national territory, and a population of 3,938,336 inhabitants (IBGE, 2021a). According to the Köppen classification, the predominant climate in the region is A type, with average temperatures of 24ºC to 26ºC and relative humidity ranging from 76 to 89%, having two well-defined seasons: winter characterized as the rainy period, and summer comprising the dry period (Figueroa; Nobre, 1990; Alvares et al., 2013).

The State is inserted in the Amazon Basin, the largest basin in the world, with a drainage area exceeding 6,000,000 km². In this immense hydrographic basin, the main waterways are: Solimões, Juruá, Javari, Negro, Japurá, Purus, and Madeira (Coelho et al., 2005).

Among the dominant soil classes in the State of Amazonas, the Ultisols are the most pronounced, comprising practically 45% of the entire state area. The Oxisols represent 26% of the area, predominantly yellow Oxisols, whose occurrence is concentrated near the central region of the State in dryland areas (Coelho et al., 2005).

The main forest typologies that occur in the State of Amazonas are floodplain forests, lowland forests, and highland forests. In lowlands are located the lowland forests ("Igapó") closest to the rivers, which are flooded most of the year, unlike the flooded areas that are more commonly subject to flooding during the rainy season. Highland forests are located in the upper zones, where flooding does not usually occur (Lopes et al., 2016).

According to the Ministry of Environment (MMA, 2019), there are 6 different forms of vegetation in the State. In the present study, these data were separated into 6 vegetation classes (Figure 1 and Table 1). In this case, ArcGIS 10.5 software was also used to read the data and associate it with evapotranspiration and fire foci for each vegetation class in the State of Amazonas.

Table 1. Forest typologies present in the State of Amazonas

Code	Vegetation types
A	Areas of pioneer formations
B	Ecological tension areas (contacts between vegetation types)
C	Open ombrophilous forest (transition forest)
D	Dense ombrophilous forest
E	Savanna
F	Oligotrophic woody vegetation of swamps and sandy accumulations

2.2 Meteorological Variables Obtained por Estimating Evapotranspiration

To estimate evapotranspiration for the ENSO period considered, data were obtained from conventional meteorological stations (CME), through the Database for Teaching and Research (BDMEP) located in the municipalities: Barcelos, Benjamin Constant, Codajás, Eirunepé, Fonte Boa, Manaus, Manicoré, São Gabriel da Cachoeira, Coari, Iauarete, Itacoatiara, Lábrea, Parintins and Tefé. These data are available in the meteorological data bank for teaching and research, at INMET portal

The following variables were acquired in txt format and later transferred to an electronic spreadsheet: maximum temperature (ºC), minimum temperature (ºC), relative humidity (%), insolation (hours/day), and wind speed (m/s). Figure 1 and Table 2 show the stations from which the variables were obtained and their respective latitudes, longitudes, and altitudes.

Table 2. Weather stations and their respective latitudes, longitudes, and altitudes.

Stations	Code (WMO)	Latitude (º)	Longitude (º)	Altitude (m)
Barcelos	82113	-0.96	-62.91	40.00
Benjamin Constant	82410	-4.38	-70.03	65.00
Codajás	82326	-3.83	-62.08	48.00
Eirunepé	82610	-6.66	-69.86	104.00
Fonte Boa	82212	-2.53	-66.16	55.57
Manaus	82331	-3.11	-59.95	67.00
Manicoré	82533	-5.81	-61.3	50.00
São Gabriel da Cachoeira	82106	-0.11	-67.00	90.00
Coari	82425	-4.08	-63.13	46.00
Iauarete	82067	0.61	-69.20	120.00
Itacoatiara	82336	-3.13	-58.43	40.00
Lábrea	82723	-7.25	-64.83	61.00
Parintins	82240	-2.63	-56.73	29.00
Tefé	82317	-3.83	-64.70	47.00

Source: (http://www.inmet.gov.br/portal/index.php?r=bdmep/bdmep).
WMO – World Meteorological Organization
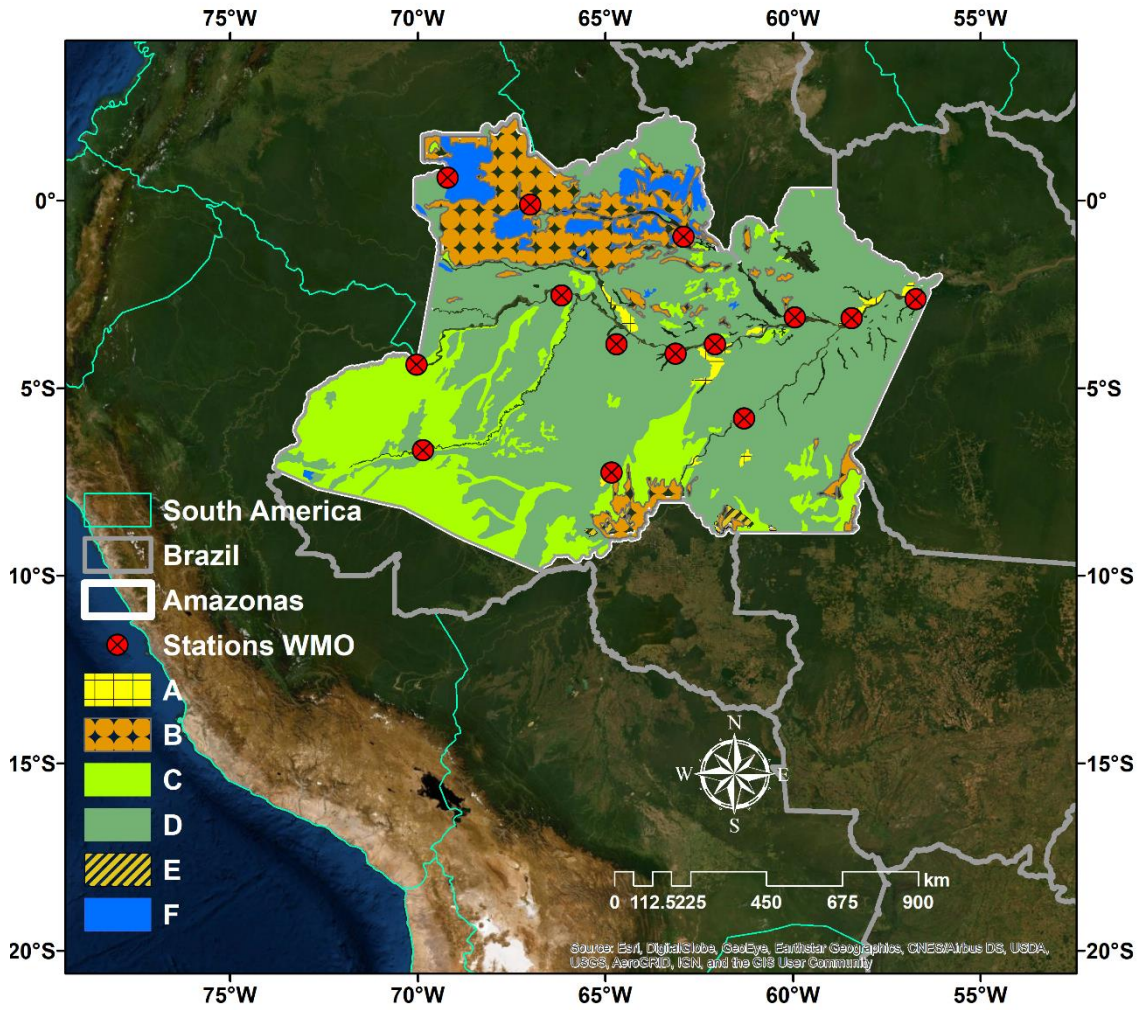
Figure 1. Geographic location of the study area highlighting the spatialization of the conventional weather stations and the forest typologies used in this study.

2. 3 Estimating Evapotranspiration

The Penman-Monteith-FAO method, considered a robust method (Allen et al., 1998), was used to estimate reference evapotranspiration (ET_0) (Equation 1), and the same method was used to estimate the MOD16 product (Mu; Zhao; Running, 2011), allowing a comparison between field data and satellite images.

$$ET_0 = \frac{0.408 * \Delta * (Rn - G) + \gamma * 900 \, T+273 * u2 * (es - ea)}{\Delta + \gamma * (1 + 0.34 * u2)} \tag{1}$$

Wherein: ET_0 – reference evapotranspiration (mm day^{-1}); Rn – net radiation on the crop surface (MJ m^{-2} day^{-1}); G – heat flow on the ground (MJ m^{-2} day^{-1}); T – daily average air temperature at 2 m height (ºC); u2 – wind speed at 2 m height (m s^{-1}); es - saturation vapor pressure (kPa); ea – current vapor pressure (kPa); (es - ea) – vapor saturation deficit (kPa); Δ – slope of the vapor pressure versus temperature curve (kPa ºC^{-1}); and γ – psychrometric constant (kPa ºC^{-1}).

Another seven methods were also used to estimate evapotranspiration for the State of Amazonas and are shown in Table 3.

Table 3. Empirical methods for estimating the ET_0.

Method ID	Equation	Variables	Reference
Val-1	$ETo = 0{,}0393\ Rs\ \sqrt{T + 95} − 0{,}19\ Rs^{0,6}\ \phi^{0,15} + 0{,}048\ (T + 20)\ (1 − RH\ 100)\ u^{0,7}$	Rs, T, ϕ, RH, u	
Val-2	$ETo = 0{,}0393\ Rs\sqrt{T + 95} − 0{,}19\ Rs^{0,6}\ \phi^{0,15} + 0{,}0037(T + 20)\ (1{,}12T − Tmin − 2)^{0,7}$	Rs, T, Tmin, ϕ	
Val-3	$ETo = 0{,}0393\ Rs\ \sqrt{T + 95} − 0{,}19\ Rs^{0,6}\ \phi^{0,15} + 0{,}078\ (T + 20)\ 1 − RH\ 100$	Rs, T, ϕ, RH	Valiantzas (2013)
Val-4	$ETo = 0{,}0393\ Rs\ \sqrt{T + 95} − 0{,}19\ Rs^{0,6}\ \phi^{0,15} + 0{,}0037\ (T + 20)\ (1.12T − Tmin − 2)^{0,7} U_{av}^{0,7}$	Rs, T, Tmin, ϕ, Uav	
Irmak-1	$ETo = -0{,}611 + 0{,}149\ Rs + 0{,}079\ T$	Rs, T	
Irmak-2	$ETo = 0{,}489 + 0{,}289\ Rn + 0{,}023\ T$	Rn, T	Irmak et al. (2003)
Alex	$ETo = 0{,}057 + 0{,}227\ C_2 + 0{,}643\ C_1 + 0{,}0124\ C1C_2$ $C1 = 0{,}6416 - 0{,}00784\ RH + 0{,}372\ Rs - 0{,}00264\ Rs\ RH$ $C2 = -0{,}0033 + 0{,}00812\ T + 0{,}101\ Rs + 0{,}00584\ Rs\ T$	Rs, T, RH	Alexandris, Kerkides and Liakatas (2006)

Rs = solar radiation (MJ m^{-2} d^{-1}); T = daily average air temperature (^{0}C); φ = latitude of the station (radians); RH = daily average relative humidity (%); u = daily average wind speed at 2 m height (m s^{-1}); T_{min} = daily minimum air temperature (^{0}C); U_{av} = local long-term average annual wind speed (m s^{-1}); Rn = net radiation (MJ m^{-2} d^{-1}).

Simplified equations to approximate the Penman-Monteith equation for estimating ET_0 were developed by Valiantzas (2013). This author named the first equation Val-1, which uses air temperature, solar radiation, relative humidity, and wind speed. This author also created simplifications of this equation for locations where data for wind speed, relative humidity, or both are not available, called Val-3, Val-4, Val-2, respectively.

The equations proposed by Irmak et al. (2003) were developed from the Penman-Monteith method (FAO-56). The first equation, Irmak-1, uses solar radiation and air temperature, and the second (Irmak-2) uses net radiation and air temperature. Alexandris et al. (2006) developed an empirical equation for daily reference evapotranspiration using solar radiation, temperature, and relative humidity data. The coefficients of the equation were determined by a bilinear surface regression analysis.

2. 4 El Niño Southern Oscillation (ENSO)

Through the digital platform of Golden Gate Weather Services (GG Weather, 2021), data were collected regarding the occurrence of the La Niña phenomenon (July 2007 to July 2008), Neutrality (January to December 2013), and El Niño (January to December 2015) (Table 4). The years are organized in quarters and the events are classified by the colors red (El Niño), blue (La Niña), and black (Neutrality).

Table 4. ENSO occurrence periods.

Year	DJF	JFM	FMA	MAM	AMJ	MJJ	JJA	JAS	ASO	SON	OND
2007	0.7	0.4	0.1	-0.1	-0.2	-0.3	-0.4	-0.6	-0.9	-1.1	-1.3
2008	-1.4	-1.3	-1.1	-0.9	-0.7	-0.5	-0.4	-0.3	-0.3	-0.4	-0.6
2013	-0.4	-0.4	-0.3	-0.2	-0.2	-0.2	-0.3	-0.3	-0.2	-0.3	-0.3
2015	0.6	0.5	0.6	0.7	0.8	1.0	1.2	1.4	1.7	2.0	2.2

*Source: GGWeather - Golden Gate Weather Services (2021).

2. 5 Remote Sensing - Products

Actual evapotranspiration images used in this study were obtained from the Moderate Resolution Imaging Spectroradiometer (MODIS) database of the MODIS Global Evapotranspiration Project (MOD16A2) product with spatial resolution equal to 500 m and temporal resolution of 8 days and is available from the year 2000 (Mu; Zhao; Running, 2011). MODIS tiles (H11V08, H10V09, H11V09, H12V09, H12V08, and H10V08) were mosaiced, converted from HDF (Hierarchical Data Format) to GeoTIFF format and from sinusoidal projection to geographic coordinate system and WGS84 datum.

The geographic location of the fire foci and the vectorized data in Shapefile format are provided by the National Aeronautics and Space Administration - NASA. Fire foci data were obtained from the MOD14 collection 6 platforms TERRA and AQUA (https://earthdata.nasa.gov/firms).

2. 6 The Standardized Precipitation-Evapotranspiration Index (SPEI)

We selected the SPEI drought index to examine drought characteristics in the years of La Niña (July 2007 to July 2008), Neutrality (January to December 2013), and El Niño (January to December 2015) phenomena. The SPEI is based on the monthly climatic water balance (D) driven by precipitation and potential evapotranspiration (PET) variables, the classification of drought status is similar to the Standardized Precipitation Index (SPI) index as shown in Table 5.

Table 5. Drought severity classes according to the SPEI index.

Drought and wet degree	Index values
Very severe wet (Vsw)	Index ≥ 2
Severe wet (Sw)	$1.5 \leq$ Index < 2
Moderate wet (Mw)	$1 \leq$ Index < 1.5
Close to normal (Cn)	$-0.99 \leq$ Index ≤ 0.99
Moderate drought (Md)	$-1.5 <$ Index ≤ 1
Severe drought (Sd)	$-2 <$ Index ≤ -1.5
Very severe drought (Vsd)	Index ≤ -2

Source: Saeidipour; Radmanesh; Eslamian (2019).

The SPEI calculation procedure is based on the original SPI calculation but uses the difference between monthly precipitation (P) and PET as shown in Equation (2).

$$D = P - PET$$

$$(2)$$

2. 7 Demographics and Main Agricultural Crops

Data from the population projection in the State of Amazonas from the Brazilian Institute of Geography and Statistics (IBGE, 2021a) and data in hectares of the main expanding agricultural crops in the State (IBGE, 2021c) were used. The crop and population projection data were used to compare with the increase in fires and drought severity from the SPEI index.

2. 8 Statistical Analyses

Monthly evapotranspiration estimates obtained from the MOD16A2 product of the MODIS sensor were compared with averages obtained by FAO-56. The other seven empirical ET_0 estimation methods were also compared with the Penman-Monteith method. The comparisons were performed for the years of extreme ENSO events for the 14 stations distributed in the State. The coefficient of determination (R^2) was used to evaluate the accuracy of evapotranspiration estimates by the different methods presented here.

Through the Boxplot statistics, the SPEI index and evapotranspiration for the different forest typologies present in the State were characterized. The correlation between the different variables used in this study was also analyzed. To analyze the trend of these variables, the Mann-Kendall test (Mann, 1945; Kendall, 1975) was applied using the *Kendall* package (MCLEOD, 2015) in R software.

3. RESULTS AND DISCUSSION

3. 1 Evapotranspiration for Stations Used

In Figure 2 the correlations between different methods in estimating evapotranspiration are shown. For the year of La Niña phenomenon (July 2007 to July 2008), the comparison between Irmak-1 and Penman-Monteith methods shows that station 82212 showed the highest R^2 value (0.994). For El Niño (2015), station 82425 recorded the highest R^2 (0.9813) and for the Neutral year (2013), 82317 showed maximum value with R^2 of 0.994.

When comparing the Irmak-2 and Penman-Monteith methods for La Niña (July 2007 to July 2008), station 82240 showed the highest R^2 (0.998). This also occurred for El Niño and Neutral, where this same station obtained R^2 of 0.995 and 0.990 respectively (Figure 2).

Station 82240 showed the highest R^2 value (0.990) for the La Niña period, in the correlation between Val-1 and Penman-Monteith. Whereas for El Niño (2015), station 82331 recorded the highest R^2 (0.998). For the Neutrality (2013) in the State, 82240 recorded the highest R^2 value (0.988) (Figure 2).

When comparing Val-2 and Penman-Monteith, it can be seen that 82240 was also the station that showed the highest R^2 value (0.998) for the year of La Niña. For El Niño (2015) and Neutrality (2013), it was also the station showing the highest R^2 values, 0.995 and 0.987, respectively (Figure 2).
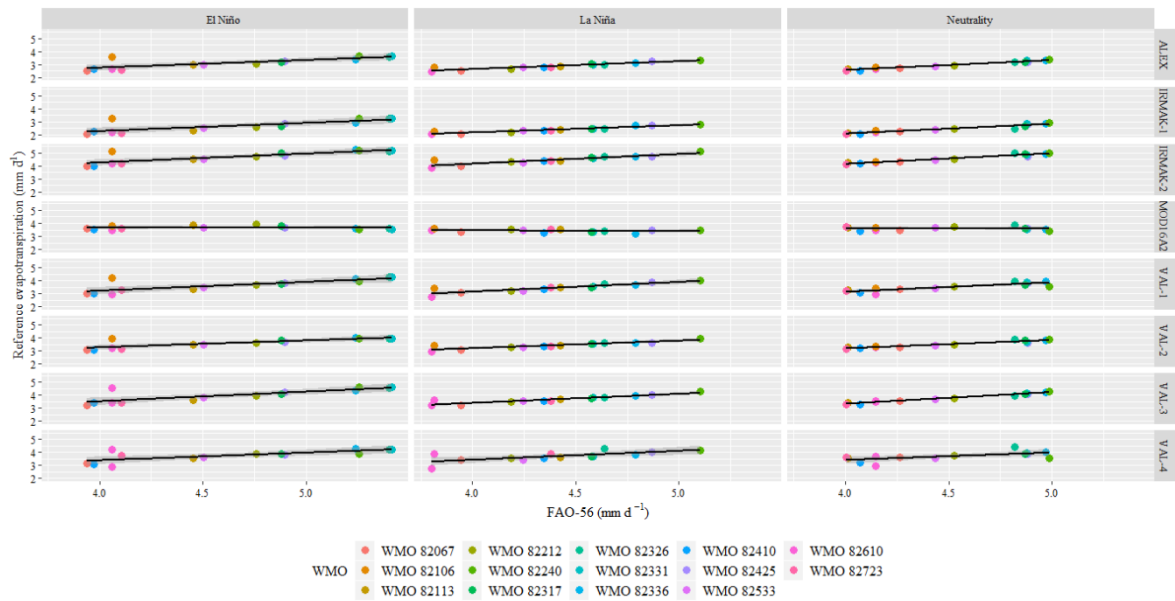
Figure 2. Correlation between different methods of estimating evapotranspiration for the 14 stations present in the State of Amazonas.

Station 82317 in the La Niña period obtained the highest R^2 value 0.997, in the comparison between the Val-3 and Penman-Monteith methods. When analyzing the El Niño of 2015, station 82212 showed the highest R^2 (0.995). For Neutrality (2013), 82212 also obtained the highest R^2 (0.991) (Figure 2).

When analyzing the results of the comparison between the Val-4 and Penman-Monteith methods, the station 82240 once again presented the highest value of R^2 (0.988) for La Niña. By comparing the methods for the El Niño phenomenon, the same station obtained maximum R^2 of 0.992 and in the Neutral period also with R^2 of 0.987 (Figure 2).

Comparing Alex (2006) and Penman-Monteith for La Niña (July 2007 to July 2008), 82410 had the highest R^2 (0.994). For the El Niño event (2015) for the State, station 82212 had the highest R^2 value (0.995). For the Neutral event (2013), station 82317 had the highest R^2 (0.994).

For La Niña (July 2007 to July 2008), the highest correlation between MOD16A2 and Penman-Monteith was found for station 82533 with R^2 0.823. Whereas for the El Niño (2015), the correlations were low and station 82723 showed the highest R^2 (0.397). When analyzing the Neutrality year (2013), 82106 showed the maximum R^2 (0.557).

It can be seen that there are differences in the correlations for the stations, showing that within the same State there is variation in evapotranspiration in each region. The variation can be influenced by different isolated or interrelated factors, such as latitude, insolation, local altitude, wind speed, type of vegetation cover, availability of water in the soil, among others (Glenn; Nagler; Huete, 2010). The different methods presented here showed good correlations with the standard FAO-56 method in the different years analyzed. They presented satisfactory results for use in estimating evapotranspiration in the State of Amazonas.

The correlations with MOD16A2 for El Niño and Neutral were low, however, in many regions, the FAO-56 approach is limited due to the lack of required climate data. Therefore, under conditions of insufficient weather data, many researchers have emphasized the use of indirect methods of estimating ET_0 from satellite products, which can capture the spatial and temporal variability at different scales (Autovino; Minacapilli; Provenzano, 2016.). Furthermore, good quality ET_0 data generated by MOD16A2 has been used successfully in several studies (Velpuri et al., 2013, Hu et al., 2015, Alemayehu et al., 2017).

3. 2 Evapotranspiration for Forest Typologies

In Figure 3 are presented the average evapotranspiration values for each forest typology present in the study area in the years of El Niño (2015), Neutrality (2013), and La Niña (July 2007 to July 2008). In this Figure, it can be observed that the typology open ombrophilous forest (C) showed the highest value of average evapotranspiration (3.75), the dense ombrophilous forest (D) recorded the second highest average value of 3.59 and the Savanna (E) corresponded to the lowest average value 3.52, for the months of Neutrality (2013).

When analyzing the El Niño period, the oligotrophic woody vegetation of swamps and sandy accumulations (F) showed the highest average value of evapotranspiration (3.96), followed by the dense ombrophilous forest (D) with an average value of 3.78. The typologies Savanna (E) and Areas of pioneer formations (A) presented the lowest values of 3.58 and 3.70, respectively.

For the La Niña period, the oligotrophic woody vegetation of swamps and sandy accumulations (F) obtained the highest average value of evapotranspiration (3.68), while savanna (E) obtained the lowest value (3.22). As shown by the results, the El Niño year presented the highest average evapotranspiration compared to the other years, and even the lowest values found in this period were close or superior to the highest averages recorded for La Niña and Neutrality.

Vegetation F, also known as Campinarana, which has as a characteristic a thin and tall tree vegetation of "riparian" type resulting from soil poverty (IBGE, 2012), showed higher evapotranspiration for the La Niña rainy event. However, under the dry El Niño period (2015), responsible for the highest temperature in a century (Jiménez - Muñoz et al., 2016), the highest average was obtained for this vegetation type. Therefore, ET_0 increases with increasing atmospheric water vapor demand, or in other words, ET0 increases as the atmosphere gets drier and when more energy is available to evaporate the water.

Costa et al. (2010) reported that their research supports previous studies, also demonstrating that evapotranspiration in the dry season is higher than in the wet season and that net surface radiation is the major controller of evapotranspiration in humid equatorial locations. Cleland et al. (2012) reported that tree species are particularly vulnerable to climate change because their phenology is generally able to track the lengthening or shortening of the dry season.

These results indicate that colder and wetter years may exhibit similar ET_0 rates compared to warmer and drier years. However, the warming and drying that occur under El Niño may cause increased tree mortality (Jiménez - Muñoz et al., 2016), which can alter the carbon cycle and lead to changes in forest structure and function and can last for several years after the event (Phillips et al., 2010).
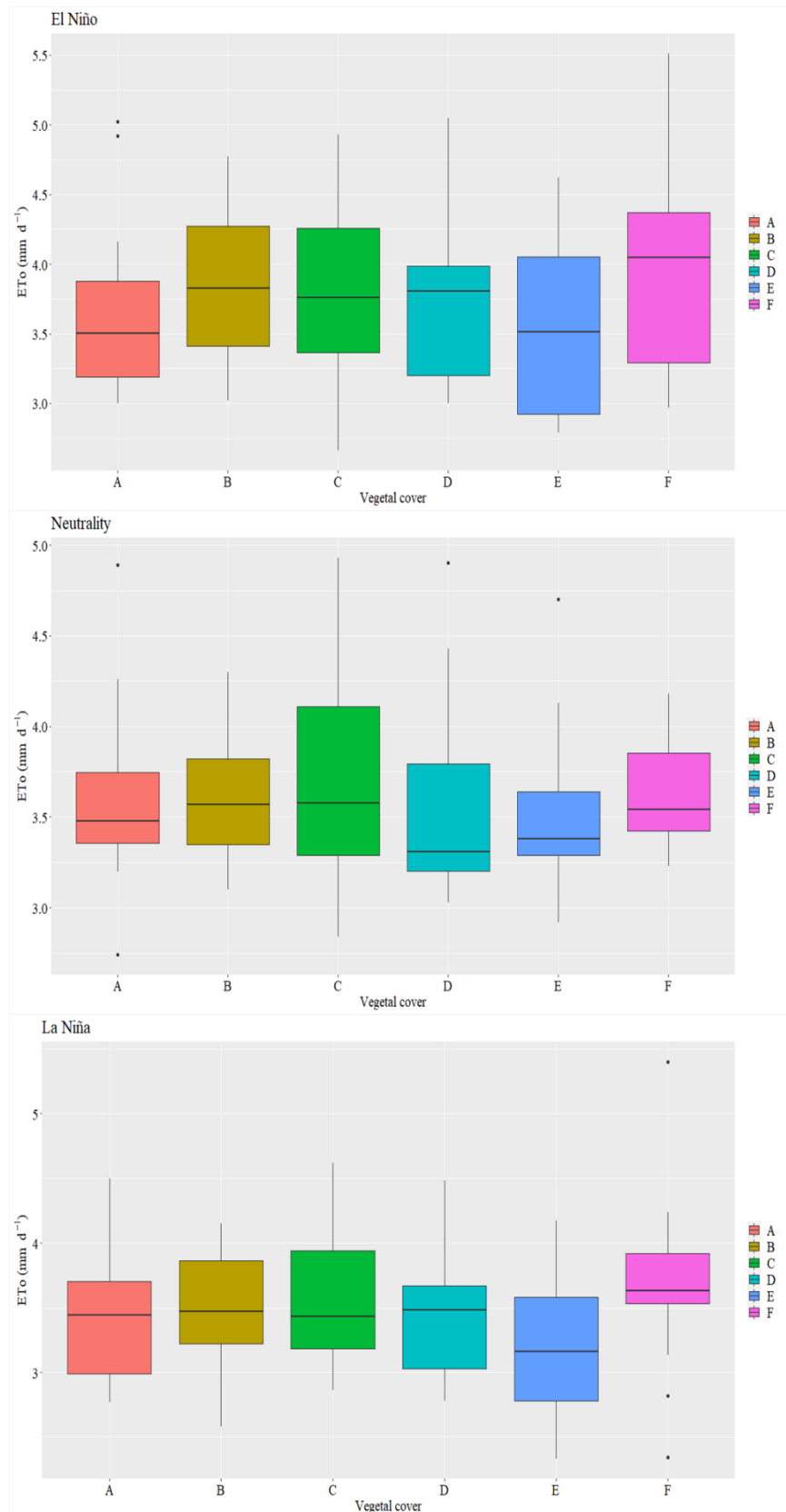
Figure 3. Average evapotranspiration values for each forest typology present in the study area in El Niño, Neutral, and La Niña years.

In Figure 4 it is possible to observe the number of fire foci for each of the six vegetation types present in the State of Amazonas in the years of the ENSO phenomenon. In 2015, a period

in which the Amazon underwent intense drought, the Dense Ombrophylous Forest (D) recorded the highest occurrences of fire foci for the months of August, September and October with sums of 4132, 5192 and 2756 foci, respectively. During La Niña of 2007 and 2008, the Dense Ombrophylous Forest (D) was also the one to present the highest foci occurrence totaling 14415, with the highest records for the period considered dry in the region. In Neutrality, there was a lower occurrence of fire foci that are also more accentuated in the dry period, and once again, typology D recorded the highest occurrences with a sum of 4999 foci (Figure 4).

The Dense Ombrophylous Forests are conditioned to high rainfall, with a regular rain distribution throughout the year (IBGE, 1992). The reduced rainfall caused by El Niño may have culminated in a higher occurrence of fires in this forest type in the State of Amazonas.

The dry seasons intensified by the ENSO phenomenon in the Amazon increase fires from anthropogenic sources spreading into the standing forest. Forest fires in the Amazon are atypically intense in these years due to the higher amount of dry combustible material deposited on the ground, killing up to 64% of the trees (Barlow and Peres, 2006).

Forest fires degrade Amazonian forests and destabilize the remaining forest cover through flammability and erosion feedback, favoring more open vegetation (Flores et al., 2019).

In addition to climate change, the Amazon Rainforests suffer from the pressures of human development in the region. Population growth up to the year 2060 in the State can be seen in Figure 5 (IBGE, 2021a). The regional growth of cities, such as Manaus, road and dam construction needed to meet population demand (Barber et al., 2014; Fearnside, 2014), further increase the pressure on Amazonian forests.
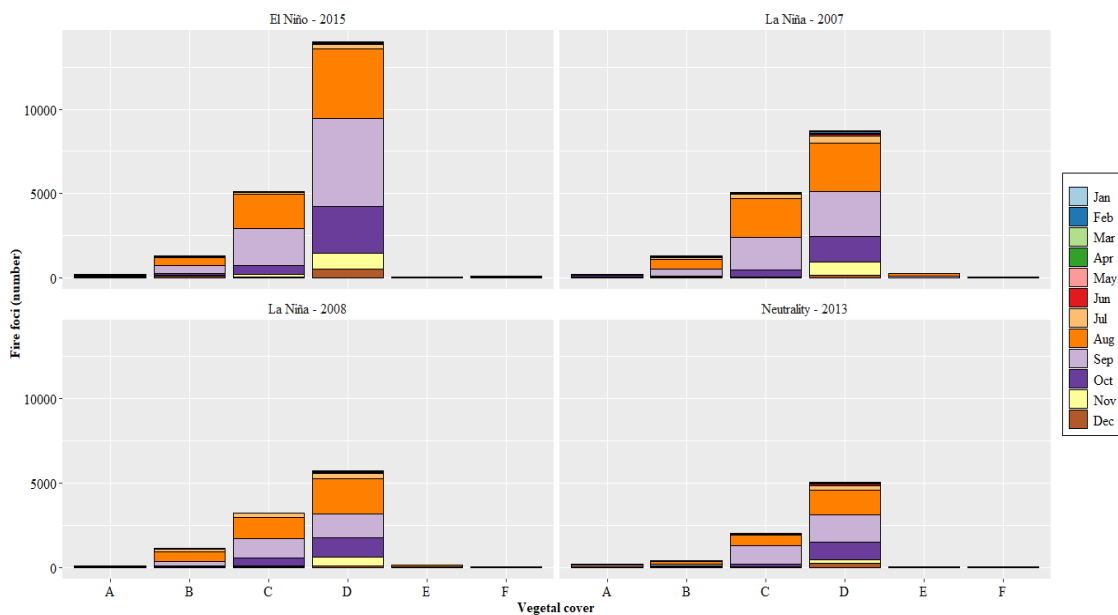
Figure 4. Fire foci for each forest typology present in the states during the La Niña, El Niño, and Neutrality years.
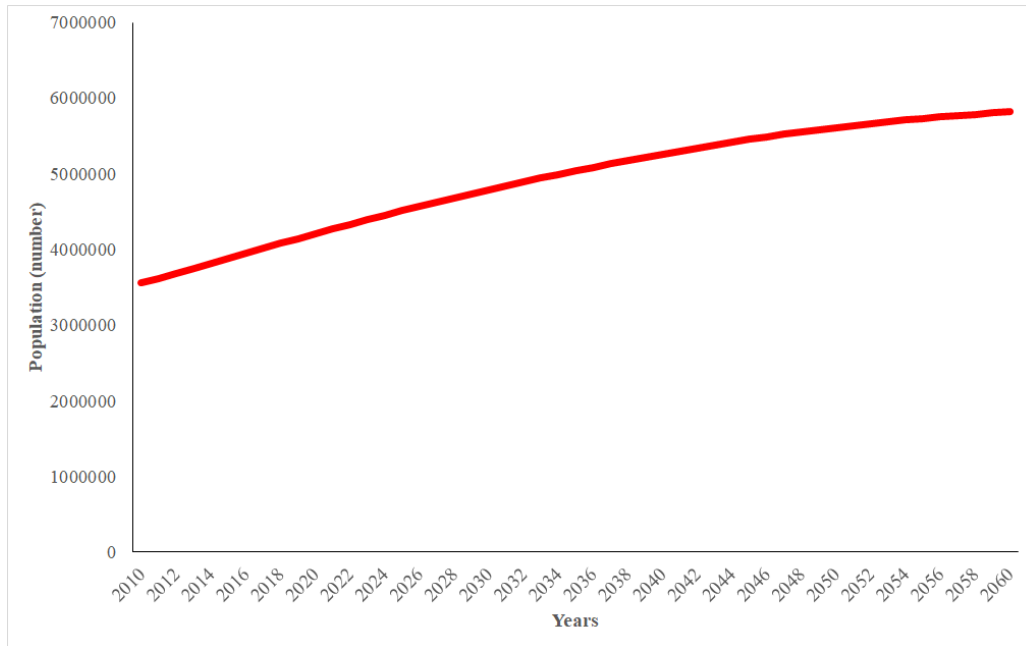
Figure 5. Population growth for the State of Amazonas.
Adapted source (IBGE, 2021a).

The SPEI index generated for the La Niña (2007 and 2008), El Niño (2015) and Neutrality (2013) is shown in Figures 6 and 7. For the entire State, it is possible to observe levels ranging from very severe humidity to very severe drought.

In the El Niño (2015), it is possible to note that throughout the year moderate to very severe droughts occurred in almost the entire State. The month of September obtained the lowest average (-1.68), which puts it in the severe drought class according to the index. Even in the months considered rainy, most regions of the State faced very severe droughts, according to the index, which caused fires even in vegetation such as the Dense Ombrophylous Forest (Figure 6 and 7).

El Niño effects, still being felt in 2016, led to an additional 2.6% of tropical forests facing extreme drought severity (Jiménez-Muñoz et al., 2016). The physiological responses of Amazonian forest trees to drought are resulting in lower carbon uptake and increased risk of mortality. Recent work has shown a strong interdependence of hydraulic function and metabolism, with drought affecting tree ability to mobilize and transport carbohydrates (Barros et al., 2019; Brienen et al., 2015).

During Neutrality 2013, we see that the State in almost its entirety has moderate to severe wet levels, especially during the period considered rainy in the region. In the dry period, the State suffers moderate drought, with some regions facing severe drought (Figures 6 and 7).

There is not much rainfall or extreme drought in the neutrality period as seen in La Niña and El Niño. However, unusual events were recorded, such as the drought evidenced in Figure 7, faced by the State in December and January, a period considered rainy in Amazonas.
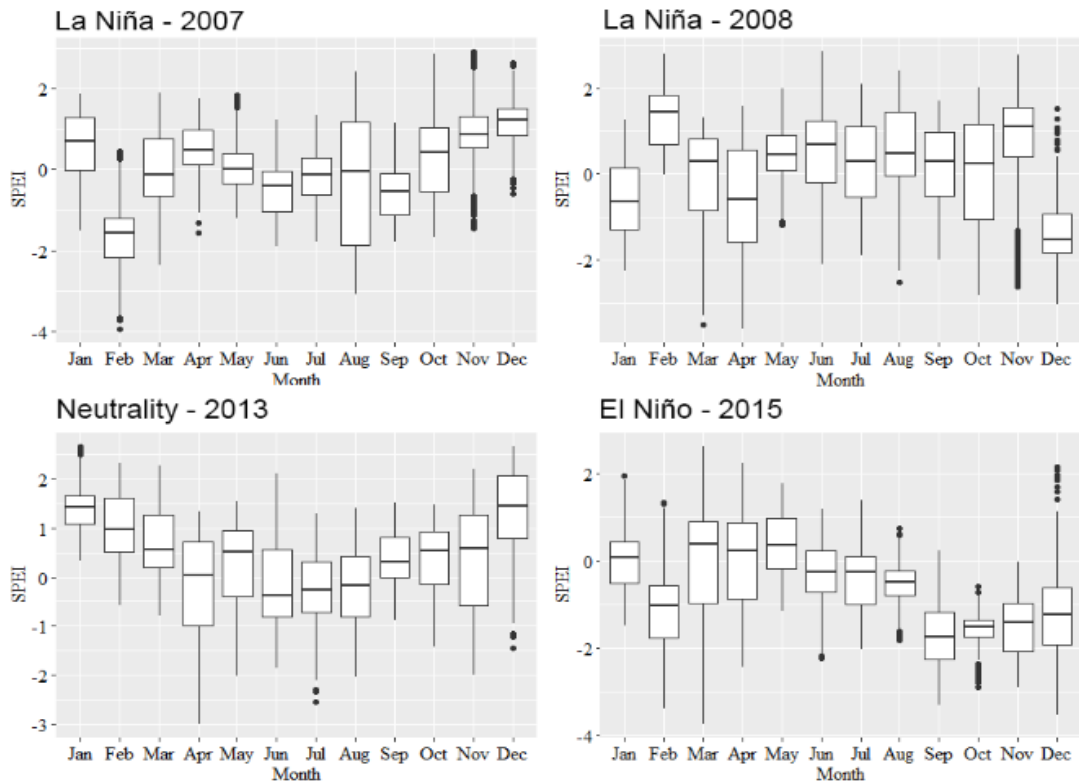
Figure 6. Boxplot of the SPEI index for La Niña, El Niño and Neutral years.
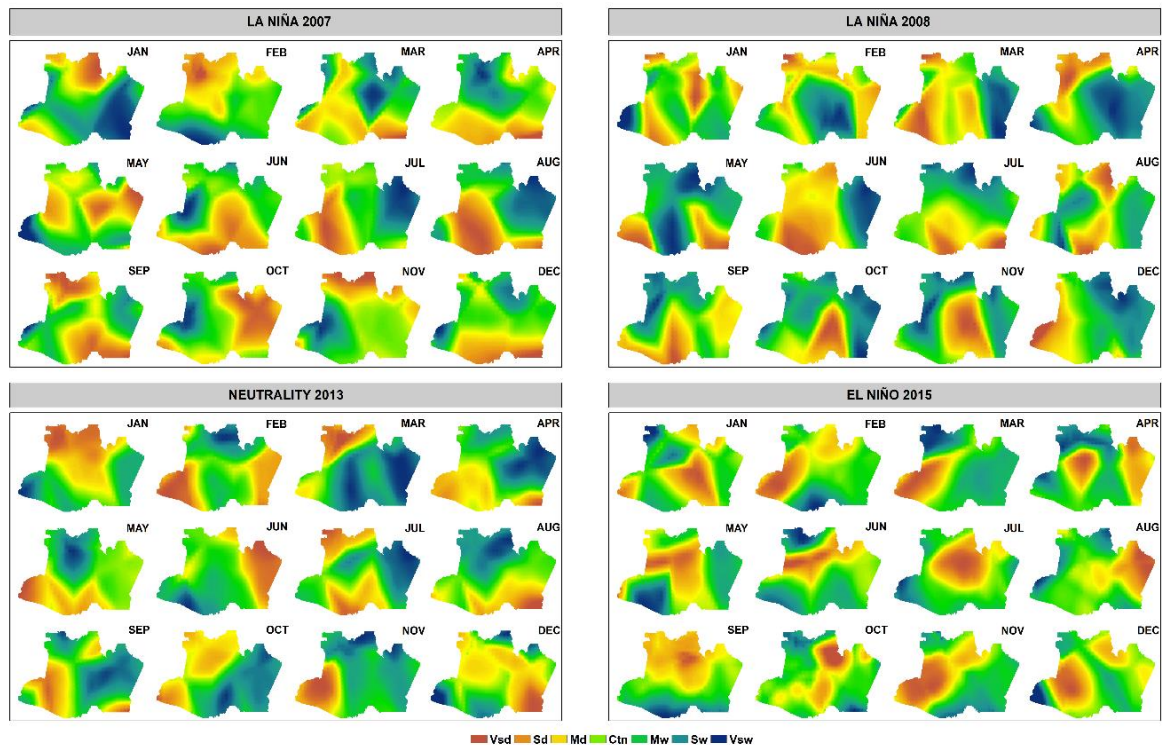
**Figure 7**. Spatialization of the SPEI index in La Niña, El Niño and Neutrality years for the State of Amazonas.

In the period of La Niña (2007 and 2008), it is already possible to note a higher occurrence of very severe wet, moderate wet, and close to normal in regions of the State for

most of the year (Figure 7). However, even faced the phenomenon that results in higher rainfall in the region during the period considered dry, some State regions suffered from severe and very severe droughts, especially in 2007. For example, the month of February, even though it is considered a rainy month in the region, recorded the lowest average of the year (-1.63), which placed it in the severe drought class (Figure 6).

In the same year, we can observe (Figure 8) an increase in the areas occupied by sugarcane and corn crops. An extension in hectares of these crops is almost always through forest conversion, bringing numerous consequences such as lower carbon sequestered from the atmosphere (Yang et al., 2018), amplification of the edge effect which makes the forest more susceptible to fire, and increased evapotranspiration. Brando et al. (2014) compared 2007 with other years and recorded for 2007 sharp increases of 462% in tree mortality in the Amazon due to interactions between droughts and fires. It is evident that not only climate variations can interfere with regional variations, but also human-made changes have a huge impact on Amazonas and can amplify the ENSO effects on Amazonas.
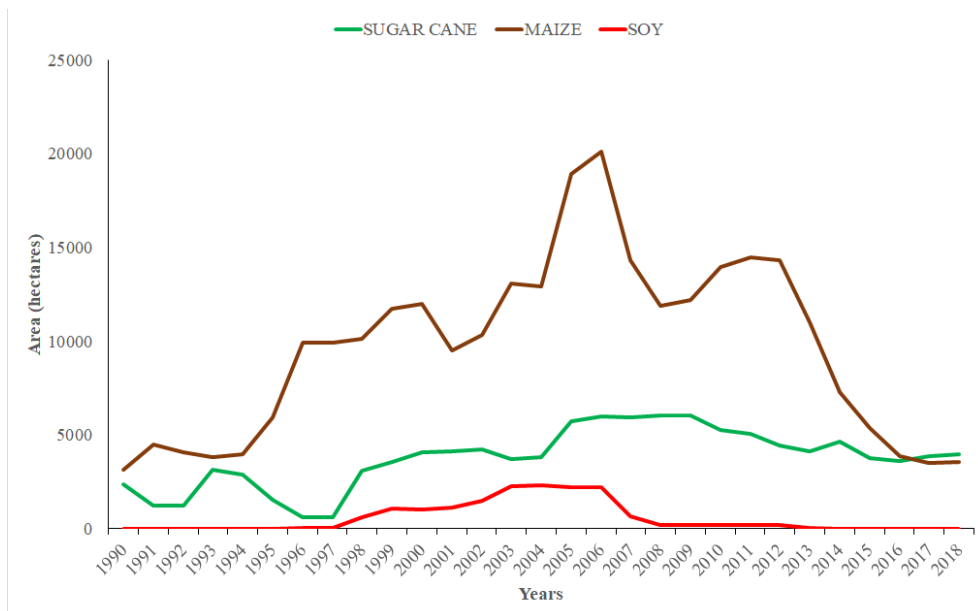

Figure 8. Area in hectares of the main annual crops grown in the State of Amazonas.

When analyzing the La Niña year, it is noted that the SPEI index has a high correlation with the forest typology F, which coincidentally presented the highest evapotranspiration rates.

It is also possible to see a strong correlation between average temperature and hotspots, indicating that the higher the temperatures, the higher the evapotranspiration rates and hence the forests become more prone to fire (Figure 9). This fact can be seen in Figure 4, where even in a La Niña year there was a high occurrence of fire foci in August, September and October.

For the Neutrality (2013), there was a high correlation between insolation and the Dense Ombrophylous Forest typology (Figure 9). In this same year, this typology proved to be very sensitive to high insolation levels, recording high evapotranspiration rates and the highest occurrences of fires in Amazonas. Figure 9 B shows the correlations between different variables in the El Niño (2015). For this year, a high correlation is observed between the SPEI and fire foci, remembering that in this period the index recorded severe drought in almost the entire State for most of the year, which consequently increases evapotranspiration, making the forest more prone to fire. This susceptibility to fire is further reinforced by the high correlation between average temperature and fire foci, indicating that the higher the temperature, the higher the occurrence of fires in the State.

The interaction between drought and high temperatures can also reduce tree growth (Vlam et al., 2014), leading to increased sensitivity of photosynthesis to rainfall (Giardina et al., 2018), as well as reduce vegetative vigor by increasing evapotranspiration (dos Santos et al., 2017).
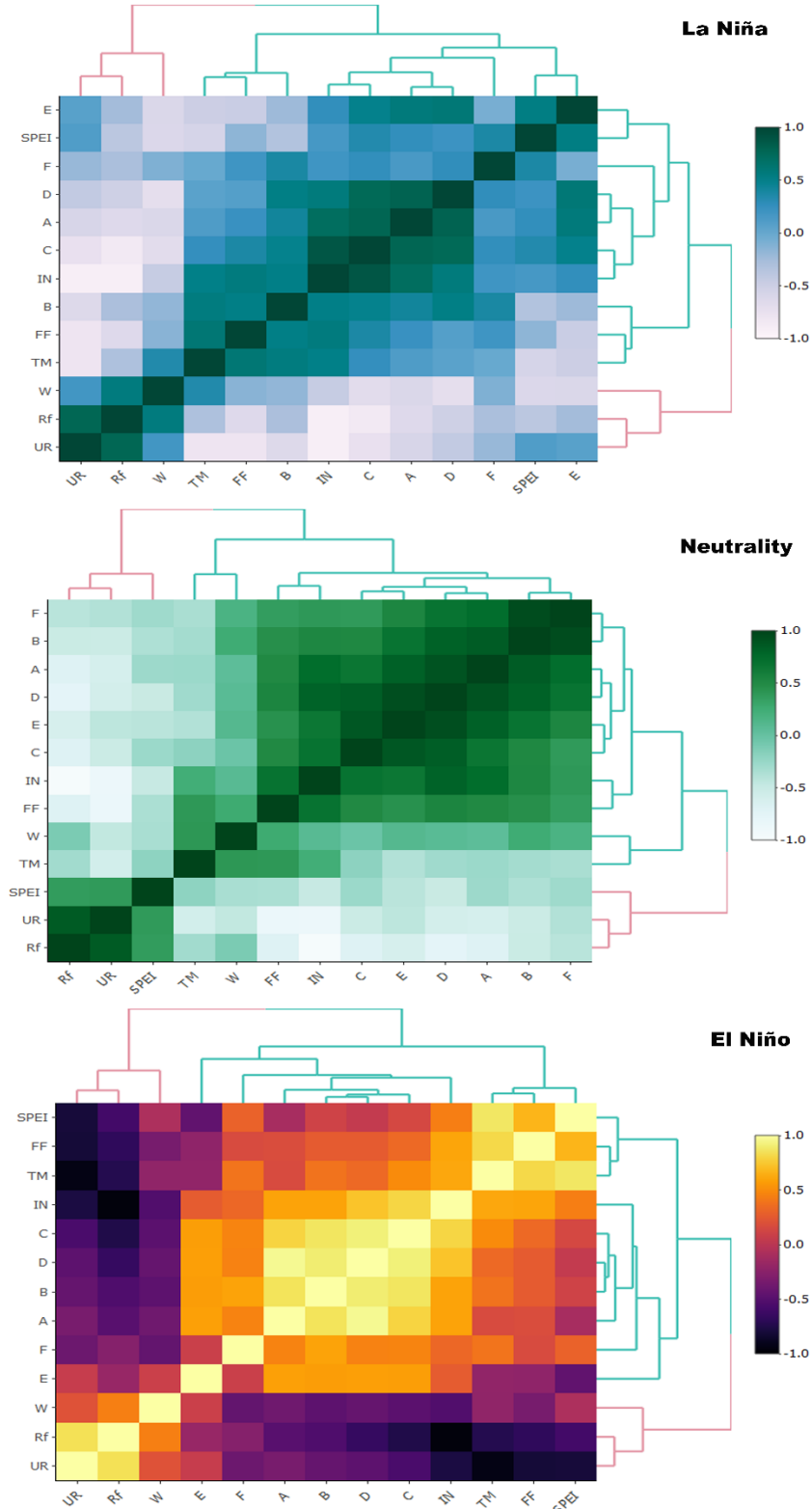
Figure 9. Correlation between different variables for La Niña (A), El Niño (B) and Neutrality (C) years. Legend: Forest typologies (A, B, C, D, E, F); RH = Relative humidity (%); Rf =

Rainfall (mm); W (Wind speed, m s^{-1}); IN = Insolation (hours); TM = Average air temperature (ºC); FF = Fire foci (number); SPEI = Standardised Precipitation-Evapotranspiration Index.

Still analyzing the 2015 period (Figure 10), an increase in coffee, banana, and orange crops is observed. The use of fire by farmers to clear their plantation areas is very common in Amazonas (Davidson et al., 2012). Severe drought events overlapping these land use activities increase the forest's susceptibility to fires.
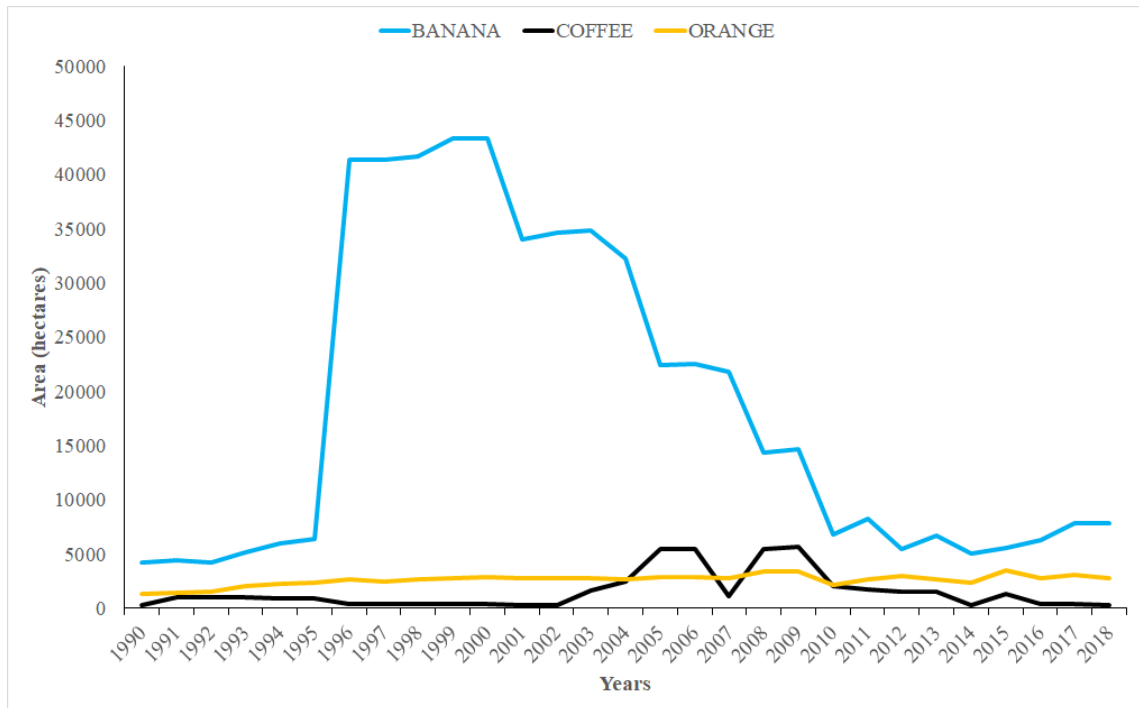
Figure 10. Area in hectares of the main perennial crops grown in the State of Amazonas.

The sugarcane crop showed an increasing and significant trend according to the Mann-Kendall test. The orange crop also showed a positive and significant trend with a p-value of 0.0006.

In the La Niña period, the variables temperature and fire foci showed positive and significant trends, which causes strong concern, because Amazon faces high rates of rainfall during La Niña, which should slow down the occurrence of fires in the State and reduce the temperature. Once again, human influence on the increase in temperature and the fires in the region is evident. The impacts of fires in the Amazon region could be avoided or decreased by reinforcing the monitoring, control, and enforcement of the current Brazilian legislation on illegal fires; creation of protected areas; and environmental education programs.

During Neutrality (2013), Mann-Kendall trend analysis showed positive and significant values for rainfall (p-value = 0.046), fire foci (p-value = 0.023), and insolation (p-value = 0.033).This result indicates that even though there is a positive rainfall trend for the State during the less rainy months, the forests become prone to fire with an increase in insolation.

For El Niño (2015), there was a positive and significant trend for insolation (p-value = 0.03), average temperature (p-value = 0.005), SPEI (p-value = 0.03), and fire foci (p-value = 0.05). This year in particular obtained record high temperatures and consequently numerous fire foi across the State.

5 CONCLUSIONS

The different methods tested for estimating evapotranspiration obtained satisfactory correlations with the standard FAO-56 method and can be used for the State of Amazonas.

The Oligotrophic Woody Forest typology of swamps and sandy accumulations showed the highest evapotranspiration rates, especially in the dry period caused by the 2015 El Niño.

The Dense Ombrophylous Forest recorded the highest rates of fire foci in the dry period of all years analyzed, particularly with the highest value in the drought caused by the 2015 El Niño.

The SPEI index recorded moderate to very severe droughts across most of the State during the 2015 El Niño.

High correlations were observed for the SPEI index and fire foci in the region in 2015. During La Niña period, average temperature and fire foci were highly correlated, demonstrating the temperature effects on fire starting in the State.

The Mann-Kendall analysis, especially for El Niño, showed a positive and significant trend for the variables insolation, average temperature, SPEI, and fire foci, showing the significant phenomenon influence on the Amazon region.

In 2020, deforestation and fire rates in Brazil were extremely high. We can expect that with fire in land management in Amazonia, the impacts of droughts associated with ENSO events will intensify. Therefore, a large area of forest edges will have higher evapotranspiration be at higher risk of fire.

Studies like this help to better understand the ENSO effects on vegetation and could prevent uncontrolled forest loss. Governance interventions involving national and financial actors, as well as local populations, also play a role in these efforts.

7 REFERENCES

Alemayehu, T., Griensven, A. van., Senay, G.B., Bauwens, W. Evapotranspiration mapping in a heterogeneous landscape using remote sensing and global weather datasets: application to the Mara Basin, East Africa. **Remote Sens., v**. 9, p. 2-24, 2017. doi: 10.3390/rs9040390

Alexandris, S., Kerkides, P., Liakatas, A. Daily reference evapotranspiration estimates by the "Copais" approach. **Agricultural Water Management**, Amsterdã, v. 82, n. 3, p. 371-386, 2006. doi: 10.1016/j.agwat.2005.08.001.

Autovino, D., Minacapilli, M., Provenzano, G. Modelling bulk surface resistance by MODIS data and assessment of MOD16A2 evapotranspiration product in an irrigation district of Southern Italy. **Agricultural Water Management**. v. 167, p. 86–9. 2016. oi.org/10.1016/j.agwat.2016.01.006.

Alvares, C. A., Stape, J. L., Sentelhas, P. C., de Moraes, G., Leonardo, J., & Sparovek, G. Köppen's climate classification map for Brazil. **Meteorologische Zeitschrift**, n. 22, n. 6, p. 711-728, 2013. Doi: 10.1127/0941-2948/2013/0507.

Barbosa, M.L.F., Delgado, R.C., Teodoro, P.E. et al. Occurrence of fre foci under diferent land uses in the State of Amazonas during the 2005 drought. **Environ Dev Sustain**., v. 21, p. 2707–2720, 2019. Doi: org/10.1007/s10668-018-0157-4.

Barbosa, H. A., Kumar T.V. L. Influence of rainfall variability on the vegetation dynamics over Northeastern Brazil. **Journal of Arid Environments**, v. 124. p. 377-387. 2016. doi.org/10.1016/j.jaridenv.2015.08.015.

Barber, C. P., Cochrane, M. A., Souza, C. M., Laurance, W. F. Roads, deforestation, and the mitigating effect of protected areas in the Amazon. **Biol. Conserv**., v. 177, p. 203–209, 2014. doi: 10.1016/j.biocon.2014.07.004.

Barlow, J., Peres, C.A. Consequences of fire disturbance for ecosystem structure and biodiversity in Amazonian forests. Emerging Threats to Tropical Forests, eds Laurance W.F, Peres C.A (Chicago University Press, Chicago), p 225–240, 2006.

Barros, F. de V., Bittencourt, P. R. L., Brum, M., Restrepo-Coupe, N., Pereira, L., Teodoro, G. S., Saleska, S. R., Borma, L. S., Christoffersen, B. O. et al. Hydraulic traits explain differential responses of Amazonianforests to the 2015 El Niño-induced drought. **New Phytologist.,** v. 223, p. 223:1253–1266, 2019. doi. 10.1111/nph.15909.

Bonfils, C., Anderson, G., Santer, B. D., Phillips, T. J., Taylor, A. E. Competing Influences of Anthropogenic Warming, ENSO, and Plant Physiology on Future Terrestrial Aridity. **American meteorological society.** v. 30, p. 6883-6904. 2017. doi.org/10.1175/JCLI-D-17-0005.1.

Bonsal, B.R., Cuell, C., Wheaton, E., Sauchyn, D.J., Barrow, E. An assessment of historical and projected future hydro-climatic variability and extremes over southern watersheds in the Canadian Prairies. **International Journal of Climatology**, v.37, p. 3934–3948, 2017. doi:org/10.1002/joc.4967.

Brando, P.M., Balch, J.K., Nepstad, D.C., Morton, D.C., Putz, F.E., Coe, M.T., Silvério, D., Macedo, M.N., Davidson, E.A., Nóbrega, C.C., Alencar, A., Soares Filho, B.S. Abrupt increases in Amazonian tree mortality due to drought–fire interactions. **Proceedings of the National Academy of Sciences**, v. 111, n. 17, p. 6347-6352, 2014. doi:10.1073/pnas.1305499111.

Brienen, R., Phillips, O., Feldpausch, T. et al. Long-term decline of the Amazon carbon sink. **Nature** v. 519, p. 344–348, 2015. doi.org/10.1038/nature14283.

Coelho, M. R. **Levantamento pedológico de uma área-piloto relacionada ao projeto BiosBrasil (Conservation and sustainable management of below-ground biodiversity: phase I), município de Benjamin Constant (AM).** Rio de Janeiro: Embrapa Solos, 2005.

Coelho, C. A. S., Denis, H. F. C., Mári, A. F. F. Precipitation diagnostics of an
exceptionally dry event in São Paulo, Brazil. Theoretical and Applied Climatology, v. 125, p. 1-16, 2015. doi.10.1007/s00704-015-1540-9.

Costa, M. H., Biajoli, M. C., Sanches, L., Malhado, A. C. M., Hutyra, L. R., da Rocha, H. R., Aguiar, R. G., de Araújo, A. C. Atmospheric versus vegetation controls of Amazonian tropical rain forest evapotranspiration: Are the wet and seasonally dry rain forests any different? **journal of geophysical research**, vol. 115, G04021, p. 1-9, 2010. doi:10.1029/2009JG001179.

Cox, P.M., Betts, R.A., Jones, C.D., Spall, S.A., Totterdell, I.J. Acceleration of global warming due to carbon-cycle feedbacks in a coupled climate model. **Nature**, v. 408, p. 184–187, 2000.

Cleland, E.E., Allen, J.M., Crimmins, T.M., Dunne, J.A., Pau, S., Travers, S.E., Wolkovich, E.M. Phenological tracking enables positive species responses to climate change. **Ecology**, v. 93, n. 8, p. 1765–1771, 2012.

Davidson E. A. et al. The Amazon basin in transition. **Nature**, v. 481(7381):321–328, 2012. doi:10.1038/nature10717.

dos Santos, S.R.Q., Sansigolo, C.A., Neves, T.T. de A.T., Campos, T.L. de O.B., dos Santos, A.P.P. Frequências dos eventos extremos de seca e chuva na Amazônia utilizando diferentes bancos de dados de precipitação. **Rev. Bras. Geogr. Física**, v. 10, p. 468-478, 2017. doi.10.5935/1984-2295.20140015.

Fearnside, P. M. Viewpoint-Brazil's Madeira river dams: a setback for environmental policy in amazonian development. Water Alter. v. 7, n. 1, p. 256-269, 2014.

Figueroa, S. N. Nobre, C. A. Precipitions distribution over central and western tropical south America. **Climanálise Boletim de Monitoramento e Análise Climática,** v. 5, n. 6, p. 36-45, 1990.

Flores, B. M., Staal, A., Jakovac, C. C., Hirota, M., Holmgren, M., Oliveira, R. S. Soil erosion as a resilience drain in disturbed tropical forests. **Plant and Soil**, 2019. doi:10.1007/s11104-019-04097-8.

GGWeather - Golden Gate Weather Services, 2019. El Niño and La Niña Years and Intensities [WWW Document]. URL https://ggweather.com/enso/oni.htm (accessed 5.10.19).

Glenn, E. P., Nagler, P. L., Huete, A. R., Vegetation Index Methods for Estimating Evapotranspiration by Remote Sensing. **Surv Geophys,** v. 31, n. 6, p 531–555, 2010. https://doi.org/10.1007/s10712-010-9102-2.

Giardina, F., Konings, A.G., Kennedy, D. et al. Tall Amazonian forests are less sensitive to precipitation variability. **Nature Geosci**, v. 11, p. 405–409, 2018. https://doi.org/10.1038/s41561-018-0133-5.

Hu G.C., Jia, L., Menenti, M. Comparison of MOD16 and LSA-SAF MSG evapotranspiration products over Europe for 2011. **Remote Sens. Environ**., v. 156, p. 510-526, 2015. https://doi.org/10.1016/j.rse.2014.10.017.

Instituto Brasileiro de Geografa e Estatística—IBGE. 2021a. Estados. Disponível em < http://www. ibge.gov.br/estadosat/perfl.php?sigla=am>. Acesso em: 10 janeiro 2020.

IBGE – Instituto Brasileiro de Geografia e Estatística, 2021b. Vegetação Brasileira 1:5.000. 000 [WWW Document]. URL https://www.ibge.gov.br/geociencias/cartas-e-mapas/informacoes-ambientais/10872-vegetacao.html?=&t=downloads (accessed 4.5.21).

IBGE – Instituto Brasileiro de Geografia e Estatistica, 2021c. Producao Agricola Municipal [WWW Document]. URL https://sidra.ibge.gov.br/tabela/5457 (accessed 10.11.21).

Irmak, S., Irmak, A.; Allen, R. G., Jones, J. W. Solar and net radiation-based equations to estimate reference evapotranspiration in humid climates. **Journal of irrigation and Drainage Engineering, Reston**., v. 129, n. 5, p. 336-347, 2003. doi: 10.1061/(ASCE)0733-9437(2003)129:5(336).

Jiménez-Muñoz, J.C., Mattar, Barichivich, C., J., Santamaría-Artigas, A., Takahashi, K., Malhi, Y., Sobrino, J.A., Schrier, G.V.D. Record-breaking warming and extreme drought in the Amazon rainforest during the course of El Niño 2015–2016**. Sci. Rep**., v. 6 p. 1-7, 2016. doi.10.1038/srep33130.

Kendall, M. G. Rank correlation Methods. London: Charles Griffin. 1975.

Lopes, M. O.; Peralta, D. F.; Carmo, D. M. D.; Silva, M. R. P. D. Estudo comparativo de comunidades de briófitas sujeitas a diferentes graus de inundação no município de São Domingos do Capim, PA, Brasil. **Hoehnea**, v. 4, n. 2, p. 159–171. 2016. https://doi.org/10.1590/2236-8906-54/2015.

Lu, Z., Liu, Z., zhu, J.; Cobb, K. M., Lu, Z. et al. A Review of Paleo El Niño-Southern Oscillation. **atmosphere Review**, v. 9, n.4, p, 130, 2018. https://doi.org/10.3390/atmos9040130.

Marengo, J. A., espinoza, J. C. Extreme seasonal droughts and floods in Amazonia: causes. **International journal of climatology**, v. 1050, n. Julho 2015, p. 1033–1050, 2016. https://doi.org/10.1002/joc.4420.

MINISTÉRIO DO MEIO AMBIENTE. Mapa de Cobertura Vegetal. Disponível em: < https://www.mma.gov.br/biomas/amaz%C3%B4nia/mapa-de-cobertura-vegetal.html >. Acesso em: 23 out. 2019.

Mu, Q., Zhao, M., Running, S. W. Improvements to a MODIS global terrestrial evapotranspiration algorithm. **Remote Sensing of Environment**, v. 115, p. 1781-1800, 2011. https://doi.org/10.1016/j.rse.2011.02.019.

NATIONAL OCEANIC ATMOSPHERIC ADMINISTRATION (NOAA). ENSO: Cold & Warm Episodes by Season. Disponível em: < http://www.cpc.ncep.noaa.gov/products/analysis_monitoring/ensostuff/ensoyears.shtml>. Acesso em: 10 abr. 2019.

Rosemback, R., Ferreira, N.J., Shimabukuro,Y. E., Conforte, J. C. Análise da dinâmica da cobertura vegetal na região sul do brasil a partir de dados modis/terra. **Revista Brasileira de Cartografia**, v. 2, p. 401–416, 2010. https://doi.org/10.1016/j.rse.2011.02.019.

Rossi, S., Soares, O. M. de B. Effects of el niño on the coastal ecosystems and their related services. **Mercator (Fortaleza)**, v. 16, p. 1–16, 2017. https://doi.org/10.4215/rm2017.e16030.

Saeidipour, M., Radmanesh F., Eslamian, S. Meteorological Drought Monitoring Using the Multivariate Index of SPEI (Case Study: Karun Basin). **AUT J. Civil Eng**., v.3, n.1, p. 85-92, 2019. doi: 10.22060/ajce.2018.14740.5494.

Sousa, A. C. de; Candido, L. A.; Andreoli, R. V. Interannual Variability of Precipitation and Moisture Flux on Amazon Using QTCM. **Revista Brasileira de Meteorologia**, v. 33, n. 1, p. 41–56, 2018. https://doi.org/10.1590/0102-7786331015.

Valiantzas, J. D. Simplified forms for the standardized FAO-56 Penman-Monteith reference evapotranspiration using limited weather data. **Jounal of Hydrology**, Amsterdã, v. 505, p. 13-23, 2013. https://doi.org/10.1016/j.jhydrol.2013.09.005

Van Der Werf, G.R.; Randerson, J.T.; Giglio L.; Gobron, N.; dolman, A.J. Climate controls on the variability of fires in the tropics and subtropics **Global Biogeochemical Cycles**, v. 22, n. 3, GB3028, p. 1-13, 2008. https://doi.org/10.1029/2007GB003122.

Velpuri, N. M., Senay, G. B., Singh, R.K., Bohms, S., Verdin, J.P. A comprehensive evaluation of two MODIS evapotranspiration products over the conterminous United States: using point and gridded FLUXNET and water balance ET. **Remote Sens. Environ**., v. 139, p. 35-45, 2013. https://doi.org/10.1016/j.rse.2013.07.013.

Vicente-Serrano, S. M., Begueria, S., Lopaz-Moreno, J. I. A multiscalar drought index sentitive to global warming: the standardized precipitation evapotranspiration index Journal of Climate, v. 23, n. 7, p. 1696-1718, 2010. DOI: 10.1175/2009JCLI2909.1.

Vlam, M., Baker, P.J., Bunyavejchewin, S., Zuidema, P. A. Temperature and rainfall strongly drive temporal growth variation in Asian tropical forest trees. **Oecologia**, v. 174, p. 1449–1461, 2014. https://doi.org/10.1007/s00442-013-2846-x.

Wright, S.J. & Calderón, O. Seasonal, El Nino and longer term changes in flower and seed production in a moist tropical forest. **Ecology Letters**, v. 9, p. 35-44. 2006. doi: 10.1111/j.1461-0248.2005.00851.x.

Yang, Y., Saatchi, S. S., Xu, L., Yu, Y., Choi, S., Phillips, N., Kennedy, R., Keller, M., Knyazikhin, Y., Myneni, R. B. Post-drought decline of the Amazon carbon sink. **Nat. Commun**. v. 9, p. 3172, 2018. DOI: 10.1038/s41467-018-05668-6.

Zhang, K., kimball, J. S., Nemani, R. R., Running, S. W., Hong, Y., gourley, J. J., Yu, Z. B. Vegetation greening and climate change promote multidecadal rises of global land evapotranspiration. **Scientific Reports**, v. 5, n. 15956, p. 1-9, 2015. DOI: 10.1038/srep15956.

CAPÍTULO III

UMA NOVA ABORDAGEM PARA O PREENCHIMENTO DE FALHAS EM DADOS DE PRODUTIVIDADE PRIMÁRIA BRUTA PROVENIENTE DE TORRES DE FLUXO NA AMAZÔNIA

RESUMO

As séries temporais de Gross Primary Productivity (GPP) são muito importantes para entendimento da dinâmica de absorção do carbono pela floresta tropical amazônica. No entanto, é comum ocorrer falhas nos dados dos sensores medidores em torres micrometeorológicas, em que o preenchimento destas falhas gera maior detalhamento na obtenção de informações. O objetivo central deste trabalho é detectar e preencher falhas observadas na série temporal de 2001 a 2020 de GPP proveniente da torre micrometeorológica K34 por meio do modelo Autoregressive Integrated Moving Average Model (ARIMA). Para tanto, foram utilizados dados de GPP provenientes de sensores acoplados a torre K34 e do produto MOD17A2H, oriundo do sensor MODIS/Terra, sendo combinados para gerar a GPP por meio da modelagem ARIMA e preencher as falhas existentes nos dados da K34. O coeficiente de determinação (R^2), raiz quadrada do erro-médio (RMSE) e erro médio absoluto (MAE) foram utilizados para avaliar a acurácia das estimativas pelos diferentes métodos (MODIS e ARIMA) estudados. O teste de Pettitt foi utilizado para detectar inflexão na série temporal, para analisar a tendência, aplicou-se o teste Mann-Kendall apenas nas imediações da torre. O teste de Pettitt mostrou uma mudança na série para 2013, com maiores valores de GPP nos meses de junho a outubro, porém o teste de Mann-Kendall não mostrou tendencia significativa para a torre K34. O ano com maior GPP média para a K34 foi 2003 com 8,82 g C m^{-2} d^{-1} e com menor valor para o ano de 2001 com 6,82 g C m^{-2} d^{-1}. O ano com maior GPP MODIS médio foi 2014 (6,80 g C m^{-2} d^{-1}), já para o ARIMA, foi 2004 com 6,12 g C m^{-2} d^{-1}. Os valores de GPP K34 foram ligeiramente maiores que os obtidos pelo MODIS e ARIMA, ainda assim, é possível notar que, na maioria dos meses as medições da torre de fluxo estão com valores próximos aos dados do MODIS e ARIMA. A GPP sazonal mostrou padrões diferentes para os dados MODIS e a K34, com MODIS apresentando seu pico na estação seca (6,67 g C m^{-2} d^{-1}) e um declínio na estação chuvosa (5,67 g C m^{-2} d^{-1}). A simulação ARIMA também obteve seu pico no período seco (5,54 g C m^{-2} d^{-1}), mostrando sua capacidade em capturar a sazonalidade da região. Na correlação entre ARIMA e K34, o modelo subestimou ligeiramente o GPP na maioria dos meses, com diferença média de 0,22 g C m^{-2} d^{-1} entre 2001 e 2020. Na correlação MODIS e ARIMA, os anos que apresentaram maior R^2 foram 2018 (0,66 g C m^{-2} d^{-1}) e 2002 (0,48 g C m^{-2} d^{-1}), com RMSE de 1,18 e 1,37 g C m^{-2} d^{-1} e MAE de 0,001 g C m^{-2} d^{-1}, respectivamente. Contornando obstáculos como dependência de outras variáveis externas e dados de postos vizinhos, a modelagem ARIMA se mostrou satisfatória para o preenchimento das falhas nos dados de GPP, se mostrando adequado para séries temporais longas com comportamento dinâmico.

Palavras-chave: Produtividade da vegetação, Absorção do carbono, monitoramento ambiental.

ABSTRACT

Gross Primary Productivity (GPP) time series are very important for understanding the dynamics of carbon absorption by the Amazon rainforest. However, it is common to occur failures in the data of the measuring sensors in micrometeorological towers, where filling these failures generates greater detail in obtaining information. The main objective of this work is to detect and fill gaps observed in the 2001 to 2020 time series of GPP from the K34 micrometeorological tower using the Autoregressive Integrated Moving Average Model (ARIMA). For this purpose, GPP data from sensors coupled to a K34 tower and from the MOD17A2H product, from the MODIS/Terra sensor, were used, being combined to generate the GPP through ARIMA modeling and filling the gaps in the K34 data. The coefficient of determination (R2), root mean square error (RMSE) and mean absolute error (MAE) were used to assess the accuracy of the estimates by the different methods (MODIS and ARIMA) studied. The Pettitt test was used to detect inflection in the time series, to analyze the trend, the Mann-Kendall test was applied only in the vicinity of the tower. The Pettitt test showed a change in the series for 2013, with higher GPP values in the months of June to October, however the Mann-Kendall test showed no significant trend for the K34 turret. The year with the highest average GPP for K34 was 2003 with 8.82 g C m-2 d-1 and with the lowest value for the year 2001 with 6.82 g C m-2 d-1. The year with the highest average MODIS GPP was 2014 (6.80 g C m-2 d-1), whereas for ARIMA, it was 2004 with 6.12 g C m-2 d-1. The values of GPP K34 were slightly higher than those obtained by MODIS and ARIMA, even so, it is possible to notice that, in most months, the flux tower measurements are with values close to the MODIS and ARIMA data. Seasonal GPP showed different patterns for MODIS and K34 data, with MODIS showing its peak in the dry season (6.67 g C m-2 d-1) and a decline in the wet season (5.67 g C m-2 d-1). The ARIMA simulation also reached its peak in the dry period (5.54 g C m-2 d-1), showing its ability to capture the seasonality of the region. In the correlation between ARIMA and K34, the model slightly underestimated the GPP in most months, with an average difference of 0.22 g C m-2 d-1 between 2001 and 2020. In the MODIS and ARIMA correlation, the years with the highest R2 were 2018 (0.66 g C m-2 d-1) and 2002 (0.48 g C m-2 d-1), with RMSE of 1.18 and 1.37 g C m-2 d-1 e MAE of 0.001 g C m-2 d-1, respectively. Overcoming obstacles such as dependence on other external variables and data from neighboring stations, ARIMA modeling proved to be satisfactory for filling gaps in GPP data, being adequate for long time series with dynamic behavior.

Keywords: Vegetation productivity, Carbon absorption, environmental monitoring.

1 INTRODUÇÃO

A quantificação do fluxo de carbono, através dos ecossistemas terrestres, tem sido uma grande e ampla área de pesquisa nas últimas décadas. As florestas tropicais, como um dos maiores biomas terrestres, desempenham papéis importantes no sequestro global de carbono (C) onde o mesmo é absorvido pela fotossíntese e incorporado a biomassa do vegetal durante seu crescimento (LI et al., 2020).

A produtividade primária bruta terrestre (Gross Primary Productivity - GPP) é a quantidade total de carbono fixada pelos ecossistemas terrestres e um dos principais componentes-chave do fluxo global de carbono (PAN et al., 2014). O aumento das concentrações atmosféricas de dióxido de carbono (CO_2) e poluentes, como o ozônio (O_3), decorrentes das mudanças de cobertura da terra induzida pelo homem, tem alterado a absorção de carbono pela produção primária bruta (BALDOCCHI; PENUELAS, 2019). Neste sentido, o conhecimento da GPP e sua resposta a variabilidade climática é fundamental para avaliar os potenciais de vulnerabilidade e adaptação do ecossistema, particularmente no contexto das mudanças de ambientes globais (PAN et al., 2014; AHLSTRÖM et al., 2015).

A floresta tropical é um dos biomas mais importantes em termos de produtividade respondendo por 34% da GPP global. Abrangendo um terço de todas as árvores do mundo, a floresta Amazônica é considerada a maior floresta tropical com 5,5 milhões de km^2 cobrindo cerca de 40% da América do Sul, além de abrigar mais de 40 mil espécies de plantas (WENG et al., 2018). Sabe-se que a Amazônia desempenha papel crucial no sistema climático e global, além de contribuir amplamente para a evapotranspiração da superfície (DE OLIVEITA et al., 2017). Apesar da logística desafiadora e do afastamento de fontes de financiamentos científicos, suas florestas tropicais, têm sido tema de diversos trabalhos ao longo dos últimos anos (RESTREPO-COUPE et al., 2013; DOUGHTY et al. 2015; WENG et al., 2018; VILANOVA et al., 2021), buscando, sobretudo, compreender a dinâmica do carbono estabelecendo relações com os possíveis impactos climáticos e vice-versa.

A GPP pode ser medido por vários métodos (WU et al., 2009; PENG; GITELSON; SAKAMOTO, 2013). Os dados provenientes de sensores remotos orbitais se apresentam como alternativa para superar as limitações da existência de dados de campo, principalmente em áreas de grande extensão no Brasil. O Moderate Resolution Imaging Spectroradiometer (MODIS) é um sensor a bordo dos satélites TERRA e AQUA que foi idealizado em parte para responder questionamentos sobre a dinâmica global do carbono. O produto MOD17A2H vem sendo utilizado, desde fevereiro de 2000, para fornecer a GPP global a uma resolução espacial de 500 m em um intervalo de 8 dias (SANTOS et al., 2021).

Medições de torre de fluxo produzem informações sobre como o metabolismo do ecossistema responde inúmeras forças biofísicas, como, temperatura, chuva, luz, CO_2, fenologia, dentre outras (YANG; VAN DER TOL, 2018). Com base em uma rede de torre de fluxo, por meio da técnica de vórtices turbulentos, os padrões da GPP podem ser quantificados. As medições de fluxo de carbono na Amazônia vêm desde o início dos anos 1980, no estudo de Shuttlewort (1988) e posteriormente em uma escala mais ampla como parte da rede de torres da Grande Escala da Biosfera-Atmosfera na Amazônia (LBA) (DA ROCHA et al., 2009; RESTREPO-COUPE et al., 2013).

O monitoramento de variáveis ambientais por meio de torres e fluxo produz um amplo conjunto de informações, onde por diversas vezes, suas séries históricas, são utilizadas para modelagem do ecossistema, eficiência no uso da luz, eficiência de uso de carbono e água, dentre outros (STOCKER et al., 2018; BALDOCCHI; PENUELAS, 2019). Entretanto, falhas podem acontecer nos equipamentos sensores ou na transmissão de informações das variáveis obtidas pelas torres micrometeorológicas, devido a intempéries naturais ou até mesmo ações antrópicas (WALTER et al., 2013).

Infelizmente, as áreas de maior escassez de dados e falhas normalmente coincidem com áreas que sofrem os maiores impactos de condições hidrológicas adversas, incêndios e desmatamento, onde mais dados poderiam ser usados para avaliar melhor a situação atual e prever cenários futuros permitindo melhores estratégias de mitigação e adaptação. O preenchimento de falhas é necessário para aproveitar séries longas (WALTER et al., 2013), e garantir uma maior qualidade na obtenção de informações, neste sentido, metodologias tem-se desenvolvido com o intuito de minimizar esse problema.

Existem diversas técnicas para executar os preenchimentos das falhas espaço-temporais, como o uso de interpolações, geoestatística, redes neurais, regressão linear, dentre outras (PAPPAS et al., 2014). O modelo Autoregressive Integrated Moving Average Model - ARIMA é um dos modelos estocásticos de séries temporais mais utilizados (ZHANG, 2003; HAN et al., 2010). Este modelo permite usar dados passados para gerar simulações futuras dos processos ambientais, mas também é usado para preencher lacunas (AFRIFA-YAMOAH et al., 2020). Um dos principais motivos para a utilização do modelo ARIMA é o uso de observações anteriores, o que permite ao modelo incorporar condições anteriores para informar os valores atuais. Desse modo, como ressaltam DORICH et al. (2020), modelos utilizados para prever o futuro podem ser usados para preenchimento de falhas, pois incorporam condições passadas para informar os valores atuais.

A hipótese dessa pesquisa é que o modelo ARIMA pode ser utilizado com acurácia para preenchimento de falhas de dados em série temporal de GPP. É nesse contexto que se apresenta esse artigo, focado no preenchimento de falhas observadas na série temporal de produtividade primária bruta, proveniente da torre micrometeorológica K34, localizada no estado do Amazonas através do modelo Autoregressive Integrated Moving Average Model – ARIMA.

2 MATERIAL E MÉTODOS

2.1 Área de Estudo

O estado do Amazonas está situado na região norte apresentando uma superfície de 1.559.148,890 km^2, sendo maior que as regiões sul e sudeste juntas, considerado o maior em extensão territorial do Brasil, com uma população de 3.938.336 habitantes (Figura 1) (IBGE, 2020). De acordo com a classificação de Köppen, o clima predominante na região pertence ao grupo A, com temperaturas médias do ar de 24ºC a 26ºC e umidade relativa do ar variando de 76% a 89%, possuindo duas estações bem definidas, o inverno caracterizado como o período

das chuvas e o verão que compreende a seca ou período menos chuvoso (ALVARES et al., 2013).

O Experimento de Grande Escala da Biosfera-Atmosfera na Amazônia (LBA) fornece uma comparação das taxas de absorção de carbono através de torres entre as principais regiões climáticas. O foco deste trabalho é a GPP provenientes da torre micrometeorológica K34 (Figura 1). A torre foi instalada na Reserva Biológica do Cuieiras do Instituto Nacional de Pesquisas da Amazônia (INPA), está situada a cerca de 60 km a noroeste de Manaus e foi erguida em 1999, apresentando uma altura de 50 m, localizada a 2° 36' 33 ″ S e 60° 12' 33″ W, numa altitude de 130 m (MALHI, et al., 2009).

O clima local é típico da Amazônia Central com temperaturas elevadas, uma boa abundância de chuvas ao longo do ano (2672,6 mm ano^{-1}) e uma curta estação seca. A vegetação é típica de floresta tropical primária não perturbada onde grande parte se encontra em planícies alagadas (ARAÚJO et al., 2002; MALHI, et al., 2009).
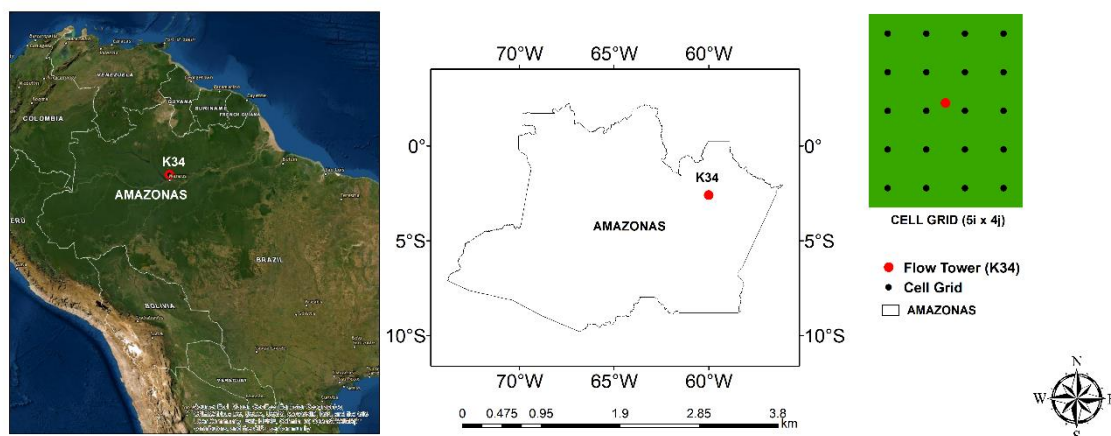
Figura 1. Localização geográfica da área de estudo.

2.2 Dados Torre de Fluxo

As torres micrometeorológicas medem GPP indiretamente como a diferença entre a troca líquida do ecossistema e a respiração do ecossistema (Re). Os dados de produtividade obtidos da K34 foram horários, por meio da técnica de covariância de vórtices turbulentos. Esse método se baseia nas condições turbulentas ou instáveis da atmosfera, em que ocorre a troca de massa e energia entre a vegetação e a camada limite atmosférica. A metodologia tem como princípio as flutuações das concentrações (covariância) de gases, energia e na velocidade vertical do vento (BALDOCCHI, 2019).

Uma descrição detalhada das principais medições, alturas e instrumentos utilizados da torre micrometeorológica K34 e métodos usados, para calcular os dados brutos da troca de CO_2 no ecossistema, estão presentes em Tabela1 e nos trabalhos de Araújo et al. (2002)e Restrepo-Coupe et al. (2013).

Tabela 1. Relação das medições, alturas e instrumentos utilizados presentes na torre micrometeorológica K34. Adaptado de Araújo et al. (2002).

Medição	Instrumento utilizado	Altura (m)
Ondas curtas entrando e saindo	Piranômetro Kipp e Zonen CM 21	44,60
Radiação fotossinteticamente ativa (PAR)	Sensor quântico LI-COR LI-190SZ	51,6
Humidade relativa	Vaisala HMP35A	51,1
Direção do vento	Vector W200P	51,45
Perfil vertical da velocidade do vento	Vector A100R	51,9; 42,5; 35,3; 28
Temperatura da superfície	Sensor infravermelho Heimann KT15	50,40

2.3 Produto MODIS

Os dados do GPP foram obtidos através do sensor MODIS plataforma Terra produto MOD17A2H, com resolução temporal de 8 dias e resolução espacial de 500 metros seguindo a metodologia adotada para o cálculo do GPP no Parque Nacional de Itatiaia por Delgado et al. (2018), durante o período de janeiro de 2001 a dezembro de 2020.

Os dados são originados a partir de um mosaico de oito dias com 500m de resolução espacial. Em qualquer dado pixel dentro do conjunto global de 500m pixels, a estimativa da GPP será calculada, essa estimativa é um composto cumulativo de valores de PPB, baseado no conceito da eficiência da utilização da radiação solar pela vegetação. Nessa lógica, a produtividade primária está linearmente relacionada com a radiação ativa absorvida pela fotossíntese (APAR), (DELGADO et al., 2018; SANTOS et al., 2021). As imagens obtidas foram transformadas em valores analíticos, para isso é necessário a transformação dos números digitais em valores biofísicos (Equação 1).

Pixel Biofísico ($Kg\ C\ m^{-2}$) = Pixel da imagem * Fator de escala (0,0001)   (1)

Os valores de GPP também foram transformados do valor acumulado a cada 8 dias para valores médios a cada 8 dias e convertidos de $Kg\ C\ m^{-2}\ dia^{-1}$ para $g\ C\ m^{-2}\ dia^{-1}$.

2.4 Modelo de Média Móvel Integrada Autorregressiva (ARIMA)

Vários métodos estatísticos foram desenvolvidos para preencher lacunas em conjuntos de dados espaço-temporais, sendo mais comumente utilizado o Autoregressive Integrated Moving Average Model (ARIMA) (ZHANG, 2003; HAN et al., 2010). O ARIMA sazonal (Equação 2) é uma das classes mais gerais de modelos para extrapolar séries temporais (SANTOS et al., 2021), sendo utilizado para preenchimento das falhas nos dados de GPP para a K34. Para realizar o preenchimento das lacunas existes, utilizou-se os valores de produtividade obtidos pelo produto MODI17A2H derivado do sensor MODIS (item 2.3) e os próprios dados de GPP da torre.

Dentro desse domínio, a abordagem ARIMA, introduzida por Box-Jenkins em 1976, tem sido empregado em muitos campos, como climatologia, hidrologia (VALIPOUR et al.,

2013), energia e economia devido à sua simplicidade, flexibilidade e fácil interpretação (FASHAE et al., 2019).

$$\left(1 - \sum_{i=1}^{p} \alpha_i L^i\right) X_t = \left(\sum_{i=1}^{q} \theta_i L^i\right) \varepsilon_t \tag{2}$$

em que: L é o operador de atraso, o α_i são os parâmetros da parte autoregressiva do modelo, o Θ_i são os parâmetros da parte da média móvel e ε_t são os termos de erro. Os termos de erro ε_t são geralmente considerados variáveis independentes e distribuídas de forma idêntica, amostradas a partir de uma distribuição normal com uma média zero.

2.5 Análises Estatísticas

Para uma melhor adequação e compreensão, os dados de GPP foram convertidos para escala mensal. A estação seca que vai de abril a setembro e a chuvosa que vai de outubro a março (ARAÚJO et al., 2002) foram investigados para avaliar o comportamento sazonal da GPP nas diferentes metodologias aqui apresentadas.

Através do pacote Time Series Analysis (TSA) no software R, o teste não paramétrico de Pettitt (Equação 3) foi utilizado para detectar a inflexão na série temporal, que serviu para analisar os mapas espaciais na unidade territorial do estado do Amazonas, utilizando para tanto os dados provenientes do sensor MODIS.

$$k_T = \max |U_{t,T}|,$$

$$U_{t,T} = \sum_{i=1}^{t} \sum_{j=t+1}^{T} sng\,(Xi - Xj)$$

$$p \cong 2\exp\left(\frac{-6\,K_T^2}{T^3 + T^2}\right) \tag{3}$$

em que: a estatística k(t) representa o ponto de mudança t significativo no qual o valor de |Ut, N| é máximo e está associado a um nível de significância (p). O ponto de mudança da série está localizado em K_T, desde que a estatística seja significativa.

Para analisar a tendência da GPP para as imediações da torre (CELL GRID 5 linhas x 4 colunas) no período de 2001 a 2020, foi aplicado o teste de Mann-Kendall, utilizando o pacote Kendallno software R (Equação 4).

$$Z_{mk} = \frac{S-1}{\sqrt{Var(S)}}; \text{when } S > 0 \tag{4}$$
$$Z_{mk} = 0; \text{when } S = 0$$
$$Z_{mk} = \frac{S+1}{\sqrt{Var(S)}}; \text{when } S < 0$$

em que: Z_{mk} é o índice Z do teste de Mann-Kendall; S é a estatística "score" e Var (S) é a variância do valor estatístico S.

O coeficiente de determinação (R^2), RMSE (Equação 5) e MAE (Equação 6) foram utilizados para avaliar a acurácia das estimativas de GPP pelos diferentes métodos aqui apresentados.

$$RMSE = \sqrt{\frac{\sum_{i=1}^{n}(p_i - o_i)^2}{n}}$$
(5)

$$MAE = \frac{\sum_{i=1}^{n}|p_i - o_i|}{n}$$
(6)

em que: p_i é o valor estimado ou previsto; o_i é o valor observado ou medido e n: número de observações.

3 RESULTADOS E DISCUSSÃO

Para toda a série de estudo que foi de 2001 a 2018, o teste de Pettitt mostrou um ponto de mudança para o ano de 2013, para este ano, foram espacializados os valores mensais da GPP MOD17A2H que são mostrados na figura 2. É possível notar que os maiores valores de GPP se apresentam nos meses que vão de junho a outubro, especialmente em 2013. A região Amazônica passava por um período de grandes enchentes relacionadas a anomalias de temperatura da superfície do mar nos oceanos Atlântico e Pacífico, que alteraram o ciclo da água em diferentes partes da bacia e períodos do ano (MARENGO; ESPINOSA, 2015; SORRIBAS et al., 2016)

Os meses de julho a outubro geralmente recebem grande quantidade de irradiação solar, que se associado com uma boa disponibilidade de água, como a que ocorreu em 2013, pode ter favorecido a PPB. Restrepo-Coupe et al. (2013) e Wu et al. (2016) em suas análises dos conjuntos de dados de torres de fluxos, mostraram que em florestas não limitadas por água da Amazônia, a GPP foi impulsionada por uma combinação de entrada de radiação e ritmos fenológicos que influenciaram a qualidade e quantidade de folhas.

Outro ponto importante é que dada a redução da cobertura de nuvens na estação seca, aumento da radiação solar, e árvores com raízes profundas não afetadas pela secagem da superfície do solo, pode-se esperar que a produção primária bruta do ecossistema da Amazônia aumente neste período.

Apesar do teste de Pettitt ter mostrado um ponto de inflexão para 2013, o teste de Mann-Kendall não mostrou tendencia significativa, para o local onde a torre está localizada, para nenhum dos anos da série de estudo, sendo o menor p-valor encontrado para o ano de 2009 (Tabela 2). A não significância do teste pode ser pelo fato de que as imediações da torre se encontram em um ambiente bastante preservado, onde os ventos predominantes do nordeste sopram sobre a vasta extensão de floresta tropical intacta antes de chegar ao local da torre, além disso, a região dispõe de uma precipitação pluviométrica média anual de 2672,6 mm ano[-1] e uma estação seca mais curta.
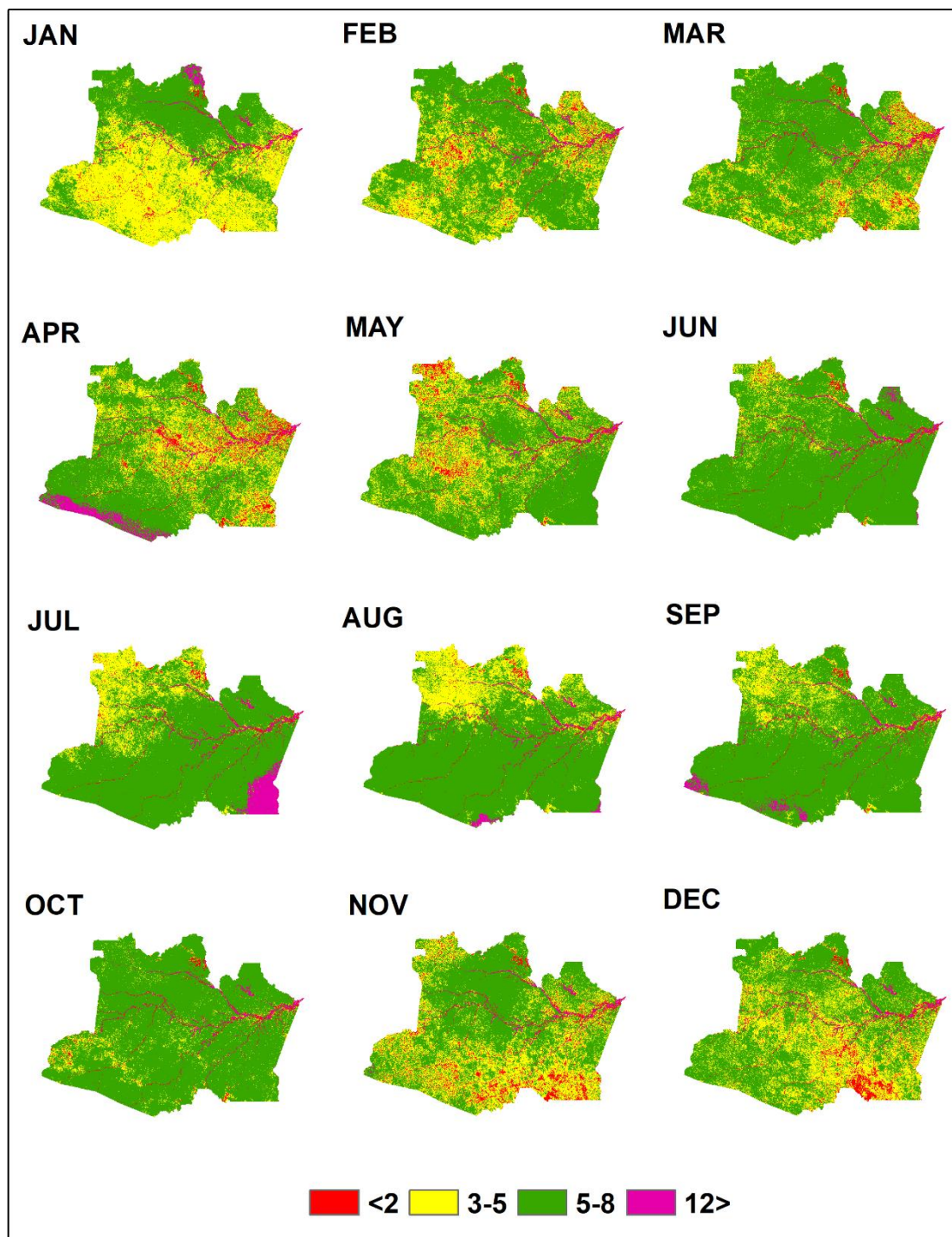
Figura 2. Valores de GPP mensal para todos os meses do ano 2013.

Tabela 2. Mann-Kendall de todos os anos para o entorno da torre (CELL GRID 5i x 4j).

Ano	Tap	S	varS	P.valor	Zmk
2001	0.107	7	211.667	0.680	0.412
2002	0.076	5	211.667	0.783	0.275
2003	0.046	3	211.667	0.891	0.137
2004	0.229	15	211.667	0.336	0.962
2005	-0.046	-3	211.667	0.891	-0.137

2006	0.076	5	211.667	0.783	0.275
2007	0.229	15	211.667	0.336	0.962
2008	0.076	5	211.667	0.783	0.275
2009	0.412	27	211.667	0.074	1.787
2010	0.137	9	211.667	0.582	0.550
2011	0.260	17	211.667	0.271	1.100
2012	0.198	13	211.667	0.409	0.825
2013	0.076	5	211.667	0.783	0.275
2014	0.290	19	211.667	0.216	1.237
2015	0.137	9	211.667	0.582	0.550
2016	0.046	3	211.667	0.891	0.137
2017	0.229	15	211.667	0.336	0.962
2018	0.046	3	211.667	0.891	0.137
2019	-0.137	-9	211.667	0.582	-0.550
2020	-0.229	-15	211.667	0.336	-0.962

Z = Análise estatística de teste de Mann-Kendall. p-valor = tendência estatisticamente significativa. varS = variância.

3.1 Produtividade Primária Bruta Mensal e Anual

A Figura 3 mostra os dados de GPP mensal obtidos do MODIS e modelagem ARIMA para todo o estado, nos anos de 2001 a 2020 e K34 de 2001 a 2006. O GPP mínimo e máximo mensal observado até o ano de 2006, onde se tem os dados da K34, foram 1,80 g C m^{-2} d^{-1} (setembro de 2001) e 11,8 g C m^{-2} d^{-1} (dezembro de 2004) respectivamente. O ano com maior GPP média para a K34 foi 2003 com 8,82 g C m^{-2} d^{-1} e 2001 apresentou o menor valor com 6,82 g C m^{-2} d^{-1}, nota-se uma diferença pequena entre os valores máximos e mínimos obtidos para o entorno da K34. Os valores de GPP da torre foram ligeiramente maiores que os obtidos pelo MODIS e a modelagem ARIMA, ainda assim, é possível notar que, na maioria dos meses as medições da torre de fluxo estão em um bom acordo com os dados do MODIS e a simulação do ARIMA.

É frequente o uso de séries temporais de torre micrometeorológicas para modelagem de ecossistemas, e há casos em que as séries temporais disponíveis podem ter observações ausentes, ser de curta duração ou mesmo ambos. Como resultado, em muitos casos, cientistas e profissionais são desafiados a trabalhar com séries curtas e fragmentadas. Ao analisar a série do estudo em questão é possível notar que, há inúmeras falhas em praticamente todos os anos para os dados da K34, as porcentagens variaram de 33% a 48%, essas falhas tornam as previsões menos precisas e por vezes contestáveis. A modelagem ARIMA simulou valores semelhantes aos onservados pela K34, preenchendo as falhas existentes para a série de 2001 a 2006, mostrando sua capacidade em simular dados de GPP.
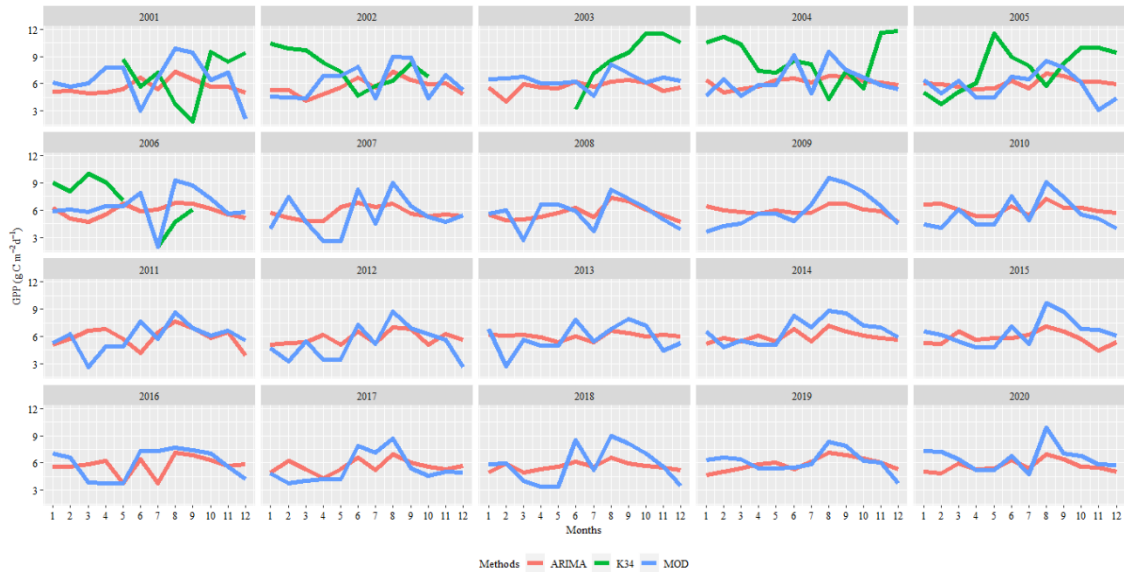
Figura 3. GPP mensal dos anos de 2001 a 2020 para todo o estado do amazonas.

Os valores de GPP obtidos do MODIS para toda a série do estudo apresentaram valores mínimos mensais de 1,95 g C m^{-2} d^{-1} (maio e julho de 2006) e máximos de 9,90 g C m^{-2} d^{-1} (agosto de 2020). Já na modelagem ARIMA o seu valor mínimo foi de 3,73 em julho de 2016 e máximo de 7,63 para agosto de 2011. Os anos com maior GPP MODIS médio foram 2014 (6,80 g C m^{-2} d^{-1}) e 2015 (6,54 g C m^{-2} d^{-1}), para o ARIMA foram 2004 (6,12 g C m^{-2} d^{-1}) e 2005 (6,06 g C m^{-2} d^{-1}).

Percebe-se que os anos com maiores GPP, tanto MODIS como ARIMA, precederam eventos meteorológicos responsável por intensos períodos de insolação, 2014 por exemplo, antecedeu umas das maiores secas já registradas na Amazônia. Uma possível explicação é que em 2014 a insolação nesta região era mais atuante, porém, com uma maior disponibilidade de água para a planta do que no ano seguinte (2015), favorecendo seus processos fisiológicos e consequentemente melhorando a absorção de carbono.

Cabe ressaltar que, mesmo se as florestas forem capazes de manter sua capacidade de produtividade em baixos níveis de precipitação, outros fatores além da GPP irão determinar se as florestas irão persistir, mudar para outro tipo de floresta ou ser substituídas por savanas. Hirota et al. (2011) relatam que sob uma precipitação pluviométrica superior a 2500 mm anuais, a cobertura florestal domina, porém, há uma redução na quantidade de árvores encontradas em precipitações pluviométricas inferiores a 750 mm anuais.

Se mudanças climáticas ou intervenções humanas resultarem na diminuição ainda maior da precipitação pluviométrica nessa estação seca, o aumento na ocorrência de incêndios pode resultar numa substituição da floresta por pastagem. As preocupações são ainda maiores se levarmos em consideração que o número de incêndios em 2020 aumentou 12% em relação a 2019 (INPE, 2021) e estamos vivendo um desmonte da fiscalização ambiental e das políticas sociais além da eliminação de agentes ambientais neste atual governo (CASTRO et al., 2020).

3.2 Sazonalidade da GPP

O ciclo de GPP observado em escala sazonal mostrou padrões diferentes para os dados do MODIS e a K34 (Figura 4). Os dados MODIS apresentaram seu pico durante a estação seca (6,67 g C m^{-2} d^{-1}) e um declínio na estação chuvosa (5,67 g C m^{-2} d^{-1}). Restrepo-Coupe et al. (2016), demostraram em seu trabalho um aumento da GPP na Amazônia equatorial para o período seco. Já os valores da K34, foram ligeiramente maiores durante a estação chuvosa (9,15 g C m^{-2} d^{-1}), com redução no período seco (6,76 g C m^{-2} d^{-1}).

Como a diferença de GPP na estação seca e chuvosa para os dados da torre K34 foram muito pequenas, sugere-se que seja devido a torre estar localizada em um local extremante preservado na Reserva Biológica do Cuieiras do Instituto Nacional de Pesquisas da Amazônia (INPA) próximo a cidade de Manaus, e a duração da estação de seca mais proeminente, para a localização da torre, ser de aproximadamente 2 meses (RESTREPO-COUPE et al., 2016).

A simulação ARIMA também mostrou seu pico de GPP no período seco (5,54 g C m^{-2} d^{-1}), mostrando sua capacidade em capturar a sazonalidade da região (Figura 4). De Oliveira et al, 2017 analisaram a GPP e obtiveram seus maiores valores durante a estação seca mostrando que na Amazônia equatorial a produtividade primária bruta é controlada principalmente pela disponibilidade de luz e fenologia, pois durante a estação seca a vegetação tem a oportunidade de aumentar sua produtividade sob o regime de precipitação existente.

Observações de árvores com raízes profundas de até 18 m e de distribuição hidráulica (DA ROCHA et al., 2004), sugerem mecanismos pelos quais as florestas conseguem manter sua produtividade durante a estação considerada seca. Von Randow et al. (2020) explicam que a região não apresenta uma forte sazonalidade e fornece água suficiente no solo que pode ser acessada pelas raízes profundas das árvores antigas para aproveitar tanto a luz quanto o abastecimento de água. Kim et al. (2012) demostram que a GPP sustentada ou crescente na estação seca é consistente com a maior disponibilidade de luz, uma vez que esses locais equatoriais experimentam picos de irradiância solar na estação seca, devido a redução da cobertura de nuvens. tanto a luz quanto o abastecimento de água.

Outro fato que ocorre também na estação seca é a redução de folhas velhas, o que resulta em mais luz penetrando no dossel para folhas mais jovens remanescentes. No geral, as folhas novas têm mais clorofilas em comparação com as folhas velhas e maior capacidade fotossintética, o que favorece a captura de carbono pela planta (CHAVANA-BRYANT et al., 2016). Fatichi; Leuzinger; Körner, (2014) refletem sobre as limitações biofísicas impostas na estação chuvosa por exemplo, baixa radiação e alto teor de umidade do solo, que fazem com que as folhas e a madeira sejam produzidas durante a estação seca.

Entretanto, estudos apontam que a GPP é impulsionada pela luz até uma certa temperatura e que durante os períodos de seca, a temperatura mais alta junto com a radiação aumentada podem exercer estresse térmico na fotossíntese das folhas iluminadas pelo sol, podendo diminuir a GPP nas florestas Tropicas Amazônicas (YAN et al., 2019).
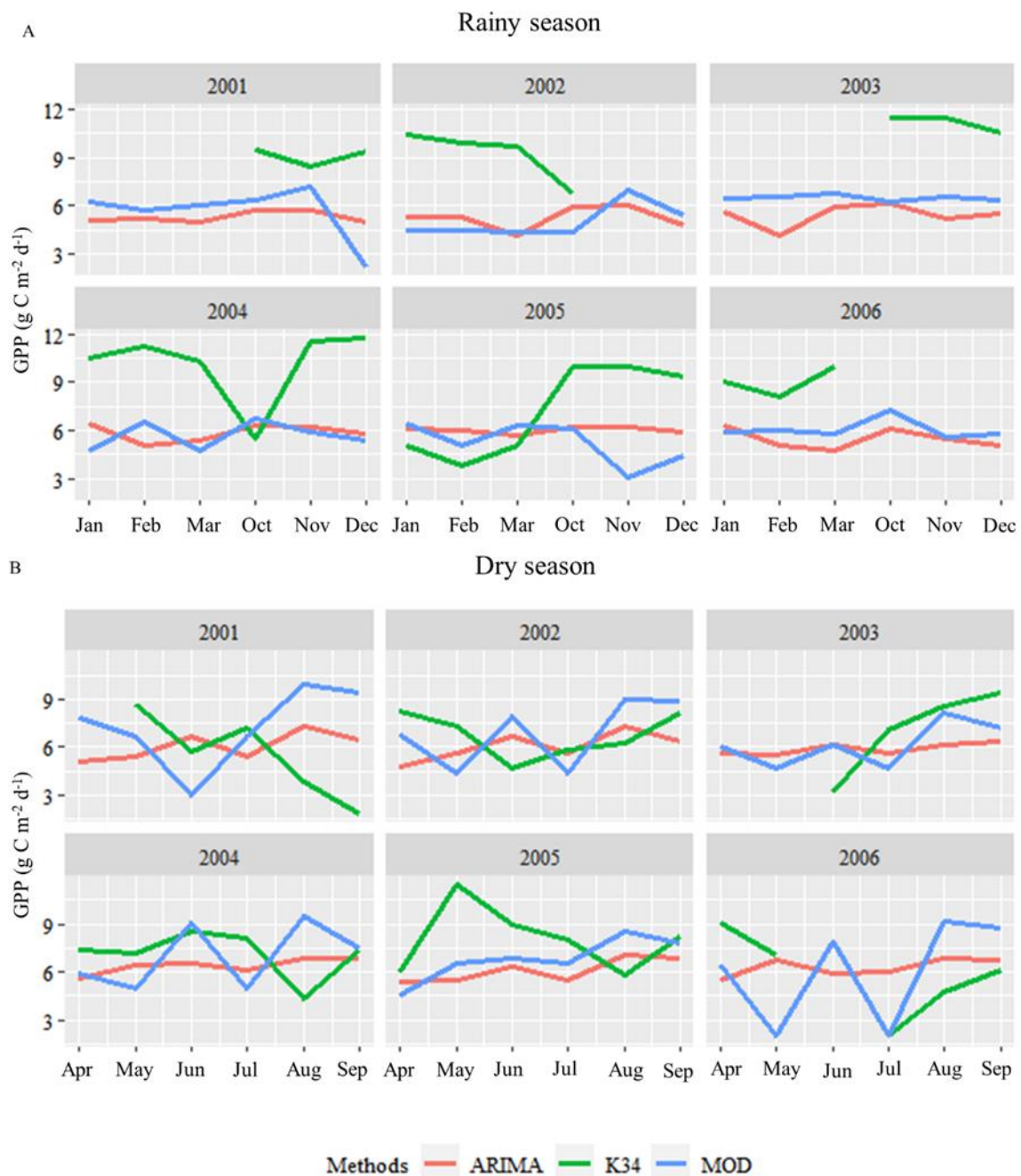
**Figura 4**. GPP para a estação considerada seca e chuvosa no estado do Amazonas.

3.3 Correlação Entre a Torre K34 e a Modelagem ARIMA

Observou-se uma correlação modesta entre o GPP Torre e o GPP advindo da modelagem ARIMA. Como pode ser visto, o ARIMA subestimou ligeiramente na maioria dos meses o GPP local, com diferença média de 0,22 g C m^{-2} d^{-1} para o período de 2001 a 2006. O ano de 2001 apresentou a melhor correlação com R^2 0,67, RMSE e MAE de 3,38 g C m^{-2} d^{-1} e 0,002 respectivamente. O ano de 2005 apresentou o menor valor de R^2 < 0,01, porém com o menor RMSE de 2,38 g C m^{-2} d^{-1} e MAE de 0,003 g C m^{-2} d^{-1} (Figura 5).

O fato da modelagem ARIMA ter sido realizada para todo o estado e os valores obtidos pela K34 são apenas para o seu entorno, pode explicar essa subestimação, pois embora pareça, superficialmente, que as florestas tropicais são muito semelhantes em toda a Amazônia, a região consiste em uma série de sub-regiões climáticas muito distintas. Outro ponto que pode ter influenciado no desempenho do modelo, resultando na modesta correlação, foi o comprimento da série estudada, que por ser relativamente curta pode ter obscurecido características como como tendência, sazonalidade e comportamentos cíclicos.

A aquisição de valores contínuos de produtividade primária bruta na Amazônia é muito importante para apoiar análises de mudanças globais. As técnicas de preenchimento de falhas são particularmente úteis no ajuste de dados ausentes em produtos usados para monitorar características que mudam gradualmente ao longo do tempo. O método ARIMA é comum para problemas de previsão de séries temporais, mas também foi testado em cenários de preenchimento de lacunas (DE ROSA et al., 2016, 2018). No sentido de que muitas técnicas de preenchimento se mostram não satisfatórias, a modelagem ARIMA se apresenta como uma metodologia consistente que pode ser utilizada, principalmente, quando não se tem disponíveis os dados de postos vizinhos para interpolações e recursos computacionais.

Os resultados aqui encontrados são ainda mais expressivos se for lembrado que a única informação utilizada para o preenchimento foi a própria série, dispensando variáveis externas e análises cruzadas entre postos de medição. REN et al. 2019 compararam o modelo ARIMA com outros métodos para preenchimento de falhas, e concluíram que a metodologia ARIMA foi eficiente no preenchimento das lacunas, além de ser capaz de capturar tendências e apresentar um desempenho melhor do que os outros modelos em termos de estatísticas de erro.
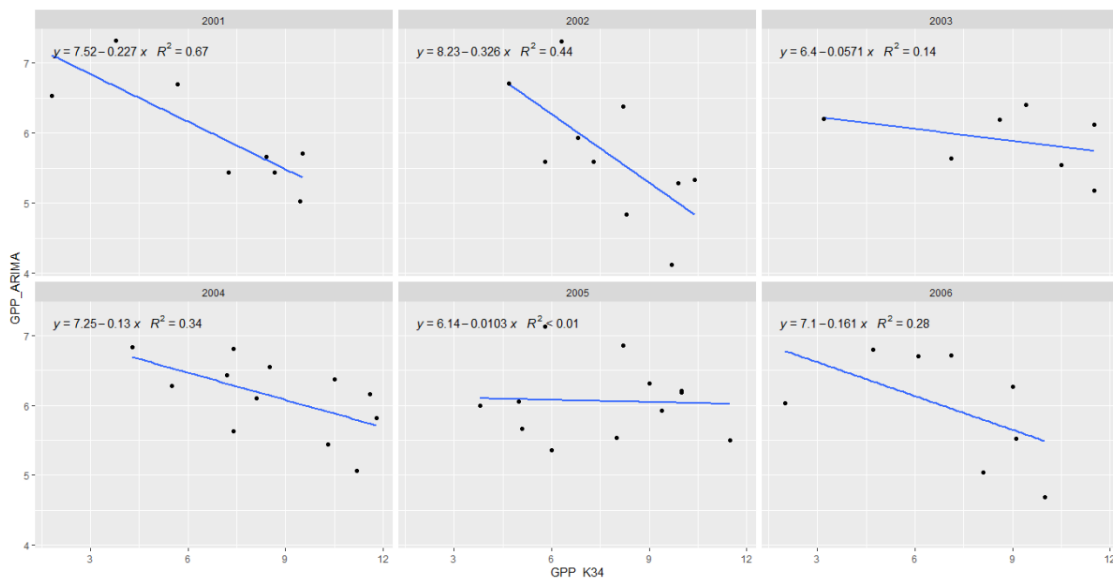
Figura 5. Correlação entre a GPP obtida pela K34 e a modelagem ARIMA.

## 3.4 Correlação Entre o MODIS e a Modelagem ARIMA

Na Figura 6 podemos ver a regressão para os dados de GPP obtidos pelo MODIS e ARIMA. Os anos que apresentaram maior correlação foram 2018 (0,66) e 2002 (0,48), com RMSE de 1,18 g C m^{-2} d^{-1} e 1,37 e MAE de 0,001 g C m^{-2} d^{-1} respectivamente. Os anos em que

ocorreram as maiores secas no estado apresentaram baixas correlações como por exemplo, 2005 e 2015 com R^2 de 0,01 para ambos. Essa menor correlação para os anos com seca extrema pode ser devido as anomalias negativas ocorridas na maioria das florestas tropicais da Amazônia durante eventos de El Niño. Liu et al. (2018) encontraram uma diminuição do GPP na América do Sul tropical devido ao evento El Niño de 2015/2016.

O R^2 médio encontrado para toda série de 2001 a 2020 foi de 0,26. Em um estudo desenvolvido por Wang et al. (2013), os autores analisaram as estimativas MODIS no norte da China e encontraram um R^2 de 0,26. De Oliveira et al. (2017) analizaram os dados de GPP das torres K67, K83 e K77 do projeto LBA para o etado do Amazonas e compararam com o produto MODIS17A2 e obtiveram R^2 médio de 0,40.

Dorich et al. (2020) compararam cinco métodos para preenchimento de lacunas nos dados de emissões de N_2O do solo, dentre eles o ARIMA, que em comparação com os demais apresentou R^2 de 0,68 e RMSE de 2,77 g C m^{-2} d^{-1}. Os autores enfatizam que a técnica de preenchimento por meio da modelagem ARIMA tem se mostrado promissora para diferentes tipos de dados. Afrifa-yamoah et al. (2020) estudaram diferentes abordagens para imputação de dados ausentes, dentre eles, o ARIMA, e obtiveram bom desempenho para o modelo, mostrando sua adequabilidade para o preenchimento de falhas em dados de temperatura.
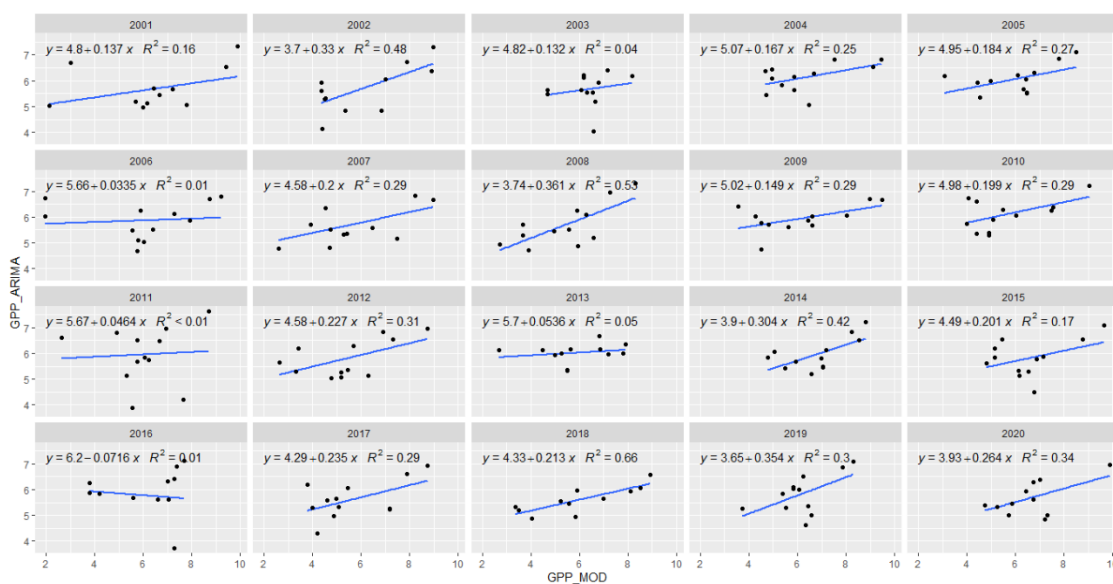
Figura 6. Regressão para os dados de GPP obtidos pelo MODIS e ARIMA.

4 CONCLUSÕES

A intenção deste trabalho foi oferecer uma alternativa às técnicas tradicionais de preenchimento de falhas em dados de torres micrometeorológicas. Contornando obstáculos como dependência de outras variáveis externas e dados de postos vizinhos, a modelagem ARIMA se mostrou satisfatória para o preenchimento das falhas nos dados de GPP.

O ARIMA foi capaz de capturar tendências de longo prazo nos dados, se mostrando adequado para séries temporais longas com comportamento dinâmico.

O uso de métodos de preenchimento de falhas, principalmente no estado do Amazonas, pode aumentar a transparência, melhorar as estimativas de produtividade da floresta, reduzir a incerteza e aumentar a capacidade de quantificar o impacto das práticas de mitigação.

5 REFERÊNCIAS

AFRIFA-YAMOAH, E.; MUELLER, U. A.; TAYLOR, S. M.; FISHER, A. J. Missing data imputation of high-resolution temporalclimate time series data. **Meteorol Applications**, v. 2, n. 1, p. e1873, 2020. https://doi.org/10.1002/met.1873.

AHLSTRÖM, A.; RAUPACH, M. R.; SCHURGERS, G.; SMITH, B.; ARNETH, A.; JUNG, M.; REICHSTEIN, M.; CANADELL, J. G.; FRIEDLINGSTEIN, P.; JAIN, A. K.; KATO, E.; POULTER, B.; SITCH, S.; STOCKER, B. D.; VIOVY, N.; WANG, Y. P.; WILTSHIRE, A.; ZAEHLE, S.; ZENG, N. The dominant role of semi-arid ecosystems in the trend and variability of the land CO_2 sink. **Science**, v. 348, n. 6237, p. 895–899. 2015. https://doi.org/10.1126/science.aaa1668.

ALVARES C. A.; STAPE J. L.; SENTELHAS P. C.; GONÇALVES J. L. M.; SPAROVEK G. Koppen's climate classification map for Brazil. **Meteorologische Zeitschrift**, v. 22, n. 6, p. 711–728, 2013. doi: 10.1127/0941-2948/2013/0507.

ARAÚJO, A. C.; NOBRE, A. D.; KRUIJT, B.; ELBERS, J. A.; DALLAROSA, R.; STEFANI, P.; VON RANDOW, C.; MANZI, A. O.; CULF, A. D.; GASH, J. H. C.; VALENTINI, R.; KABAT, P. Comparative measurements of carbon dioxide fluxes from two nearby towers in a central Amazonian rainforest: The Manaus LBA site. **Journal of Geophysical Research – Atmospheres**, v. 107, n. 20, p. 8090, 2002. https://doi.org/10.1029/2001JD000676.

BALDOCCHI, D.; PENUELAS, J. The physics and ecology of mining carbon dioxide from the atmosphere by ecosystems. **Global Change Biology**, v. 25, n. 4, p. 1191-1197, 2019. https://doi.org/10.1111/gcb.14559.

CASTRO, F.D.; LOPES, G.R.; BRONDIZIO, E.S. The Brazilian Amazon in times of COVID-19: from crisis to transformation? **Ambiente & Sociedade**, v. 23, p. 1-9, 2020. doi: http://dx.doi.org/10.1590/1809-4422asoc20200123vu2020l3id.

CHAVANA-BRYANT, C.; MALHI, Y.; WU, J.; ASNER, G. P.; ANASTASIOU, A.; ENQUIST, B. J. et al. Leaf aging of Amazonian canopy trees as revealed by spectral and physiochemical measurements. **New Phytologist,** v. 214, n. 3, p. 1049– 1063, 2016. https://doi.org/10.1111/nph.13853.

DA ROCHA, H. R.; GOULDEN, M. L.; MILLER, S. D.; MENTON, M. C.; PINTO, L. D. V. O.; DE FREITAS, H. C.; FIGUEIRA, A. M. e S. Seasonality of water and heat fluxes over a tropical forest in eastern Amazonia. **Ecological Applications**, v.14, n. 4, p. 22– 32, 2004. https://doi.org/10.1890/02-6001.

DA ROCHA, H. R.; MANZI, A. O.; CABRAL, O. M.; MILLER, S. D.; GOULDEN, M. L.; SALESKA, S. R.; RESTREPO-COUPE, N.; WOFSY, S.C.; BORMA, L.S.; ARTAXO, P.; VOURLITIS, G.; NOGUEIRA, J. S.; CARDOSO, F. L.; NOBRE, A. D.; KRUIJT, B.; FREITAS, H. C.; VON RANDOW, C.; AGUIAR, R. G.; MAIA J. F. Patterns of water and heat flux across a biome gradient from tropical forest to savanna in Brazil. **Journal of Geophysical Research: Biogeosciences,** v. 114, n. G1, p. 8, 2009. https://doi.org/10.1029/2007JG000640.

DE OLIVEIRA, G.; BRUNSELL, A. N.; MORAES, C. E.; SHIMABUKURO, E. Y.; BERTANI, G.; DOS SANTOS, V. T.; ARAGAO, E. O. C. L. Evaluation of MODIS-based

estimates of water-use efficiency in Amazonia. **International Journal of Remote Sensing**, v. 38, n. 19, p. 5291-5309. 2017. https://doi.org/10.1080/01431161.2017.1339924.

DE ROSA, D.; ROWLINGS, D. W.; BIALA, J.; SCHEER, C.; BASSO, B.; GRACE, P. R. N_2O and CO_2 emissions following repeated application of organic and mineral N fertiliser from a vegetable crop rotation. **Science of The Total Environment**, v. 637-638, n. 0048-9697, p. 813-824, 2018. https://doi.org/10.1016/j.scitotenv.2018.05.046.

DE ROSA, D.; ROWLINGS, D.R.; BIALA, J.; SCHEER, C.; BASSO, B.; MCGREE, J.; GRACE, P.R. Effect of organic and mineral N fertilizers on N2O emissions from an intensive vegetable rotation. **Biology and Fertility of Soils**, v. 52, p. 895–908, 2016. https://doi.org/10.1007/s00374-016-1117-5

DELGADO, R. C.; PEREIRA, M. G.; TEODORO, P. E.; SANTOS, G. L. DOS; CARVALHO, D. C. DE; MAGISTRALI, I. C.; VILANOVA, R. S. Seasonality of gross primary production in the Atlantic Forest of Brazil. **Global Ecology and Conservation**, v. 14, p. 1–12, 2018. https://doi.org/10.1016/j.gecco.2018.e00392.

DORICH, C. D.; DE ROSA, D.; BARTON, L.; GRACE, P.; ROWLINGS, D.; MIGLIORATI, M. DE A.; WAGNER-RIDDLE, C.; KEY, C.; WANG, D.; FEHR, B.; CONANT, R. T. Global Research Alliance N_2O chamber methodology guidelines: Guidelines for gap-filling missing measurements**. Journal of Environmental Quality**, v. 49, n. 5, p. 1186-1202, 2020. https://doi.org/10.1002/jeq2.20138.

DOUGHTY, C. E.; METCALFE, D. B.; GIRARDIN, C.; AMEZQUITA, F.; DURAND, L.; HUASCO, W.; SILVA-ESPEJO, J. E.; ARAUJO-MURAKAMI, A.; DA COSTA, M. C.; DA COSTA, A. C. L.; ROCHA, W.; MEIR, P.; GALBRAITH, D.; MALHI, Y. Source and Sink Carbon Dynamics and Carbon Allocation in the Amazon Basin. **Global Biogeochemical Cycles**, v. 29, n. 5, p. 645–655, 2015. doi:10.1002/2014gb005028.

FASHAE, A.; OLUSOLA, A. O.; NDUBUISI, I.; UDOMBOSO, C. U. Comparing ANN and ARIMA model in predicting the dischargeof River Opeki from 2010 to 2020 Olutoyin, **River Research and Applications,** v. 35, n. 2, p. 169–177, 2019. https://doi.org/10.1002/rra.3391.

FATICHI, S.; LEUZINGER, S.; KÖRNER, C. Moving beyond photosynthesis: from carbon source to sink-driven vegetation modeling. **New Phytologist**, v. 201, n. 4, p. 1086– 1095. 2014. https://doi.org/10.1111/nph.12614.

HAN, P.; WANG, P. X.; ZHANG, S. Y.; ZHU, D. H. Drought forecasting based on the remote sensing data using ARIMA models, **Mathematical and Computer Modelling**, v. 51, p. 1398–1403, 2010. https://doi.org/10.1016/j.mcm.2009.10.031.

Hirota, M.; Milena Holmgren, M.; Egbert H. Van Nes, E. H.; Scheffer. M. Global Resilience of Tropical Forest and Savanna to Critical Transitions. **Science,** v. 334, n. 6053, p. 232-235, 2011. doi: 10.1126/science.1210657.

INSTITUTO BRASILEIRO DE GEOGRAFIA E ESTATÍSTICA (IBGE). Censo Demográfico, 2010. Disponível em: <www.**ibge**.gov.br>. Acesso em: 15 de janeiro de 2020.

KIM, Y.; KNOX, R. G.; LONGO, M.; MEDVIGY, D.; HUTYRA, L. R.; PYLE, E. H.; WOFSY, C. S.; BRAS, L. R.; MOORCROFT, R. P. Seasonal carbon dynamics and water fluxes in an Amazon rainforest. **Global Change Biology**, v, 18, n. 4, p. 1322– 1334, 2012. https://doi.org/10.1111/j.1365-2486.2011.02629.x.

LI, Z.; AHLSTRÖM, A.; TIAN, F.; GÄRTNER, A.; JIANG, M.; XIA, J. Minimum carbon uptake controls the interannual variability of ecosystem productivity in tropical evergreen forests. **Global and Planetary Change**, v. 195, p. 103343, 2020. https://doi.org/10.1016/j.gloplacha.2020.103343.

LIU, J.; BOWMAN, K. W.; SCHIMEL, D. S.; PARAZOO, N. C.; JIANG, Z.; LEE, M.; BLOOM, A. A.; WUNCH, D.; FRANKENBERG, C.; SUN, Y.; O'DELL, C. W.; GURNEY, K. R.; MENEMENLIS, D.; GIERACH, M.; CRISP, D.; ELDERING, A. Contrasting carbon cycle responses of the tropical continents to the 2015–2016 El Niño. **Science**, v. 358, n. 6360 eaam5690. 2017. https://doi.org/10.1126/science.aam5690.

MALHI, Y.; ARAGÃO, O. C. L. E.; METCALFE, D. B.; PAIVA, R.; QUESADA, C. A.; ALMEIDA, S.; ANDERSON, L.; BRANDO, P.; CHAMBERS, J. Q.; Da COSTA, C. L. A.; HUTYRA, R. L.; OLIVEIRA, P.; PATIÑO, S. PYLE, H. E.; ROBERTSON, L. A.; TEIXEIRA, M. L. Comprehensive assessment of carbon productivity, allocation and storage in three Amazonian forests. **Global Change Biology**, v. 15, n. 5, p. 1255-1274, 2009. https://doi-org.ez30.periodicos.capes.gov.br/10.1111/j.1365-2486.2008.01780.x.

MARENGO, J. A.; ESPINOSA, F. C. Extreme seasonal droughts and floods in Amazonia: causes, trends and impacts. **International Journal of Climatology**, v. 36, n. 3, p. 1033-1050, 2015. doi: 10.1002/joc.4420.

National Institute for Space Research (INPE). Disponível em <http://www.obt.inpe.br/OBT/assuntos/programas/amazonia/degrad>. Acesso em: 14 de fevereiro de 2021.

PAN, S.; TIAN, H.; DANGAL, S. R.S.; Ouyang, Z.; Tao, B.; Ren, W.; Lu, C.; Running, S. W. Modeling and monitoring terrestrial primary production in a changing global environment: toward a multiscale synthesis of observation and simulation. **Advances in Meteorology**, v. 2014, n. 6426, p.1 - 17, 2014. doi:10.1155/2014/965936.

PAPPAS, C.; PAPALEXIOU, S.M.; KOUTSOYIANNIS, D. A quick gap filling of missing hydrometeorological data. J. **Journal of Geophysical Research – Atmospheres,** v. 119, p. 9290–9300, 2014. https://doiorg.ez30.periodicos.capes.gov.br/10.1002/2014JD021633.

PENG. Y.; GITELSON, A.; SAKAMOTO, T. Remote estimation of gross primary productivity in crops using MODIS 250 m data. **Remote Sensing of Environment**, v 128, p. 186-196, 2013. DOI:10.1016/j.rse.2012.10.005.

Ren, H.; Cromwell, E.; Kravitz, B.; Chen, X. Using Deep Learning to Fill Spatio-Temporal Data Gaps in Hydrological Monitoring Networks. **Hydrology and Earth System Sciences,** 2019. https://doi.org/10.5194/hess-2019-196.

RESTREPO-COUPE N.; DA ROCHA H. R.; DA ARAUJO A. C.; BORMA, L. S.; CHRISTOFFERSEN, B.; CABRAL, O. M. R.; DE CAMARGO, P. B.; CARDOSO, F. L.; DA COSTA, A. C. L.; FITZJARRALD, D. R.; GOULDEN, M. L.; KRUIJT, B.; MAIA, J. M. F.; MALHI, Y. S.; MANZI, A. O.; MILLER, S. D.; NOBRE, A. D.; VON RANDOW, C.; SÁ, LEONARDO D. A.; SAKAI, R. K.; TOTA, J.; WOFSY, S. C.; ZANCHI, F. B.; SALESKA, S. R. What drives the seasonality of photosynthesis across the Amazon basin? A cross-site analysis of eddy flux tower measurements from the Brasil flux network. **Agricultural and Forest Meteorology**, v. 182 - 183, n. 0168-1923, p. 128–144, 2013. https://doi.org/10.1016/j.agrformet.2013.04.031.

RESTREPO-COUPE, N.; HUETE, A.; DAVIES, K.; CLEVERLY, J.; BERINGER, J.; EAMUS, D.; VAN GORSEL, E.; HUTLEY, L. B.; MEYER, W. S.; MODIS vegetation products as proxies of photosynthetic potential along a gradient of meteorologically and biologically driven ecosystem productivity, **Biogeosciences**, v. 13, n. 19, p. 5587–5608, 2016. https://doi.org/10.5194/bg-13-5587-2016.

SANTOS, R. O. DE.; DELGADO, R. C.; VILANOVA, R. S.; DE SANTANA, R. O.; ANDRADE, C. F DE.; TEODORO, P. E.; SILVA JUNIOR, C. A.; CAPRISTO-SILVA, G. F.; LIMA, M. NMDI application for monitoring different vegetation covers in the Atlantic Forest biome, Brazil. **Weather and Climate Extremes**, v. 33, n. 100329, 2021. https://doi.org/10.1016/j.wace.2021.100329.

SHUTTLEWORTH, W.J. Evaporation from Amazonian rainforest. **Proceedings of the Royal Society of London. Series B. Biological Sciences**, v. 233, n. 1272, p. 321-346. 1988. https://doi.org/10.1098/rspb.1988.0024.

SORRIBAS, M. V.; PAIVA, C. D. R.; MELACK, M. J.; BRAVO, M. J.; JONES, C.; CARVALHO, L.; BEIGHLEY, E.; FORSBERG, B.; HEIL COSTA, H. M. Projections of climate change effects on discharge and inundation in the Amazon basin. **Climatic Change**, v. 135, p. 555–570, 2016. doi: 10.1007/s10584-016-1640-2.

Stocker, B.D.; Zscheischler, J.; Keenan, T.F.; Prentice, I.C.; Seneviratne, S.I.; Peñuelas, J. Drought impacts on terrestrial primary production underestimated by satellite monitoring. **Nature Geoscience**, v. 12, p. 264, 2019. https://doi.org/10.1038/s41561-019-0318-6.

VALIPOUR, M. Use of surface water supply index to assess-ing of water resources management in Colorado and Oregon, US. **Adv. Agric. Sci. Eng. Res.**, v. 3, n. 2, p. 631–640, 2013. doi:10.5707/aaser.v3i2.247.

VILANOVA, R. S.; DELGADO, R. C.; ABEL, E. L. S.; TEODORO, P. E.; SILVA JUNIOR, C. A; WANDERLEY, H. S.; SILVA, G. F. C. Past and future assessment of vegetation activity for the state of Amazonas-Brazil. **Remote Sensing Applications: Society and Environment**, v. 17, n. 100278, 2020. https://doi.org/10.1016/j.rsase.2019.100278.

VON RANDOW, R. DE C. S.; TOMASELLA, J.; VON RANDOW, C.; DE ARAÚJO, A. C.; MANZI, A. O.; HUTJES, R.; KRUIJT, B. Evapotranspiration and gross primary productivity of secondary vegetation in Amazonia inferred by eddy covariance. **Agricultural and Forest Meteorology**, v. 294, n. 108141, p. 0168-1923. 2020. https://doi.org/10.1016/j.agrformet.2020.108141.

WALTER. O. Y.; KIHORO, J.; A; HENRY; W. K. Imputation of incomplete non- stationary seasonal time series data. **Mathematical Theory and Modeling**, v. 3, n. 12, p. 2224-5804, 2013.

WENG, W.; LUEDEKE, M. K. B.; ZEMP, D. C., LAKES, T.; AND KROPP, J. P. Aerial and surface rivers: downwind impacts on water availability from land use changes in Amazonia**. Hydrology and Earth System Sciences,** v. 22, n. 1, p. 911–927, 2018. doi: 10.5194/hess-2017-526.

WU, C. Y; NIU, Z.; TANG, Q.; HUANG, W. J.; RIVARD B. J. L. Feng Remote estimation of gross primary production in wheat using chlorophyll-related vegetation indices. **Agricultural and Forest Meteorology,** v. 149, p. 1015 – 1021, 2009. https://doi.org/10.1016/j.agrformet.2008.12.007.

WU, J.; ALBERT, L. P.; LOPES, A. P.; et al. Leaf development and demography explain photosynthetic seasonality in Amazon evergreen forests. **Science**, v. 351, n. 6276, p. 972–976. 2016. doi: 10.1126/science.aad5068.

YAN, H.; WANG, S.; HUETE, A.; SHUGART, H. H. Effects of light component and water stress on photosynthesis of Amazon rainforests during the 2015/2016 El Niño drought. **Journal of Geophysical Research: Biogeosciences**, v. 24, n. 6, p. 1574–1590, 2019. doi:10.1029/2018JG004988.

YANG, P.; VAN DER TOL, C. Linking canopy scattering of far-red sun-induced chlorophyll fluorescence with reflectance. **Remote Sensing of Environment**, v. 209, p. 456– 467, 2018. https://doi.org/10.1016/j.rse.2018.02.029.

ZHANG, G. P. Time series forecasting using a hybrid ARIMA and neural network model. **Neurocomputing**, v. 50, p. 159–175, 2003. https://doi.org/10.1016/S0925-2312(01)00702-0.

CONCLUSÕES GERAIS

Estudos para as florestas tropicais são cada vez mais importantes, devido as inúmeras pressões que o bioma enfrenta constantemente. Os resultados apresentados neste trabalho, mostraram que diferentes métodos para estimativa da evapotranspiração podem ser utilizados no estado do Amazonas, o que possibilita a aquisição da variável mesmo quando não se dispõe de muitos dados.

O Vegetation Health Index (VHI), com poucos estudos para a região, mostrou-se uma forte ferramenta na detecção da saúde da vegetação. Constatou-se ainda, a forte influência dos fenômenos ENOS na evapotranspiração das diferentes tipologias florestais estudadas. A modelagem ARIMA foi capaz de capturar tendências de longo prazo nos dados de produtividade, provenientes de torres micrometeorológicas, se mostrando satisfatória para o preenchimento das falhas nos dados de GPP.

Trabalhos como este ajudam a entender melhor os efeitos do fenômeno ENOS e degradação antrópica sobre a vegetação, além de mostrar a importância da preservação de nossas florestas e investimentos políticos para obtenção de dados mais consistentes e com menos falhas nas regiões mais remotas, como o estado do Amazonas.